Universidad
Rey Juan Carlos

TESIS DOCTORAL

A Stochastic Switched Optimal Control Approach to Formation Mission Design for Commercial Aircraft

Autora:
María Cerezo Magaña

Director:
Ernesto Staffetti Giammaria

Programa de Doctorado en Tecnologías de la Información y las Comunicaciones

Escuela Internacional de Doctorado

2022

Acknowledgements

En primer lugar, me gustaría expresar mi más sincera gratitud a Ernesto Staffetti, mi director. Gracias por tu guía, por todo tu tiempo, por tu esfuerzo y empeño en que este trabajo haya ido cogiendo forma y pueda estar orgullosa de él. Gracias por tener en cuenta mis opiniones siempre, por hacerme sentir escuchada y por todas las horas invertidas en cerrar cada fleco que quedaba suelto. Gracias también por tus ánimos y por tener siempre un rato para charlar de trivialidades. No puedo olvidar a Alberto Olivares, gracias. Tu ayuda para que esta tesis haya salido adelante es también incalculable. Gracias por ese nuevo punto de vista que siempre hacía replantear todo de nuevo, mejorándolo. Gracias por todos tus comentarios, por tu tiempo. Gracias por tu sinceridad y por tu buen hacer.

I would like to thank Dr. Sander Hartjes, who supervised my stay at TU Delft. Thank you for your time and advice. It is a pity that my stay coincided with your academia departure. I would also like to thank all the people of the Air Transport & Operations group.

Sin lugar a dudas, estos años y esta tesis no hubieran sido los mismos sin mis compañeros y compañeras de departamento. Gracias, en primer lugar, por los viernes de cerveza. No por la cerveza en sí, que también, sino por vuestra compañía. Sin duda, uno de los peores efectos colaterales de la pandemia, ha sido llevarse esos viernes. Gracias Mihaela, por ser la mejor compañera que se puede tener, pero sobre todo, por ser una gran amiga. Gracias Óscar, Edu, por escucharme, por vuestros consejos, por todos esos brindis y por los que nos quedan. Gracias Antonio, por tu confianza, por estar siempre dispuesto a echarme una mano. Gracias Fernando, por los ratos compartidos en el despacho entre viajes, escalada y montaña. Gracias Pepa, por la tensión compartida de estos últimos meses. Gracias Rebeca, Ana, Nacho, Álex, Cris, Estela, por cada charla.

Gracias a todas y todos que, sin saberlo, me habéis ayudado a llegar hasta aquí. Gracias Jose, Laura, Elisa, Marta, Tere, Álex, por seguir haciendo el mundo girar. Gracias a ti en especial, Carlos, por ser como un hermano para mi. Gracias a todo el equipo Placax, a los super Saiyans, por las risas y por los pegues.

Gracias a mi familia. Gracias tata, por estar ahí desde el primer día de mi vida. Gracias tío Félix, por mostrar siempre ese interés por mi y por mi trabajo. Gracias tío Basi, por enseñarme que siempre podemos aportar un granito de arena para hacer de este mundo algo mejor. Gracias papá y mamá, porque con vosotros los te quieros y los abrazos nunca son suficientes. Gracias por apoyarme siempre, gracias por haberme enseñado a creer en mi.

Finalmente, a mi familia de bichitos. A ti, Juan, no puedo decirte simplemente gracias porque es insuficiente. Por ser mi amigo, mi compañero de viaje y de vida. Por los enanos. Porque contigo todo es más bonito. Y por supuesto, Lucas y Adriana, porque desde el primer segundo en el que os vi, supe que haría lo que fuera por veros sonreír. Esta tesis es vuestra.

Publications and financial support

The results of the research activity described in this PhD thesis have been published in the following journal articles

- M. Cerezo-Magaña, A. Olivares, and E. Staffetti, Formation mission design for commercial aircraft using switched optimal control techniques, *IEEE Transactions on Aerospace and Electronic Systems*, vol. 57, no. 4, pp. 2540–2557, 2021.
- M. Cerezo-Magaña, A. Olivares, and E. Staffetti, A Stochastic Switched Optimal Control Approach to Formation Mission Design for Commercial Aircraft, *IEEE Transactions on Aerospace and Electronic Systems*, in Press, 2022.

and have been presented at the following international conferences and workshops

- M. Cerezo-Magaña, A. Olivares, and E. Staffetti, Cooperative aircraft trajectory planning using stochastic optimal control techniques, *International Workshop on Uncertainty and Air Traffic Management*, 2017.
- M. Cerezo-Magaña, A. Olivares, and E. Staffetti, Assessment of the effect of the fuel savings scheme in Formation Flight Planning using Switched Optimal Control Techniques, *8th European Conference for Aeronautics and Space Sciences*, 2019.

The research activity described in PhD thesis has been partially supported by the following research projects

- Formation flight for a future highly efficient commercial aviation, financed by the Spanish Government (Reference code: TRA2017-91203-EXP). Universidad Rey Juan Carlos 2018-2021. Principal Investigator: Ernesto Staffetti.
- Managing meteorological uncertainty for a more efficient air traffic system: Meteorological uncertainty processing and trajectory tracking, financed by the Spanish Government (Reference code: RTI2018-098471-B-C33). Consortium: Universidad de Sevilla, Universidad Carlos III, Universidad Rey Juan Carlos. Universidad Rey Juan Carlos 2019-2022. Principal Investigators: Ernesto Staffetti and Alberto Olivares.

Abstract

Currently, the main challenge for global aviation is to ensure that the predicted growth in air traffic for the coming decades remains sustainable from an environmental point of view, and that the air traffic management system meets the expected demand for increased capacity. Formation flight offers great promise in terms of improving both the environmental impact of aviation and the capacity of the air traffic management system.

This thesis addresses the formation mission design problem for commercial aircraft in the presence of uncertainties. Specifically, it considers uncertainties in the departure times of the aircraft and in the fuel burn savings for the trailing aircraft. Given several commercial flights, the problem consists in arranging them in formation or solo flights and finding the trajectories that minimize the expected value of the direct operating cost of the flights. Since each aircraft can fly solo or in different positions inside a formation, the mission is modeled as a stochastic switched dynamical system, in which flight modes of the aircraft are described by sets of stochastic ordinary differential equations, the discrete states of the system describe the combination of flight modes of the individual aircraft, and the switching logic among the discrete states is defined by logical constraints.

The formation mission design problem is formulated as an optimal control problem of a stochastic switched dynamical system and solved using nonintrusive generalized polynomial chaos based stochastic collocation. The stochastic collocation method converts the stochastic switched optimal control problem into an augmented deterministic switched optimal control problem. With this approach, a small number of sample points of the random parameters are used to jointly solve particular instances of the switched optimal control problem. The obtained solutions are then expressed as orthogonal polynomial expansions in terms of the random parameters using these sample points. Depending on the distributions of the random parameters, different types of orthogonal polynomials can be chosen to achieve better precision. This technique allows statistical and global sensitivity analysis of the stochastic solutions to be conducted at a low computational cost. The augmented deterministic switched optimal control problem has been then solved using an embedding approach, which allows switching decision among discrete states to be modeled without relying on binary variables. The resulting problem is a classical optimal control problem which has been solved using a knotting pseudospectral method.

The aim of this study is to establish if, in the presence of uncertainties, a formation mission is beneficial with respect to solo flight in terms of the expected value of the direct operating costs. Several numerical experiments have been conducted in which uncertainties regarding the departure times and on the fuel saving during formation flight have been considered. The obtained results demonstrate that benefits can be achieved even in the presence of these uncertainties and that formation flight has great potential to reduce fuel consumption and emissions in commercial aviation.

Resumen extendido

Antecedentes

Conseguir un futuro sostenible del tráfico aéreo mundial es uno de los principales retos de la aviación internacional. De hecho, el sector de la aviación es uno de los principales responsables de las emisiones de gases de efecto invernadero y del calentamiento global. Antes de la pandemia ocasionada por la COVID-19, la Asociación Internacional de Transporte Aéreo (IATA) estimaba que el número de pasajeros se duplicaría en las próximas dos décadas, agravando la problemática actual. A pesar de que las estimaciones previstas se han visto severamente afectadas por la pandemia, se espera una vuelta a la normalidad en los próximos años y una tasa de crecimiento del tráfico aéreo mundial similar a valores previos a la crisis. Este incremento esperado del tráfico aéreo, hace aún más difícil asegurar un futuro sostenible del sector. Por todo ello, el sector de la aviación es clave en el compromiso hacia un futuro más sostenible, exigiendo la búsqueda de nuevas soluciones que mitiguen su impacto negativo en el planeta por parte de todos los actores implicados. En este sentido, el vuelo en formación tiene un gran potencial para contribuir significativamente, no solo a la mitigación del impacto medio ambiental de la aviación, sino también al aumento de la capacidad del sistema de gestión del tráfico aéreo (ATM).

En el vuelo en formación, dos o más aeronaves vuelan a distancias cortas entre ellas. Este concepto surgió de la observación del vuelo en formación de diferentes especies de aves durante sus migraciones. Posteriormente, se demostró que el vuelo en formación mejora no solo la eficiencia de vuelo para las aves, sino que también ofrece un beneficio aerodinámico significativo para las aeronaves, ofreciendo una reducción en el consumo de combustible y en la emisión de gases contaminantes. Los beneficios conseguidos debidos al vuelo en formación dependen de varios factores, siendo la separación longitudinal entre las aeronaves uno de los principales. Las formaciones en las que las aeronaves vuelan a distancias longitudinales entre 10 y 40 envergaduras son denominadas formaciones extendidas. Este tipo de formaciones representan una solución de compromiso entre seguridad operacional y eficiencia.

En esta tesis se aborda el estudio de formaciones extendidas en la aviación comercial. En particular, se estudia el diseño de misiones de vuelo en formación rentables desde un punto de vista económico y medio ambiental, en presencia de diferentes fuentes de incertidumbre, en concreto, los tiempos de salida de las aeronaves y el ahorro de combustible obtenido debido al vuelo en formación.

Objetivos

El principal objetivo de esta tesis es resolver el problema de diseño de misiones de vuelo en formación para aeronaves comerciales en presencia de incertidumbres. El planificador de

misiones estocásticas de vuelo en formación propuesto debe incluir modelos dinámicos precisos del vuelo en formación de la aeronave, información sobre los vuelos como, por ejemplo, el lugar y las horas de salida y llegada, la predicción meteorológica, el modelo de los efectos de la formación sobre el consumo de combustible para la aeronave seguidora, las funciones de densidad de probabilidad que caracterizan los parámetros del problema y el funcional objetivo que refleje los costes directos operativos de la misión.

El planificador estocástico de misiones de vuelo en formación presentado en esta tesis, debe encontrar la solución óptima del problema, para un máximo de tres aeronaves candidatas al vuelo en formación, estableciendo si el vuelo en formación es óptimo o no, y determinando las trayectorias estocásticas óptimas de cada aeronave. La solución debe incluir los valores esperados y las desviaciones típicas de las coordenadas geográficas y de la temporización de los puntos de encuentro y de separación entre las aeronaves, así como los valores esperados y las desviaciones típicas de los tiempos de llegada de las aeronaves.

Metodología

En primer lugar, se ha resuelto el problema determinista de diseño de misiones de vuelo en formación. Este ha sido formulado como un problema de control óptimo para un sistema dinámico de tipo *switched* con restricciones lógicas en forma disyuntiva. Gracias al uso de técnicas de control óptimo, en la formulación del problema se pueden incluir modelos dinámicos precisos de las aeronaves y predicciones meteorológicas, para así mejorar la predictibilidad de las trayectorias y las estimaciones del ahorro de combustible. Para la resolución de este problema de control óptimo se ha utilizado la técnica denominada *embedding*. El uso de esta técnica permite tratar la dinámica conmutada del sistema y las restricciones lógicas disyuntivas de forma eficiente. Además, la lógica de conmutación entre estados discretos puede ser modelada sin usar variables binarias, el número de conmutaciones no debe ser establecido por adelantado y el valor óptimo de los tiempos de conmutación entre los diferentes estados discretos es obtenido sin la necesidad de introducir dichos tiempos como incógnitas del problema de control óptimo. Por tanto, el problema resultante es un problema de control óptimo clásico, el cual puede ser resuelto usando técnicas numéricas de control óptimo tradicionales. En concreto, en esta tesis, se han utilizado las técnicas numéricas llamadas *pseudospectral knotting methods*.

En segundo lugar, se ha resuelto el problema de diseño de misiones de vuelo en formación bajo incertidumbre, el cual ha sido formulado como un problema de control óptimo de un sistema estocástico de tipo *switched*. Este problema se ha resuelto usando métodos no intrusivos de colocación estocástica, en particular se ha utilizado el método denominado *generalized polynomial chaos*. Gracias a esta metodología, el problema mencionado es transformado en un problema de control óptimo determinista de tipo *switched* aumentado en un espacio de estados de mayor dimensión. Este problema puede ser resuelto utilizando la metodología descrita anteriormente para el problema determinista.

Por último, se ha realizado un análisis estadístico y de sensibilidad global de la solución estocástica obtenida. Gracias a la metodología usada para resolver el problema de diseño de misiones de vuelo en formación en presencia de incertidumbres, dicho análisis se puede realizar con un bajo coste computacional.

Resultados

Los resultados obtenidos demuestran que el vuelo en formación es económica y medio ambientalmente rentable para aeronaves comerciales, no solo bajo un marco determinista sino también en presencia de incertidumbres. En particular, se han llevado a cabo varios experimentos numéricos teniendo en cuenta incertidumbre en los tiempo de salida de las aeronaves y en el ahorro de combustible obtenido gracias al vuelo en formación.

Los resultados obtenidos demuestran que la metodología propuesta es idónea para ser incorporada en los sistemas terrestres usados por los despachadores de vuelo, como sistema de apoyo para el diseño de misiones de vuelo en formación para aerolíneas o alianzas entre aerolíneas. Gracias a la metodología empleada, los tiempos de computación se reducen significativamente con respecto a enfoques previos al problema de diseño de misiones estocásticas de vuelo en formación, haciendo que el algoritmo propuesto en esta tesis sea adecuado para cualquier fase de planificación del vuelo,es decir, para las fases estratégicas y tácticas de planificación, y también la fase operacional del vuelo.

Conclusiones

La metodología propuesta para el diseño de misiones de vuelo en formación en presencia de incertidumbre ha sido probada en diferentes escenarios basados en modelos de aeronaves y predicción meteorológica realistas, demostrando la efectividad de la metodología propuesta en esta tesis.

En primer lugar, gracias a la formulación del problema como un problema de control óptimo de un sistema de tipo *switched* estocástico, se pueden incluir modelos dinámicos precisos de las aeronaves y del vuelo en formación, así como predicciones meteorológicas, lo cual mejora la predictibilidad de las trayectorias y la estimación de los beneficios en términos de ahorro de combustible obtenidos gracias al vuelo en formación.

Además, la metodología utilizada para el tratamiento de la dinámica de conmutación del problema así como de las restricciones lógicas disyuntivas del mismo, la técnica *embedding*, permite una disminución significativa del tiempo de computación necesario para la obtención de la solución. Asimismo, es fácilmente escalable para problemas de diseño de misiones de vuelo en formación en las que se consideren un mayor número de aeronaves involucradas.

Por último, el problema de diseño de misiones de vuelo en formación en presencia de incertidumbre ha sido resuelto por métodos no intrusivos de colocación estocástica, los cuales son adecuados no sólo para la resolución del problema, sino también para poder llevar a cabo un análisis estadístico y de sensibilidad global de la solución estocástica obtenida.

"*You tell me when you want it and where you want it to land, and I'll do it backwards and tell you when to take off*"

Katherine Johnson

Contents

List of Figures

List of Tables

List of Acronyms

ATM	Air traffic management
BADA	Base of aircraft data
CAGR	Compound annual growth rate
CI	Cost index
CNF	Conjunctive normal form
CORSIA	Carbon offsetting and reduction scheme for international aviation
DAE	Differential algebraic equations
DGAC	Direction générale de l'aviation civile
DOC	Direct operating costs
DoF	Degrees of freedom
DSNA	Direction des services de la navigation aérienne
EASA	European aviation safety agency
ECEF	Earth-centered, Earth-fixed
ECMWF	European centre for medium-range weather forecasts
EOCP	Embedded optimal control problem
f-LGR	Flipped Legendre-Gauss-Radau
FAA	Federal aviation administration
FF	Formation flight
FMS	Flight management system
GHG	Greenhouse gases
gPC	Generalized polynomial chaos
IAA	Irish aviation authority
IATA	International air transport association
ICAO	International civil aviation organization
IPCC	Intergovernmental panel on climate change
IPOPT	Interior point optimizer
LiDAR	Light detection and ranging

LG	Legendre-Gauss
LGL	Legendre-Gauss-Lobatto
LGR	Legendre-Gauss-Radau
MSL	Mean sea level
NATS	National air traffic services
NLP	Nonlinear programming
OCP	Optimal control problem
ODE	Ordinary differential equations
PCE	Polynomial chaos expansion
PDF	Probability density function
PMP	Pontryagin's minimum principle
PSM	PSeudospectral methods
RBF	Radial basis functions
RV	Rendezvous
SAS	Scandinavian airlines system
SEOCP	Stochastic embedded optimal control problem
SF	Solo flight
SOCP	Switched optimal control problem
SP	Splitting
SSOCP	Stochastic switched optimal control problem

List of Symbols

F_{LH}	Local horizon reference frame
F_{ECEF}	Earth-centered, Earth-fixed reference frame
F_{WF}	Wind-fixed reference frame
χ	Heading angle
γ	Flight path angle
μ	Bank angle
λ	Longitude
ϕ	Latitude
h	Altitude
V	True airspeed
m	Mass
t	Time
T	Thrust force
L	Lift force
D	Drag force
W	Weight of the aircraft
D_i	Induced drag force
C_L	Lift coefficient
C_D	Drag coefficient
C_{D0}	Parasitic drag coefficient
C_{Di}	Induced drag coefficient
K	Lift-induced drag coefficient
ϵ	Rate of induced drag reduction
w_i	Induced velocity
u_l	Local velocity
α	Angle of attack
α_e	Apparent angle of attack
α_i	Induced angle of attack
u_∞	Free flowing fluid velocity

q	Dynamic pressure
ρ	Air density
p	Air pressure
S	Reference wing surface area
g	Acceleration due to gravity
κ	Adiabatic index of air
M	Mach number
V_{CAS}	Calibrated airspeed
V_{TAS}	True airspeed
V_{MO}	Maximum operating calibrated speeds
M_{MO}	Maximum operating Mach number
V_s	Stall speed
AR	Aspect ratio
b	Wingspan
e	Efficiency factor
V_{W_E}	Eastward component of the wind velocity
V_{W_N}	Northward component of the wind velocity
η	Thrust specific fuel consumption
C_{f_1}	First empirical thrust specific fuel consumption coefficient
C_{f_2}	Second empirical thrust specific fuel consumption coefficient
$C_{T_{C,1}}$	First empirical thrust coefficient
$C_{T_{C,2}}$	Second empirical thrust coefficient
$C_{T_{C,3}}$	Third empirical thrust coefficient
$C_{T_{cr}}$	Maximum cruise thrust coefficient
$\mathcal{D}$	Great-circle distance
R_E	Earth radius
H_p	Geopotential pressure altitude
x	State variables vector
u	Control variables vector
J	Bolza cost functional
$\mathcal{M}$	Mayer cost functional
$\mathcal{L}$	Lagrange cost functional
θ	Vector of random variables
E	Expected value operator
VAR	Variance operator

Subscripts

S	Switched
SS	Stochastic switched
E	Embedded
I	Initial
F	Final
p	Aircraft p

To Lucas & Adriana.

Chapter 1

Introduction

1.1 Motivation

The aviation sector represents a major challenge to the environment, being one of the top ten emitters of greenhouse gases (GHG) in the world, and accounting for approximately 4% of human contribution to the global warming [Klöwer et al., 2021, Lee et al., 2009]. According to a recent report by the intergovernmental panel on climate change (IPCC) [IPCC, 2018], a leading climate science body, aviation is a crucial sector to the threat of climate change and global warming. Indeed, although air transport is only responsible for 14% of the transport sector's carbon dioxide emissions, far less than other modes of transport like light-duty vehicles (30%) and heavy-duty vehicles (36%), it seems to be harder to decarbonize. The reason for this lies in the predicted growth rate for air traffic, which is projected to be greater than for other modes of transport.

The predicted growth rate for air traffic is another concerning aspect. Before the COVID-19 crisis, the compound annual growth rate (CAGR) forecast over the next two decades, assessed by the international air transport association (IATA), estimated that the number of flights was expected to continue increasing by 3.5% annually, which translates to twice the current number of passengers by 2040 [IATA, 2016]. It is well known that the COVID-19 pandemic has severely affected the whole aviation sector, international commercial flights in particular, and, consequently, air traffic has plummeted by more than two thirds compared with previous levels.[1] At present, vaccination rates, travel restrictions, and quarantine procedures are rendering it unclear how quickly the aviation sector will return to normal values. However, air traffic growth is expected to recover to pre-crisis levels within the next few years, while continuing to increase annually [Lai et al., 2022]. This continuous growth in air traffic demand imposes the search for new solutions to mitigate its potential negative effects on our planet.

[1] https://www.eurocontrol.int/covid19

Unfortunately, the measures taken by the aviation sector until recently are considered to be insufficient to mitigate its impact on climate change. Current policies should be strengthened and a firm commitment from all the stakeholders is essential to success. For instance, the IATA is looking for improvements in different areas in order to achieve a reduction in net aviation CO_2 emissions of 50% by 2050, relative to 2005 levels [IATA, 2013]. The different measures considered can be classified into technical improvements, including more efficient aircraft and engines, operational measures, including more efficient flight procedures and airport operations, and the search of alternative, more sustainable fuels [Abrantes et al., 2021]. Fig. 1.1 gives a schematic overview of the potential contribution of the mentioned measures to the reduction of the net CO_2 emissions of international aviation.

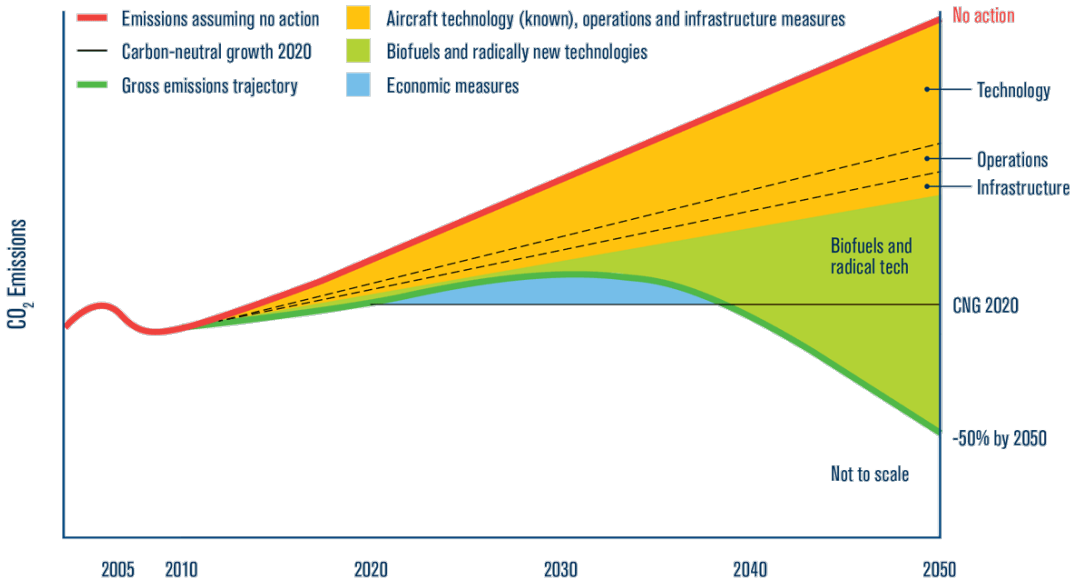

Fig. 1.1: Potential contribution of different measures to the reduction of the net CO_2 emissions of international aviation. Source: IATA [IATA, 2013].

As such, the predicted effects of the aviation sector on climate change are greater than desired [IPCC, 2018, ICAO, 2016], and a great effort is required to mitigate them. In this regard, formation flight has the potential to make a significant contribution. Furthermore, formation flight offers great promise not only with regard to mitigating the environmental impact of aviation but also in terms of increasing air traffic management (ATM) capacity and reducing air traffic control workload, which represents another major challenge of the sector.

1.2 Formation flight

Formation flight is where two or more aircraft fly at a short distance from each other. The notion of formation flight arose from the observation of nature, in particular from the different species of bird that fly in formation during their migrations

[Lissaman and Shollenberger, 1970]. Aircraft formation flight was first introduced in military aviation for mutual defense during missions, concentrating the fire power during attacks, and, consequently, improving combat efficiency. Later, it was demonstrated that formation flight led to notable efficiency improvements for the birds and that substantial fuel savings were also possible for aircraft flying in formation. The reduction achieved strongly depends on the longitudinal distance between aircraft, this being negligible over approximately 40 wingspans. Formations in which aircraft fly at a longitudinal distance between 10 and 40 wingspans are called extended formations [Durango et al., 2016]. They represent a trade-off between safety and efficiency. This thesis will investigate the possibility of implementing extended formations in commercial aviation. In particular, the focus is on the possibility of implementing economically and environmentally beneficial formation flights in the presence of different sources of uncertainty, namely the departure times of the flights and the fuel savings during formation flight.

Fig. 1.2: Two civil aircraft in formation flight. Source: Airbus[2]

The key enabling factors for this concept of operation consist of a formation control system to keep the aircraft flying in formation at the optimal relative position to optimize the fuel burn savings for the trailing aircraft and an ATM system capable of synchronizing flights departing from different airports to ensure that the formation mission occurs as planned. Within a formation flight, instabilities such as meandering and external factors may affect the motion of the vortices. It is therefore important to maintain the relative position between the follower aircraft and the leader's wake vortices precisely, as the fuel burn savings are very sensitive to that relative positioning. This can be done using a formation control system capable of continuously locating the wake vortices, maintaining the aircraft in the optimal

[2] https://www.airbus.com/en/innovation/disruptive-concepts/biomimicry/fellofly

relative position, and, in this way, optimizing the fuel savings during the formation flight [Caprace et al., 2019]. While technical issues related to maintaining an efficient and safe formation flight have been solved in recent years, some concerns have yet to be addressed. In particular, a major change in airworthiness standards, policies, and procedures is required. At the 40^{th} international civil aviation organization (ICAO) Assembly, formation flight was proposed as a strategic objective, and the necessity of developing a new operational concept including reduced separations between aircraft to allow formation flights was established [Abeyratne, 2020].

Due to its potential for reducing fuel consumption and GHG emissions, formation flight has recently attracted increasing interest, and the studies on the aerodynamics of formation flight have given way to studies on formation flight planning. The majority of the commercial formation flight planning studies are based on geometric models which do not allow use of either accurate dynamic models or meteorological forecasts. The past few years have brought with them some research studies [Hartjes et al., 2018, Hartjes et al., 2019] in which the mission design problem has been studied for two- and three-aircraft formations using a multiphase optimal control approach. This methodology has clear advantages compared to previous ones since the optimal control approach allows the use of accurate models, improving the predictability of the trajectories. However, using the multiphase approach implies having a fixed switching structure in advance, that is to say, knowing the transition among phases established in advance. Since the switching structure of the optimal solution is unknown for the formation mission design problem, any combination should be addressed and, then, the obtained solutions must be compared to establish which one corresponds to the minimum operation-related aircraft costs, also known as direct operating costs (DOC) [Camilleri, 2018]. Thus, this approach is feasible if the number of flights considered is low and both the type of formation and the relative position of each aircraft in the formation are fixed. Otherwise, the number of combinations quickly increases with the number of flights, making the previous approach hardly scalable.

A more general framework is therefore needed, which is able to design formation missions solving a single optimal control problem (OCP) in which neither the number of phases nor the switching structure is known in advance. Moreover, this approach should be easily scalable to design, for instance, formation missions involving more than three flights. For this purpose, the formation mission design problem can be formulated as an OCP of a switched dynamical system. These systems are described by both continuous and discrete dynamics in which the transitions among discrete states are not established in advance. In particular, each aircraft has different flight modes, namely solo flight and flight in different positions within a formation, and their combination is represented by the discrete state of the switched dynamical system, which models their joint dynamic behavior. Each flight mode will be represented by different dynamical equations, which may or may not include formation flight benefits in terms of fuel savings. Additionally, logical constraints in disjunctive form, based on the streamwise distance

between aircraft, model the switching logic among the discrete states of the system. To solve the proposed problem, the embedding technique [Bengea et al., 2011] has been employed to obtain a new smooth formulation of the problem in which the switching dynamics are defined without binary variables together with equality and inequality constraints. The obtained problem can be solved using classical optimal control techniques.

In addition to using accurate models, the operational concept of the formation flight entails a deeper understanding of how uncertainties affect the trajectories of each aircraft involved in the formation. In particular, addressing the uncertainty quantification in formation flight design problems is essential to improving the predictability of the trajectories and achieving more realistic solutions and estimations of the costs and the formation benefits. There are different sources of uncertainties which can affect the whole ATM system. One of the main ones is uncertainty in flight departure times, which causes trajectory uncertainty and ATM-context inefficiencies [Rivas and Vazquez, 2016]. Timing is also a crucial factor in formation missions. Effectively, considering the usual cruise speed of most long-haul commercial aircraft, missing the rendezvous location by, for instance, ten minutes means spatially missing the partner aircraft by 150 km. Such cases require catch-up maneuvers, which result in a loss of performance compared to the planned formation mission. As such, uncertainties in departure times have been considered in the formation mission design problem, along with uncertainties in the fuel savings during formation flight. These uncertain parameters have been modeled as random variables described by probability density functions.

1.3 Description of the problem

The stochastic formation flight mission design problem can be formulated as follows. Given several commercial flights together with the relevant weather forecast, the problem consists in establishing how to organize them in formation, of two- or three-aircraft, or solo flights and in finding the trajectories that minimize the expected DOC value of the formation mission. To solve it, the formation mission design problem is formulated as an OCP of a stochastic switched dynamical system and solved using nonintrusive generalized polynomial chaos (gPC) based stochastic collocation [Matsuno et al., 2015, Li et al., 2014]. The gPC method converts the stochastic switched OCP into an augmented deterministic switched OCP, which can be solved using the embedding approach together with classical numerical optimal control techniques. This technique allows statistical and global sensitivity analysis of the stochastic solutions to be conducted at a low computational cost.

The solution of the formation mission design problem in the presence of uncertainties is stochastic, i.e, its components are random processes, which can be characterized by their mean and standard deviation functions. The expected values and the standard deviations of the latitude and longitude of the optimal trajectories with respect to the expected value of the timing and the expected values and standard deviations of the timing of the trajectory as

functions of the expected value of the distance are useful for ATM purposes such as conflict detection and traffic synchronization. The expected values and standard deviations of the fuel consumption and final time of each flight of the formation mission permit the DOC to be estimated in such a way that airlines can establish to what extent a formation mission is economically beneficial.

The relative contributions of each random variable to the variability of the latitude and longitude of the optimal trajectories of each aircraft as functions of the expected value of timing and the variability of the timing of the trajectories of each aircraft as functions of the expected value of the distance allow both the ATM staff to establish which sources of uncertainty must be reduced to increase the predictability of the trajectories and airlines to determine what sources of uncertainty must be reduced to decrease the DOC.

It is well known that uncertainty regarding the weather forecast, in particular the wind field, is of particular interest in the context of optimization trajectories. However, the stochastic impact of the wind field in the formation mission design problem has not been considered. Being a random function of space and time, a wind field should be modeled as a stochastic process. Although generalized polynomial chaos can be employed to represent stochastic processes, specific techniques are needed for their representation, such as the Karhunen–Loève expansion. As a consequence, the dimensionality of the problem increases, as does the complexity of dealing with it. Therefore, it is assumed that the aircraft model is accurately known, as is the corresponding weather forecast. Neither storms nor operational uncertainties have been considered. The study of the formation mission design problem in the presence of stochastic processes such as uncertain wind field, is left for future research. In this thesis, only random variables have been considered.

Recently, the aviation industry has shown renewed interest in achieving the real implementation of commercial formation flight. Indeed, during the completion of this thesis, the Airbus Fello'fly project [Airbus, b] has been carried out, in which Airbus collaborated with airlines, air navigation service providers, and civil aviation authorities to tackle the challenges of formation flight and demonstrate its operational feasibility. The first flight test in the field of transoceanic flights was conducted in November 2021.[3] This test, in which a system for formation flight control proved itself in an operational environment, shows that this technology has reached the highest readiness level, according to the European Union's scale [Héder, 2017].

1.4 Objectives of the thesis

The general objective of this thesis is to solve the formation mission design problem for commercial aircraft in the presence of uncertainties.

The stochastic formation mission planner should include accurate dynamic models of the aircraft involved in the formation mission, the relevant flight data such as departure and

[3] https://simpleflying.com/airbus-a350s-bird-like-flight/

arrival times and locations, wind forecast, a model of the effects of flying in formation on the fuel consumption of the trailing aircraft, the probability density functions that characterize the uncertain parameters of the problem, and an objective functional reflecting the DOC of the formation mission.

The stochastic formation mission planner presented in this thesis, which is based on stochastic optimal control, finds the optimal solution for up to three aircraft candidates to fly in formation, establishing how to arrange them in formation or solo and determining the stochastic optimal trajectories. The stochastic solution of the formation mission planning problem includes the expected values and standard deviations of the latitude, longitude, and timing of the optimal trajectories. The solution also includes the expected values and standard deviations of the latitude, longitude, and timing of the rendezvous and splitting points as well as the expected values and standard deviations of the arrival times of the flights. Finally, by performing the sensitivity analysis of the solutions, the relative influence of the uncertain parameters of the problem on the variability of the stochastic solution components can be estimated. The schematic representation of the elements of the formation mission planner is given in Fig. 1.3.

The general objective of this thesis has been divided into several specific objectives:

- Reviewing existing literature on formation mission planning.
- Developing accurate dynamic models of commercial aircraft.
- Devising a method for incorporating the wind forecast into an optimal control problem.
- Formulating the deterministic formation mission design problem as an OCP of a switched dynamical system.
- Developing appropriate optimal control techniques to solve the deterministic formation mission design problem.
- Formulating the stochastic formation mission design problem as a stochastic OCP of a switched dynamical system.
- Developing the appropriate optimal control techniques to solve the stochastic formation mission design problem.
- Numerically solving several instances of the stochastic formation mission design problem in the presence of uncertainties regarding aircraft departure times and the fuel savings during formation flight to demonstrate the effectiveness of the method.
- Performing sensitivity analyses of the stochastic solution to estimate the relative influence of the uncertain parameters of the problem on the variability of the solution components.

The solutions obtained demonstrate that formation flight is environmentally and economically beneficial in the presence of uncertainties regarding the departure times of the aircraft currently observed at major international airports and the fuel savings achieved during formation flight.

The formation mission planner presented in this thesis is intended to be incorporated into a ground-based system which could be used by flight dispatchers as a support system to design formation missions for airlines or airline alliances. Flight dispatchers are employed by airlines who are responsible for compiling and modifying the flight plan. They also monitor the aircraft during flight. The computational time of the proposed algorithm makes it suitable for the strategic and tactical planning phases of the flight, as well as for the operational phase, in other words, during flight.

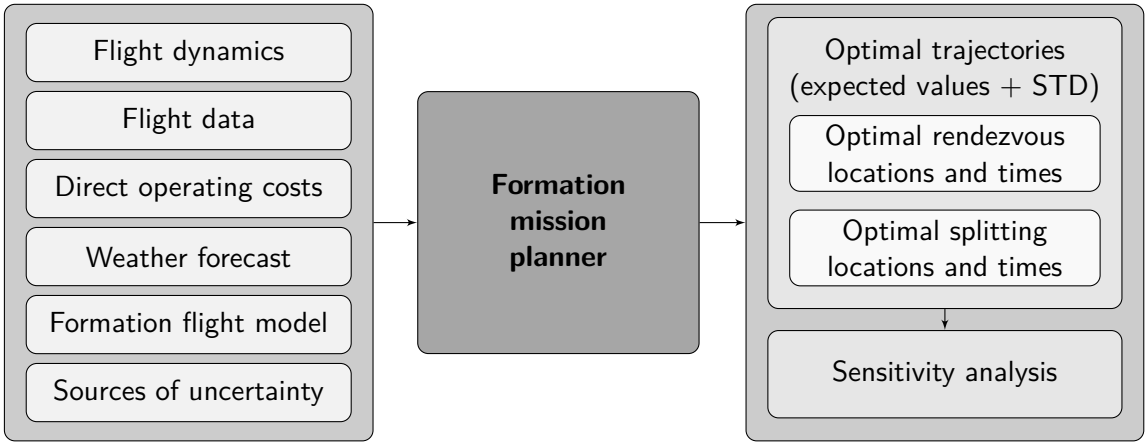

Fig. 1.3: Schematic representation of the elements of the stochastic formation mission planner presented in this thesis.

1.5 Contributions of the thesis

The contributions of this thesis to the state of the art in formation mission planning can be summarized as follows:

Contribution A: First, an innovative approach to the deterministic formation mission design problem is proposed which is formulated as an optimal problem of a switched dynamical system with logical constraints in disjunctive form and solved using an embedding approach. The optimal control formulation of the problem allows accurate dynamic models of aircraft and meteorological forecasts to be included in the problem formulation in order to improve the predictability of the trajectories and the estimation of the fuel savings. Modeling the formation mission as a switched dynamical system allows previous approaches such as the multiphase approach, to be avoided. The embedding method employed to solve the resulting OCP of a switched dynamical system is able

to deal with both the switching dynamics of the system and the logical constraints in disjunctive form in an efficient way. Additionally, the switching logic among discrete states can be modeled without using binary variables, the number of switches does not have to be established in advance, and the optimal values of the switching times between discrete states are obtained without introducing them as unknowns of the OCP. Therefore, the resulting problem is a classical OCP, which has been solved using a pseudospectral knotting method leading to significant reductions in the computational time with respect to previous approaches.

Contribution B: Then, considering the presence of uncertainties in the problem, the methodology for the solution of the stochastic formation mission design problem has been introduced, which is formulated as an OCP of a stochastic switched system. The uncertainties are represented by random variables characterized by probability density functions. This problem is solved using an approach based on gPC, in which the stochastic switched OCP is transformed into an augmented deterministic switched OCP in a higher dimensional state space. This problem is thus solved using the same methodology described in Contribution A. Several numerical experiments have been conducted in which uncertainties regarding the departure times and the fuel saving during formation flight have been considered, demonstrating its effectiveness.

Contribution C: Finally, the methodology used to solve the formation mission design problem in the presence of uncertainties makes it possible to conduct statistical and global sensitivity analysis of the stochastic solution at a low computational cost. The statistic analysis consists in the computation of the expected values and standard deviations of the geographical coordinates and timing of the aircraft trajectories obtained in the stochastic solution. The purpose of the sensitivity analysis is to estimate the relative contribution of the random parameters to the variability of the components of the stochastic solution with the aim of reducing its variability acting on the source of uncertainty.

1.6 Outline of the thesis

The rest of the document is organized as follows. In Chapter 2, an overview of formation flight is given. In Chapter 3, the model of the system that represents the formation flight is introduced. In Chapter 4, the optimal control method employed to solve the deterministic formation mission design problem is introduced. In Chapter 5, a general overview to numerical methods for optimal control is given. In Chapter 6, the stochastic optimal control method employed to solve the stochastic formation mission design problem is introduced. In Chapter 7, the methodology introduced in Chapter 4 is employed to solve three different formation mission design problems in the absence of uncertainties. In Chapter 8, the methodology

introduced in Chapter 6 is employed to solve two different formation mission design problems in the presence of uncertainties. Finally, the conclusions and a discussion of the future work are outlined in Chapter 9.

Chapter 2

Formation Flight

This chapter gives an overview of formation flight. First, the potential advantages and challenges of the introduction of formation flight in commercial aviation are discussed. Later, the most important studies on formation flight are surveyed. After that, the principles of formation flight are introduced. Finally, the main types of formation are described along with the influence of several parameters in fuel savings achieved in formation flight such as the longitudinal spacing between aircraft, the shape of the formation, the relative position of the heaviest aircraft, and the number of aircraft within a formation.

2.1 Introduction: Advantages and challenges of formation flight

As stated in Chapter 1, the current GHG emissions caused by civil aviation have become a priority at international level. Formation flight has the potential not only to mitigate the environmental impact of aviation but also to increase the capacity of the ATM. According to [ICAO, 1944], "*the formation operates as a single aircraft with regard to navigation and position reporting*," meaning that two or three aircraft flying in formation would be treated as a single aircraft for air traffic control purposes. This would help to reduce their workload. Furthermore, formation flight may even provide enhanced inter-aircraft communication, since the proximity between aircraft enables cost reductions and limits jamming sensitivity [Klavins, 2004].

Therefore, the question that naturally arises is what needs to be changed in the current paradigm to ensure effective implementation of formation flight in commercial aviation. Surprisingly, making today's aircraft appropriate to fly in formation does not require significant changes to the current aircraft appearance. However, the possibility of implementing formation flight in commercial aviation depends upon several factors, such as defining a new concept of operation for formation flight of commercial aircraft, changing the international airworthiness regulation, updating the ATM system in such a way that formation flights

and solo flights can share the same airspace, creating alliances among airlines for sharing the benefit derived from formation flight, and developing the avionics systems for formation control. These complex issues will be discussed in the following sections.

2.1.1 Operational concept and airworthiness regulation for formation flight

Safety is the greatest concern in commercial flights, and the short longitudinal distances between aircraft needed for formation flight are not currently allowed. However, both the european aviation safety agency (EASA) and the federal aviation Administration (FAA) have been considering formation flight for commercial aircraft in recent years [Durango et al., 2016]. In 2019, at the ICAO 40^{th} Assembly [Abeyratne, 2020] [Assembly 40th, 2019], formation flight was presented as a strategic objective and the following challenges for the upcoming triennium were established:

- A new operational concept should be established, including new separation schemes, specific procedures, and reduced separations to allow the formation.
- International standards and recommended practices should be developed by a multidisciplinary technical panel in which industry groups should be included.

2.1.2 Sharing benefits among airlines

As mentioned in Chapter 1, not all the aircraft flying in an extended formation benefit individually from formation flight since only the trailing aircraft save fuel. Additionally, flying in formation requires a spatial and temporal modification to the optimal individual trajectories, which could correspond to higher DOC for some of the flights. This means that formation flight offers a reduction in the total cost of the formation mission, i.e, considering all aircraft in the formation, not in the costs of the individual flights.

Furthermore, it is improbable that two or three flights that are good candidates for inclusion in a formation mission belong to the same airline. This means that the actual implementation of formation flight for commercial aircraft requires the creation of alliances among airlines to share the costs and benefits derived from formation flight. In the ICAO standards and recommendations mentioned above, a special mention to actions on airline alliances should be included [Xu et al., 2014].

2.1.3 Avionic systems for formation control

As outlined in Chapter 1, fuel savings in formation flight are generated for the trailing aircraft flying in the upwash of the wake vortex generated by the leader aircraft. To optimize the fuel savings, the trailing aircraft has to be positioned with precision with respect to the wake vortex of the leader aircraft. Thus, achieving a better understanding of generation and evolution of the wake vortices is mandatory for the real implementation of formation flight,

together with the creation of reliable technology for detecting them and positioning aircraft with respect them.

As shown in [Hallock and Holzäpfel, 2018], a review of recent research on wake vortex research, characterizing them is highly complex, mostly because of the large number of parameters involved in the model. Some of them are related to the leader aircraft that generates the vortex, such as weight, wingspan, speed, high lift devices settings, and thrust. Other parameters are related to the trailing aircraft, such as the weight or the speed, which are also involved in the case of formation flight. Meteorological variables, such as wind field and turbulence, also come into play when modeling wake vortices. However, as pointed out in [Ning, 2011], considering typical atmospheric conditions, the wake vortex of the leader aircraft causes low turbulence disturbances for the trailing aircraft in those extended formations in which the streamwise distance between the leader and trailing aircraft is greater than 10 wingspans.

Several research studies have demonstrated the possibility of "visualizing" the wake vortices of the leader aircraft for accurate positioning of the trailing aircraft with respect to the leader's wake vortex [Caprace et al., 2019]. This positioning system is based on the light detection and ranging (LiDAR) onboard technology [Michel et al., 2020], which allows the wake vortex generated by the leader aircraft to be accurately tracked by the trailing aircraft. Experimental flight tests have been conducted with an onboard LiDAR in the trailing aircraft providing real-time measurements of velocities of the wake vortex generated by the leader. Dynamic flight simulations described in [Vechtel et al., 2018] demonstrate that it is possible to maintain the position of the trailing aircraft in the wake vortex generated by the leader accurately using a regular autopilot.

These results demonstrate that formation control systems have been improved in recent years, permitting the trailing aircraft to position itself with precision in the optimal location while surfing the vortex generated by the leader aircraft.

The main aircraft manufacturers have begun developing the technology to implement formation flight. Airbus, the major European aircraft manufacturer, is undertaking an ambitious project called Fello'fly [Airbus, a] which aims to demonstrate the technical, operational, and commercial viability of formation flight for long-haul commercial flights. In this project, Airbus is collaborating with two European airlines, Frenchbee and scandinavian airlines system (SAS), as well as air navigation service providers such as France's direction des services de la navigation aérienne (DSNA), the UK's national air traffic services (NATS) and EUROCONTROL, NAVCANADA, and the irish aviation authority (IAA) in order to tackle the challenges of formation flight. The project also benefits from the support of the Direction Gènèrale de l'Aviation Civile (DGAC), the French Civil Aviation Authority. The objective of this project is not only to demonstrate the operational feasibility of the project but also to identify safety procedures and standards for transatlantic operations, enabling a controlled entry into service by 2025.

On November 9, 2021, the first formation flight test was carried out in the field of transoceanic flights.[1] Two wide-body Airbus aircraft, A350-900 and A350-1000, performed the first transatlantic formation flight from Toulouse–Blagnac Airport to Montréal–Trudeau International Airport. In this formation flight test, the observed reduction in fuel consumption was over 5% and 6 tons of CO_2 were saved.

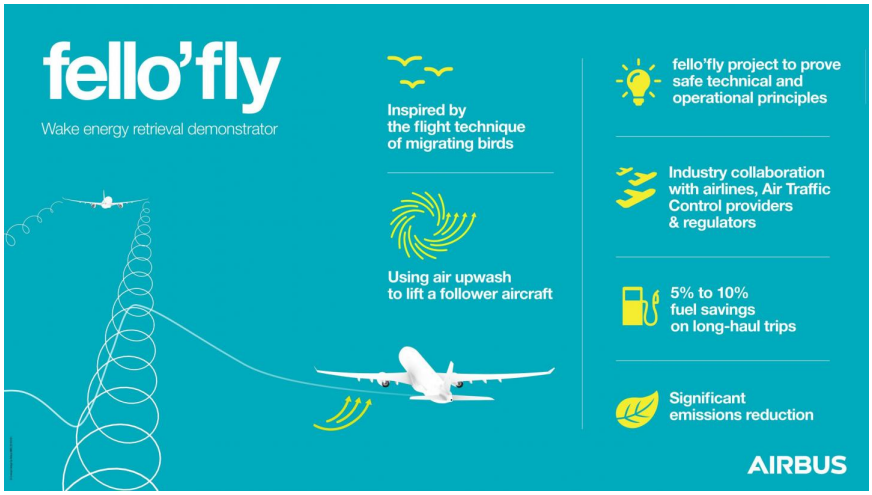

Fig. 2.1: Fello'fly Airbus project [Airbus, a].

Boeing has also conducted research activity on formation flight involving flight tests on Boeing's ecoDemonstrator platform [Flanzer et al., 2020].

2.2 Studies on formation flight

2.2.1 Studies on the aerodynamics of formation flight

Studying nature and trying to imitate it has often been a very effective way to find innovative solutions to human problems. Formation flight is undoubtedly a fine example of this. The concept of formation flight arose from the observation of nature, where many species of bird fly in formation during their migrations. In 1914, Wieselsberger established the aerodynamic aspects concerning the power savings which may give birds flying in formation an aerodynamic benefit [Wieselsberger, 1914]. Over the next half-century, this aerodynamic theory was developed including less simplified analysis. In [Lissaman and Shollenberger, 1970], the authors theoretically affirm that a flock of 25 birds flying in V-formation could achieve a range increase of over 70% with respect to solo flight. Additionally, the aerodynamic benefit achieved by birds in a formation can also be obtained by any body immersed in a fluid, including fishes, airplanes, and submarines.

At a later point in time, the efficiency obtained in flock formations was therefore extended to aircraft formations. These initial studies mainly focused on the aerodynamics

[1] https://simpleflying.com/airbus-a350s-bird-like-flight/

of formation flight to assess the potential benefits in terms of induced drag reductions and, consequently, potential fuel burn reductions [Ning et al., 2011, Kless et al., 2013, Slotnick, 2014]. Experimental studies on formation flight have also been carried out. One of the most exhaustive works was conducted within the Surfing Aircraft Vortices for Energy ($AVE) project [Bieniawski et al., 2014]. The results obtained using two C-17 aircraft, at longitudinal distances of between 18 and 70 wingspans, revealed fuel savings of up to 11% [Haalas et al., 2014, Flanzer et al., 2014] for the trailing aircraft. The results of another experimental study [Vachon et al., 2002], obtained using two F/A-18 flying closer, at a longitudinal distance of up to 6.6 wingspans, returned fuel savings of just over 18% for the trailing aircraft.

In addition to these studies on the aerodynamics of formation flight focused on estimating the potential induced drag and fuel burn reductions, other research activities have been conducted to study different practical aspects of formation flight, such as the formation control problem under actuator and sensor faults [Liu et al., 2019] and the collision avoidance in formation flight [Seo et al., 2017].

2.2.2 Studies on formation flight planning

Studies on the aerodynamics of formation flight have given way to studies on formation flight planning [Xu et al., 2014, Kent and Richards, 2015, Blake and Flanzer, 2016, Bower et al., 2009, Hartjes et al., 2018, Hartjes et al., 2019, Kent and Richards, 2021], most of which focus on extended formations. In these studies, the formation flight planning problem has been solved as a bilevel optimization problem, in which the higher level problem is the optimal partner allocation problem and the lower level problem is the mission design problem. A conceptual representation of these two problems is given in Fig. 2.2. Consider a set of transoceanic flights, represented in blue in Fig. 2.2(a). Solving the partner allocation problem for this set of flights consists in establishing how to group them into smaller subsets which contain potential partners of beneficial formation missions in terms of overall DOC. For instance, to solve the partner allocation problem for the eastbound set of flights, first the westbound flights are disregarded and then potential partners are selected based on the distance between the departure and arrival airports and the schedule of each flight. The subsets of flights with potential for profitable formations, $s_1, s_2, \ldots, s_s$, are shown in orange in Fig. 2.2(b), Fig. 2.2(c), and Fig. 2.2(d). Note that although these figures represent subsets of three flights, these sets can have cardinality two or three.

Once the subsets of flights that are potential candidates for profitable formation missions have been compiled, the formation mission design problem is solved for each subset of flights to determine the optimal trajectories of the aircraft. The optimal routes calculated solving the formation mission design problem for each group of flights are represented in green in Fig. 2.2(e), Fig. 2.2(f), and Fig. 2.2(g). They correspond to a three-aircraft formation mission,

a two-aircraft formation flight plus one solo flight, and a three-aircraft solo flight mission, respectively. As can be seen in the figures, the flights of subsets s_2 and s_s do not result in three-aircraft formation missions. Therefore, better partners for these flights should be sought.

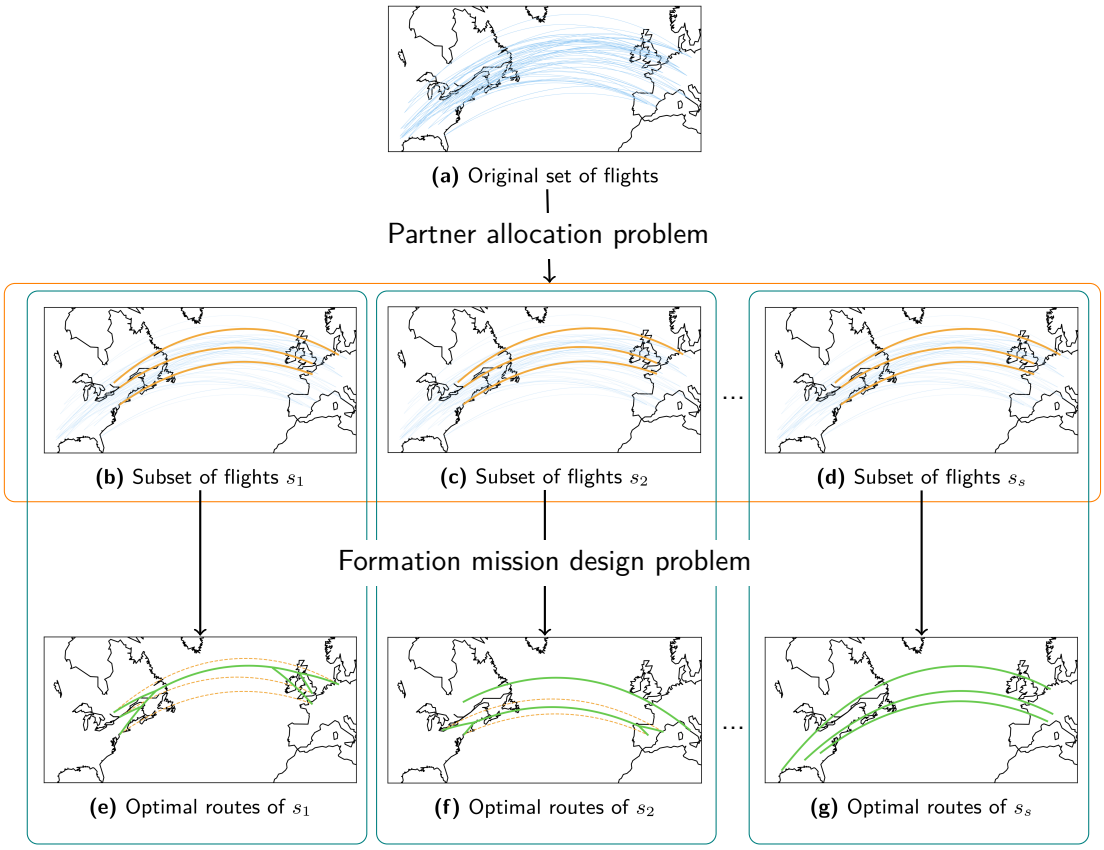

Fig. 2.2: Conceptual representation of the partner allocation and the formation mission design problems. (a) Original set of flights. (b), (c), and (d) groups of flights determined in the partner allocation problem. (e), (f), and (g) optimal routes obtained in the formation mission design problem.

Although the mission design and the partner allocation problems are intrinsically very different, the existing interconnection between them has resulted in their being addressed together in several studies such as [Xu et al., 2014] and [Kent and Richards, 2015], in which the Breguet range equation and the Fermat point extension problem were employed, respectively. [Kent and Richards, 2021] the most recent formation flight research at the time of writing this thesis, also investigated the potential for two commercial aircraft flying in formation for different cases using an analytical geometric method. Other examples are [Blake and Flanzer, 2016, Bower et al., 2009], in which geometric methods were also employed. In these approaches, the inherent combinatorial complexity of the partner allocation problem, which quickly grows with the number of flights, forced the introduction of simplifications such as using approximated dynamic models of the aircraft and neglecting

the meteorological forecast.

In [Hartjes et al., 2018], the mission design problem was studied for two-aircraft formations using a multiphase optimal control approach. In this case, the number of phases and the structure of the formation missions is unique and known in advance. There are five phases. The first two correspond to the flights from the departure locations to the rendezvous point, after which the formation flight, which corresponds to the third phase, starts. The other two flight phases correspond to the flights from the splitting point to the arrival locations. In this case, a solution is found using multiphase optimal control techniques and compared with the solution of a solo flight mission to establish which results in minimum DOC. The same framework used in [Hartjes et al., 2018] is extended in [Hartjes et al., 2019] to design three-aircraft formation missions. However, only in the latter was a wind field model, obtained from a weather database using a polynomial regression, taken into account. In contrast to two-aircraft formation missions, the structure of three-aircraft formation missions is not unique and, consequently, many different cases must be considered, including the case in which one or all the aircraft fly solo. The obtained solutions must be then compared to establish which corresponds to the minimum DOC. This drawback is due to the fact that the multiphase optimal control approach is only able to tackle optimal control problems with a fixed switching structure, in other words, with transitions among phases established in advance. This approach is feasible if the number of flights considered is low and the type of formation and the relative position of each aircraft in the formation are fixed. Otherwise, the number of combinations quickly increases with the number of flights, making the previous approach hardly scalable.

In this thesis, only the mission design problem has been addressed using optimal control techniques, including accurate dynamic models of the aircraft and the wind forecast. A new approach to this problem is proposed, which avoids the multiphase approach employed in [Hartjes et al., 2018, Hartjes et al., 2019].

2.3 Principles of formation flight

Formation flight is based on the fact that any aircraft moving through a fluid generates lift by imparting a swirling motion to the air. In particular, an aircraft flying in the cruise phase produces a vortex wake which mainly maintains its structure and intensity for several kilometers. This wake is characterized by a downwash region in the center of the wake and two similar upwash regions outside of the vortex core. A schematic representation of these upwash and downwash regions is given in Fig. 2.3. A second aircraft flying in either of these upwash regions, will increase its apparent angle of attack obtaining useful energy. The increment of the apparent angle of attack produces an effective forward rotation of the lift vector, $\vec{L}$, resulting in a lower lift-dependent component of drag, D_i. Thus, a significant decrease in induced drag is achieved [Ning et al., 2011]. For a better understanding, the apparent and

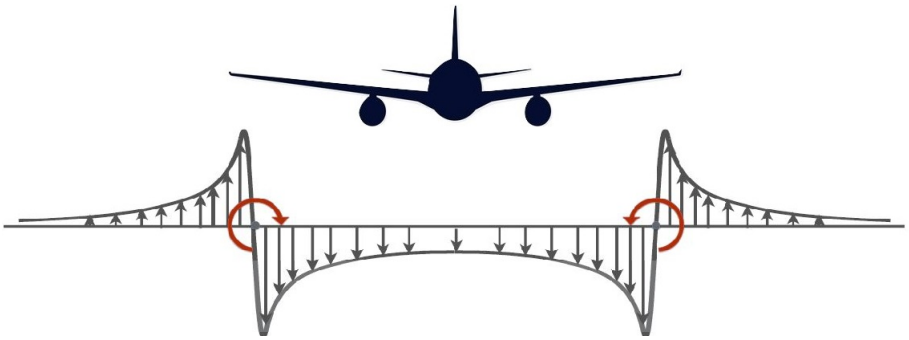

Fig. 2.3: Vertical component of the induced air velocity field (not to scale). Figure adapted from [Ning, 2011].

induced angle of attack, α_e and α_i respectively, the local and induced velocities, u_l and w_i respectively, and the lift and induced drag vector for both solo and formation flight are given in Fig. 2.4, where sub-index SF has been used to indicate "Solo Flight" and sub-index FF indicates "Formation Flight". Additionally, the components related to SF are represented in blue, whereas the components related to FF are represented in green. The total angle of attack, α, together with the free flowing fluid velocity, u_∞, have been represented in black. Notice that the total angle of attack is defined by the following sum of the apparent and the induced angle of attack,

$$\alpha = \alpha_{i,SF} + \alpha_{e,SF} = \alpha_{i,FF} + \alpha_{e,FF}. \tag{2.1}$$

From Eq. (2.1), it is easy to see that an increase of the apparent angle of attack is obtained due to the formation flight, which results in a decrease of the induced angle of attack. Consequently, both the induced velocity and the induced drag are reduced.

2.4 Types of formations

Formations can be classified based on the longitudinal distance between aircraft in close and extended formations or based on their relative positions in V, inverted-V, and echelon formations.

2.4.1 Close and extended formations

Regarding the optimal positioning, the lateral and the streamwise distance gain significance. In particular, the longitudinal spacing between aircraft, usually expressed in terms of wingspans, is used to classify formations. In the literature, the formations in which the longitudinal distance between the leader and trailing aircraft is less than 10 wingspans are called close formations, whereas those in which this distance is between 10 and 40 wingspans are called extended formations [Durango et al., 2016]. Close formations provide the greatest

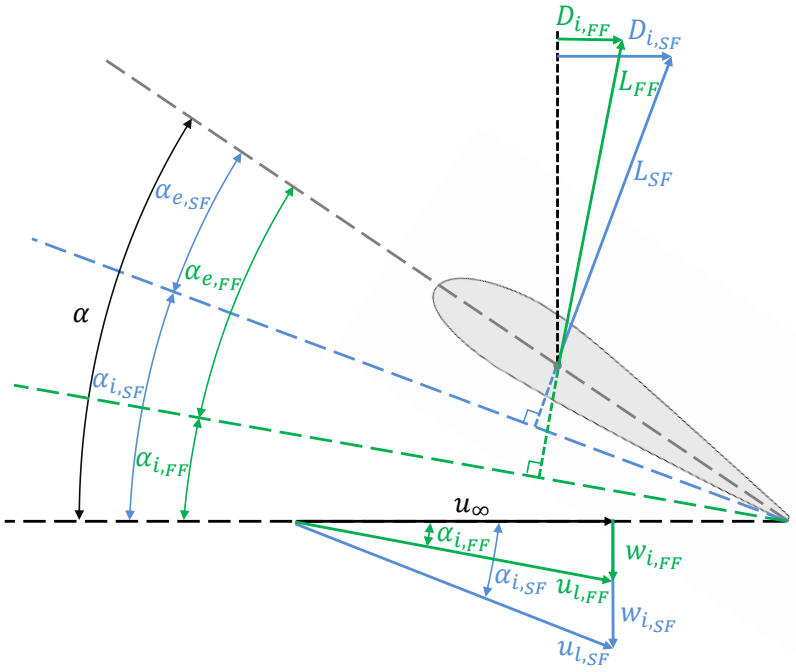

Fig. 2.4: Impact of the formation flight on the induced velocity, on the apparent angle of attack and on the induced drag.

benefits in terms of induced drag reduction while the potential induced drag reduction is lower in extended formations, especially in separations of more than 20 wingspans. However, extended formations are intrinsically safer than close formations - a crucial aspect in commercial flights. Therefore, in this thesis, only extended formations are permitted. In particular, a conservative approach in which the formation benefits are negligible for separations of more than 20 wingspans is considered, and longitudinal distances lower than 10 wingspans are prohibited.

2.4.2 V, inverted-V, and in-line formations

Furthermore, if three or more aircraft are involved in the formation, a second classification can be made according to the shape of the formation. In this case, three types of formations can be distinguished: the V formation, the inverted V formation and the in-line or echelon formation. These different types of formation are represented in Fig. 2.5.

The V formation is the most common in the nature, being that chosen by birds to fly in formation. Considering three-aircraft formation flights, in a V formation, one aircraft is the leader, and the two trailing aircraft fly in the upwash regions of the two wake vortices generated by the leader aircraft. In the inverted-V formation, as its name suggests, the configuration is the opposite: there are two leaders and one trailing aircraft, which, flying in the upwash regions of the wake vortices generated by the two leader aircraft, benefits twice

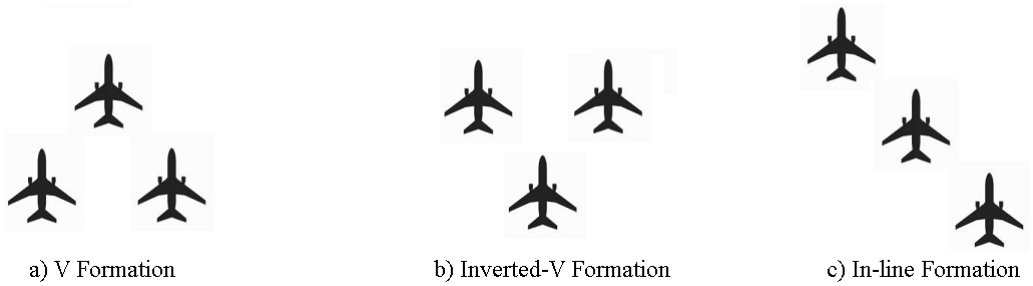

Fig. 2.5: three-aircraft formation configurations: V, inverted-V, and in-line formation (not to scale).

from formation flight. Finally, in the in-line formation, there is one leader aircraft followed by one first trailing aircraft, usually referred to as the intermediate aircraft, which is followed by another trailing aircraft.

In both the V formation and in-line formation, two aircraft benefit from the formation, while in the inverted-V formation, just one of them benefits. In the inverted-V formation, the trailing aircraft has a more symmetric load condition, which is clearly an advantage for the stability and control of the aircraft. However, in the inverted-V formation, finding the optimal position of the trailing aircraft is more challenging because it must be determined with respect to two aircraft at the same time, making this type of formation difficult to implement and the fuel savings more sensitive to position errors. As shown in [Ning et al., 2011], inverted-V formation offers lower benefits when compared to other types of formation.

In [Ning et al., 2011], other aerodynamic aspects of formation flight were studied, particularly for extended formations. The obtained results show that inverted-V formations would be less affected by viscous and compressibility effects due to a more symmetric loading compared with the others types of formation. Even though it is possible, choosing the type of formation and the relative position of each aircraft in the formation have not been included in the formulation of the formation mission design problem proposed in this thesis. Thus, in the numerical experiments conducted in this thesis, the in-line formation has been chosen and the relative position of each aircraft in the formation has been established in advance.

2.4.3 Choice of the leader aircraft of a formation

This section discusses the choice of the leader aircraft of a formation based on the relative weight of the aircraft.

By definition, the overall drag D can be expressed by the sum of two terms: the zero-lift drag, $D_0 = \frac{1}{2}\rho V^2 S C_{D0}$, and the induced drag, $D_i = \frac{1}{2}\rho V^2 S K {C_L}^2$, therefore

$$D = D_0 + D_i = \frac{1}{2}\rho V^2 S (C_{D0} + K {C_L}^2), \tag{2.2}$$

where ρ is the air density, S is the reference wing surface area, V is the aircraft airspeed, and W is the aircraft weight.

In straight and level flight, the induced drag can be expressed in terms of the weight of the aircraft as:

$$D_i = \frac{KW^2}{\frac{1}{2}\rho V^2 S}. \tag{2.3}$$

According to Eq. (2.3), placing the heavy aircraft as the trailing aircraft would lead to greater benefits. The heavier the trailing aircraft, the higher induced drag D_i will be and, consequently, higher benefits will be achieved from the formation flight for the same rate of induced drag reduction. Some studies on formation flight planning such as [Hartjes et al., 2018, Hartjes et al., 2019] are based on this statement.

However, the weight of the leader aircraft also has an impact on the wake intensity. The heavier the leader aircraft, the stronger the wake vortex intensity will be and therefore greater rates of induced drag reduction could be achieved [Marks and Gollnick, 2016]. This runs contrary to the above statement, leading to the conclusion that, depending on the particular conditions of the formation flight, the ideal relative position of the heaviest aircraft within a formation may change. [Voskuijl, 2017], addressed a comparison between different scenarios for two-aircraft formations, pre-establishing the heavy aircraft as both, the leader and the trailing aircraft, in each scenario. According to the results obtained, the authors conclude that, in the proposed scenarios, the total fuel burn reduction is higher when the heaviest aircraft is flying as the trailing one.

In this thesis, following [Voskuijl, 2017] and [Ning, 2011], it will be assumed that the leader vortex is not significantly influenced by the weight of the aircraft and, therefore, that the highest fuel savings are obtained by positioning the heaviest aircraft as the trailing one.

2.4.4 Influence of the number of aircraft on the fuel savings

In [Lissaman and Shollenberger, 1970], formations composed by different numbers of birds were analyzed, concluding that the more birds involved, the better drag savings were obtained, up to a theoretical limit. In this aspect, formation flight differs between birds and aircraft. Indeed, it has been proven in [Ning et al., 2011] that increasing the number of aircraft in the formation asymptotically reduces the benefits obtained from the formation flight. Additionally, the difficulty in synchronizing more than three flights makes formations of more than three aircraft operationally impractical [Durango et al., 2016, Ning et al., 2011]. For these reasons, only formations of up to three aircraft have been considered in this thesis.

2.5 Conclusions

Formation flight has great potential to contribute significantly to reducing fuel consumption and the environmental impact of the air transport sector while increasing its capacity. These advantages can be achieved by updating aircraft avionics and air traffic management

technologies and procedures. Its potentialities have been widely demonstrated from the aerodynamic point of view via numerical simulations and flight tests. Flight safety aspects have been also addressed, leading to the proposal of extended formations for commercial formation flight, which are intrinsically safer than close formations. Although formation flight is still not a reality for commercial aviation, international aviation organizations, aircraft manufacturers, airlines, air traffic service providers, and researchers are collaborating to make formation flight for commercial aircraft possible in the near future. The challenging Fello'fly Airbus project is a great indication of this.

Chapter 3

Model of the System

This chapter introduces the model of the system that represents the formation flight. The use of accurate dynamic models of aircraft and reliable meteorological forecast is mandatory in order to improve the predictability of the trajectories and obtain realistic estimations of the fuel savings. First, the dynamic model used to represent aircraft in solo flight is presented, together with the path constraints. Later, the dynamic model used to represent aircraft in formation flight is described. After that, the wind model is presented. Finally, the model of the direct operating costs of airlines is discussed.

3.1 Solo flight model

In aircraft trajectory optimization problems developed within the ATM context, a three degrees of freedom point-mass dynamic model of the aircraft is usually employed. In this model, the aircraft is represented as a point with variable mass due to the fuel consumption, moving in a four-dimensional space characterized by the three spatial dimensions together with time.

In this section, first, the reference systems are introduced. Later, some usual assumptions made to build an aircraft model to be used in the ATM context are described. After that, some simplifications are introduced to the model. Finally, the flight envelope is presented.

3.1.1 Reference systems

Several specific reference systems are used in flight mechanics to represent the elements involved in the motion of the aircraft, such as forces, torques, and velocities. The aim of these reference systems is to obtain practical expressions of the kinematic and dynamic equations of the aircraft [Tierno et al., 2012]. The reference systems of interest are the following: the Earth-Centered, Earth-Fixed (ECEF) reference frame, the local horizon reference frame, and

the wind-fixed reference frame.

ECEF reference frame

The ECEF reference frame, F_{ECEF}, as its name suggests, is a geocentric system, the axes of which are fixed with respect to the Earth's surface and rotate with the Earth. In particular, its origin is the center of gravity of the Earth and its axes are defined as follows: the x axis, x_{ECEF}, points towards the intersection of the Equator and the Greenwich meridian; the z axis, z_{ECEF}, points towards the North Pole; and, finally, the y axis, y_{ECEF}, completes a right-hand-oriented axes system.

Local horizon reference frame

The local horizon reference frame, F_{LH}, has its origin at the center of mass of the aircraft and its axes are defined as follows: the z axis, z_{LH}, points towards the center of the Earth; the x axis, x_{LH}, is contained in a horizontal plane and points towards a fixed direction of it, in this case, the north direction; and, finally, the y axis, y_{LH}, is also contained in a horizontal plane completing a right-hand-oriented axes system, pointing therefore towards the east direction.

Wind-fixed reference frame

To define the wind-fixed reference frame, the following assumption is made:

Assumption A: The aircraft has a plane of symmetry.

Thus, the wind-fixed reference frame, F_{WF}, is an aircraft-centered system, the axes of which rotate with the airspeed vector. In particular, its origin is the center of mass of the aircraft and its axes are defined as follows: the x axis, x_W, is aligned with the airspeed vector; the z axis, z_W, is contained in the plane of symmetry of the aircraft, orthogonal to x_W, and points downward in the usual flight attitude; and, finally, the y axis, y_W, is orthogonal to the plane of symmetry of the aircraft, completing a right-hand-oriented axes system.

The local horizon reference frame, F_{LH}, can be obtained from the ECEF reference frame, F_{ECEF}, through the rotations defined by the well known Euler angles, i.e., three consecutive rotations in the three-dimensional Euclidean space in a particular order, in this case, following the Tait-Bryan conversion, the order is z-y-x. Before performing these rotations, a translation is needed in order to make the origins of both reference systems match.

Similarly, the wind-fixed reference frame can be easily obtained from the local horizon reference frame by using the rotations defined by the Euler angles. For further information about the reference frames or about Euler's rotation theorem, please see [Hull, 2007].

3.1.2 Modeling assumptions

The following modeling assumptions are usually introduced in ATM-related studies [Hull, 2007, Tierno et al., 2012].

The first assumption comes from considering the ECEF reference system as an inertial reference system which is actually a non-inertial reference system.

> Assumption B: The Earth is considered flat, nonrotating and the ECEF reference frame can be considered inertial.

Other modeling assumptions made in this thesis are the following:

> Assumption C: The Earth is approximated as a sphere. In addition, typical aircraft cruise altitudes mean the acceleration due to gravity can be safely considered as a constant value: $g = 9.81\ m/s^2$.
>
> Assumption D: The vertical component of the wind speed is considered to be negligible. Dynamic effects of wind are neglected.
>
> Assumption E: All dynamic effects associated with elastic deformations, degrees of freedom of articulated subsystems such as flaps or rudders, or kinetic momentum of rotating subsystems with respect to the aircraft are neglected.
>
> Assumption F: The only external forces acting on the aircraft are the propulsive, aerodynamic, and gravitational forces.

As a consequence of the former hypotheses, the aircraft is considered as a rigid solid with six degrees of freedom. The set of differential equations involving forces and torques that describes the dynamics of the aircraft should be solved simultaneously. However, the following assumption is introduced to simplify the solution:

> Assumption G: Control surface deflections have quite lower effects on the aerodynamic forces than the corresponding effects on the aerodynamic torques.

This assumption allows forces and torques scalar equations to be decoupled leading to a three degrees of freedom point variable-mass dynamic model of the aircraft. Additional hypotheses made in this thesis are the following:

> Assumption H: Since most jet airplanes have engines rigidly coupled with the aircraft structure, aircraft are assumed to have fixed engines in this thesis.
>
> Assumption I: The aircraft is considered as a point variable-mass, as can be seen in the fuel mass flow equation. However, the low rate of variation of the mass of the aircraft leads it to be considered as a constant for the derivation of the kinematics and dynamics equations of motion.

Assumption J: A symmetric and coordinated flight is assumed and, hence, the airspeed vector, the propulsive forces and the aerodynamic forces are contained in the plane of symmetry of the aircraft.

Assumption K: A small thrust angle of attack is considered.

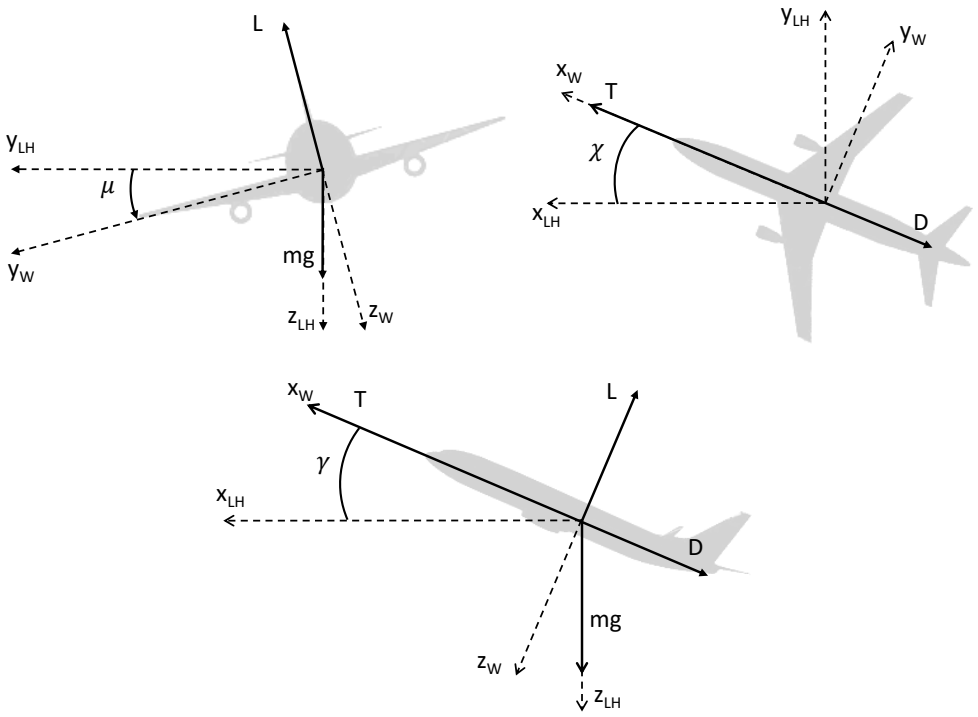

Fig. 3.1: Frontal, top, and lateral views of the aircraft together with the forces acting on it.

Considering the above assumptions and expressing the Euler's rotation using the Tait-Bryan convention for the wind-fixed reference frame with respect to the local horizon reference frame, the following angles will be used in the dynamics model of the aircraft:

- The heading angle, χ, $(0 \leqslant \chi \leqslant 2\pi)$, defined as the angle between the x_{LH} axis and the airspeed vector projection on the horizontal plane.
- The flight path angle, γ, $(-\pi/2 \leqslant \gamma \leqslant +\pi/2)$, defined as the angle between the airspeed vector and its projection on the horizontal plane.
- The bank angle, μ, $(-\pi \leqslant \mu \leqslant +\pi)$, defined as the angle between the y_W axis and the $(y_W - z_W)$ plane intersection with the horizontal plane.

A schematic representation of the forces acting on an aircraft together with the heading, flight path, and bank angles is given in Fig. 3.1.

3.1.3 Equations of motion

Taking into account the above assumptions, the motion of the aircraft can be described as a three degrees of freedom point variable-mass dynamic model defined by three dynamic equations, three kinematic equations, and one equation describing the fuel consumption flow rate. The equations of motion are hence defined by the following ordinary differential equations (ODE) system:

$$\begin{aligned}
\dot{\phi} &= \frac{V\cos\chi\cos\gamma + V_{W_N}}{R_E + h}, \\
\dot{\lambda} &= \frac{V\sin\chi\cos\gamma + V_{W_E}}{\cos\phi\cdot(R_E + h)}, \\
\dot{h} &= V\sin\gamma, \\
m\dot{V} &= T - D - mg\sin\gamma, \\
-mg\cos\gamma\sin\mu &= mV\left(\dot{\gamma}\sin\mu - \dot{\chi}\cos\gamma\cos\mu\right), \\
L - mg\cos\gamma\cos\mu &= mV\left(\dot{\gamma}\cos\mu + \dot{\chi}\cos\gamma\sin\mu\right), \\
\dot{m} &= -T\eta,
\end{aligned} \tag{3.1}$$

where ϕ, λ, and h are the three-dimensional position variables, latitude, longitude, and altitude, respectively, V is the true airspeed, χ represents the heading angle, γ represents the flight path angle, and m is the mass of the aircraft. T is the thrust force and μ the bank angle. The lift force is $L = qSC_L$, where $q = \frac{1}{2}\rho V^2$ is the dynamic pressure, ρ is the air density, and S is the reference wing surface area. The aerodynamic drag force is $D = qSC_D$, where C_D is the drag coefficient. R_E is the Earth's radius.

A relationship between both aerodynamic coefficients, C_L and C_D, exists, which is known as drag polar, that is $C_D = C_D(C_L)$. In this thesis, the following assumption about the drag polar has been made.

Assumption L: A parabolic drag polar is assumed.

Hence, considering Assumption L, a parabolic drag polar can be expressed as: $C_D = C_{D0} + KC_L^2$, where C_{D0} is the zero-lift drag component and K is the induced drag coefficient.

Other parameters and variables include the Earth's radius R_E and the gravitational acceleration g. V_{W_E} and V_{W_N} are the components of the wind velocity vector in eastward and northward directions, respectively. η is the thrust-specific fuel consumption. In particular, using Eurocontrol's base of aircraft data (BADA)[1] performance model for jet engines, the following equation applies:

$$\eta = C_{f_1}\left(1 + \frac{V}{C_{f_2}}\right), \tag{3.2}$$

[1] https://www.eurocontrol.int/model/bada

where C_{f_1} and C_{f_2} are empirical thrust-specific fuel consumption coefficients.

The BADA performance model provides accurate aircraft performance modeling such as fuel consumption, aerodynamic performance, and speed model, among others, for several types of commercial aircraft along different flight segments. Additionally, flight envelope information is also provided. Two families of aircraft performance modeling are available: BADA Family 3 and the newest BADA Family 4. In this thesis, BADA version 3.6 [Eurocontrol, 2013] has been used.

In general, the state and control variables are functions of time. The aerodynamic forces, L and D, are functions of their aerodynamic coefficient as well as of the atmospheric variables such as the density of the air ρ and the true airspeed of the aircraft V. Likewise, atmospheric variables depend on the position of the aircraft. Additionally, using the drag polar relationship, the relation between both aerodynamic coefficients can be taken into account. Finally, the components of the wind field depend on the position of the aircraft. For the sake of simplicity of the exposition, all these functional dependencies have been omitted.

Rearranging the last two dynamic equations in the ODE system (3.1), the explicit expressions for $\dot{\gamma}$ and $\dot{\chi}$ can be obtained, producing the following equivalent ODE system:

$$\begin{aligned}
\dot{\phi} &= \frac{V\cos\chi\cos\gamma + V_{W_N}}{R_E + h},\\
\dot{\lambda} &= \frac{V\sin\chi\cos\gamma + V_{W_E}}{\cos\phi\cdot(R_E + h)},\\
\dot{h} &= V\sin\gamma,\\
\dot{V} &= \frac{T - D - mg\sin\gamma}{m},\\
\dot{\chi} &= \frac{L\sin\mu}{mV\cos\gamma},\\
\dot{\gamma} &= \frac{L\cos\mu - mg\cos\gamma}{mV},\\
\dot{m} &= -T\eta,
\end{aligned} \tag{3.3}$$

where the state vector has seven components: the three dimensional position variables, ϕ, λ, and h, the true airspeed V, the heading angle χ, the flight path angle γ, and the mass of the aircraft m. In this set of equations, the control vector has three components: the thrust force T, the lift coefficient C_L, and the bank angle μ. Thus, for aircraft p, the state vector is $x_p = (\phi_p, \lambda_p, h_p, V_p, \chi_p, \gamma_p, m_p)\,, \forall p \in \{1,\ldots,N_a\}$, and the control vector is $u_p = \left(T_p, C_{L_p}, \mu_p\right), \forall p \in \{1,\ldots,N_a\}$, with N_a the number of aircraft involved in the mission design problem.

3.1.4 Flight envelope

Flight envelope constraints represent aircraft performance limitations. These constraints make reference to flight altitude, load factor, and airspeed, among others, and they can be stated in the form $\eta_l(t) \leq \eta(t) \leq \eta_u(t)$, where η is the state or control variable and η_l and η_u are the minimum and maximum allowed values of the variable, respectively. The BADA has been employed again to impose the following constraints:

$$\begin{aligned} V_{min} \leq \; V_{CAS} \leq \; & V_{MO}, \\ m_{min} \leq \; m \leq \; & m_{max}, \\ M \leq \; & M_{MO}, \\ T_{min} \leq \; T \leq \; & T_{max}, \\ C_{Lmin} \leq \; C_L \leq \; & C_{Lmax}, \end{aligned} \tag{3.4}$$

where V_{CAS} is the calibrated airspeed, V_{min} and V_{MO} are the minimum and maximum operating calibrated speeds, respectively, m_{min} and m_{max} are the minimum and maximum aircraft masses, respectively, M is the Mach number and M_{MO} is the maximum operating Mach number, T_{min} and T_{max} are the minimum and maximum available engine thrusts, respectively, and $C_{L_{min}}$ and $C_{L_{max}}$ are the minimum and maximum lift coefficients, respectively. Finally, μ_{max} is the maximum bank angle set by the air navigation regulations in civil flight. Furthermore, the BADA includes the equation $V_{min} = C_{V_{min}} V_s$, where $C_{V_{min}}$ is the minimum speed coefficient and V_s is the stall speed for each flight phase.

The V_{CAS} can be calculated as a function of the true airspeed V_{TAS} [Eurocontrol, 2013], by the following expression:

$$V_{TAS} = \left[\frac{2}{\upsilon} \frac{p}{\rho} \left\{ \left(1 + \frac{p_0}{p} \left[\left(1 + \frac{\upsilon}{2} \frac{\rho_0}{p_0} V_{CAS}^2 \right)^{1/\upsilon} - 1 \right] \right)^{\upsilon} - 1 \right\} \right]^{0.5}, \tag{3.5}$$

where p is the air pressure, ρ is the air density, and $p_0 = 101325\ Pa$ and $\rho_0 = 1.225\ kg/m^3$ are the air pressure and the air density at mean sea level (MSL), respectively. Finally, υ is defined as $\upsilon = \dfrac{\kappa - 1}{\kappa}$, where $\kappa = 1.4$ is the adiabatic index of air.

For turbofan-propelled aircraft, assuming standard atmosphere conditions, the maximum thrust T_{max} is defined by the following empirical expression:

$$T_{max} = C_{T_{cr}} \cdot C_{T_{C,1}} \cdot \left[1 - \frac{H_p}{C_{T_{C,2}}} + C_{T_{C,3}} \cdot H_p^2 \right], \tag{3.6}$$

where $C_{T_{cr}}$ is the maximum cruise thrust coefficient, $C_{T_{C,1}}$, $C_{T_{C,2}}$, and $C_{T_{C,3}}$ are the empirical thrust coefficients, and H_p is the geopotential pressure altitude.

3.2 Formation flight aircraft dynamics

The differential algebraic equations (DAE) system (3.3) is applicable to any aircraft in any phase of solo flight. However, depending on the aircraft type, the aerodynamic coefficients, the wingspan, and the reference surface, among others, the parameters of this DAE system change. In formation flight, further modifications must be introduced into the dynamic equations of the trailing aircraft.

As stated in Chapter 2, extended formations are intrinsically safer than close formations, which is why only extended formations have been considered in this thesis. In extended formations, aircraft fly with a longitudinal separation of more than 10 wingspans but the potential fuel burn reduction for the trailing aircraft has a significant decrease beyond 20-wingspans'separation. Therefore, in this thesis, the formation benefits are considered negligible for separations of more than 20 wingspans and the constraint introduced to model the distance which leads to fuel burn reductions in the trailing aircraft during formation flight is the following:

$$10b \leq \mathcal{D}_{pq} \leq 20b, \quad \forall p, q \in \{1, \ldots, N_a\}, p < q, \tag{3.7}$$

where b is the wingspan of the leader aircraft and $\mathcal{D}_{pq}$ is the great-circle distance between aircraft p and q at time t.

The haversine formula has been used to determine the great-circle distance $\mathcal{D}$ between two points given their latitudes and longitudes:

$$\mathcal{D} = 2R_E \arcsin\left(\sqrt{\sin^2\left(\frac{\phi_q - \phi_p}{2}\right) + \cos(\phi_p)\cos(\phi_q)\sin^2\left(\frac{\lambda_q - \lambda_p}{2}\right)}\right), \tag{3.8}$$

where (ϕ_q, λ_q) and (ϕ_p, λ_p) are the latitude and longitude of aircraft q and p, respectively, at any time.

As mentioned in Chapter 2, due to the formation flight, a significant decrease in induced drag is achieved for the trailing aircraft. According to Assumption L, the expression of the parabolic drag polar is

$$C_D = C_{D0} + C_{Di}, \tag{3.9}$$

where C_{D0} is the parasitic drag, which represents the aerodynamics clean performance of the aircraft, and C_{Di} is the induced drag, that is, the drag component due to lift. The induced drag can be expressed by

$$C_{Di} = \frac{C_L^2}{\pi \cdot AR \cdot e} = KC_L^2, \tag{3.10}$$

where $AR = b^2/S$ is the aspect ratio, e is an efficiency factor, which will be equal to the unity for elliptical lift distribution and lower than the unity for any other distribution, and

Solo flight	Formation flight
$\mathcal{D}_{pq} \geq 20b$	$10b \leq \mathcal{D}_{pq} \leq 20b$
$C_D = C_{D0} + KC_L^2$	$C_D = C_{D0} + (1-\epsilon)KC_L^2$

Table 3.1: Longitudinal distance constraints and parabolic drag polar in solo and formation flights.

$K = 1/(\pi \cdot AR \cdot e)$ is the lift-induced drag coefficient.

As mentioned in Chapter 2, due to formation flight, a significant decrease in the induced drag, KC_L^2, is achieved for the trailing aircraft, hence, the parabolic drag polar for a trailing aircraft flying in a formation can be expressed as [Hartjes et al., 2018], [Hartjes et al., 2019]

$$C_D = C_{D0} + (1-\epsilon)KC_L^2, \tag{3.11}$$

where ϵ represents the rate of induced drag reduction achieved for the trailing aircraft. The value of ϵ is highly dependent on the type of aircraft involved in the formation, the streamwise and the lateral distance between aircraft, the type of formation flight, and the wind, among others. According to [Ning, 2011], in which a zero wind field has been assumed, a maximum reduction in the induced drag of $30 \pm 3\%$ is achieved in a two-aircraft formation and a maximum reduction in the induced drag of $40 \pm 6\%$ in a three-aircraft formation (95% confidence intervals).

Therefore, during formation flight, the dynamics model of the leader aircraft is represented by the ODE system (3.3) with the standard parabolic drag polar, whereas the dynamic model of the trailing aircraft is represented by the same set of equations but replacing the standard parabolic drag polar by Eq. (3.11). The selection of the form of the drag polar is made based on the longitudinal distance between aircraft, as schematically illustrated in Table 3.1.

Considering that aircraft will not join in formation during the take-off, landing, and approach phases of flight [Hartjes et al., 2018], in the mission design problem studied in this thesis, only the cruise phase of the flights is considered. Moreover, the motion of the aircraft involved in the formation flight is restricted to the horizontal plane at cruise flight level, not allowing changes in the flight level. Thus, in addition to the assumptions of Section 3.1, the following assumption is made:

Assumption M: The flight path angle is zero, $\gamma = 0$.

Considering Assumption M, the dynamic models of the aircraft can be simplified. The resulting simplified model is a two degrees of freedom point variable-mass dynamic obtained by substituting $\gamma = 0$ in the DAE system (3.3). The motion of the aircraft restricted to the

horizontal cruise plane is described by the following set of kinematics and dynamics DAE:

$$\begin{aligned}
\dot{\phi} &= \frac{V\cos\chi + V_{W_N}}{R_E + h},\\
\dot{\lambda} &= \frac{V\sin\chi + V_{W_E}}{\cos\phi\cdot(R_E + h)},\\
\dot{V} &= \frac{T - D}{m},\\
\dot{\chi} &= \frac{L\sin\mu}{mV},\\
\dot{m} &= -T\eta,
\end{aligned} \tag{3.12}$$

together with the following algebraic equation:

$$L = \frac{mg}{\cos\mu}, \tag{3.13}$$

where the state vector has only five components, two less than DAE system (3.3): the two dimensional position variables, latitude and longitude, denoted by ϕ and λ, respectively; the heading angle χ; the true airspeed V; and the mass of the aircraft m.

In this set of equations, the control vector formally includes three components: the thrust force T, the lift coefficient C_L, and the bank angle μ. However, two control variables are directly related due to the requirement of equilibrium of forces given by Eq. (3.13) and, therefore, the number of control variables is two. Thus, for aircraft p, the state vector is $x_p = (\phi_p, \lambda_p, V_p, \chi_p, m_p)\,, \forall p \in \{1,\ldots,N_a\}$, and the control vector is $u_p = \left(T_p, \mu_p(C_{L_p})\right), \forall p \in \{1,\ldots,N_a\}$, with N_a the number of aircraft involved in the mission design problem.

Note that, for problem conditioning and numerical stability, normalized versions of both the DAE system (3.12) and Eq. (3.13) have been used in this thesis in the numerical experiments described in chapters 7 and 8.

Concerning the formation flight modeling, the following assumption has been adopted:

> Assumption N: The benefits obtained by flying in a formation are modeled as a rate of reduction in fuel burn consumption.

Considering Assumption N, the fuel savings factor can be directly introduced in the last differential equation of the DAE system (3.12) instead of considering the reduction in the induced drag. With $\mathcal{R}_{\text{fuel}}$ being the rate of reduction in fuel burn consumption due to the formation flight, the mass flow rate equation for the trailing aircraft during the formation flight can be expressed as

$$\dot{m} = -[1 - \mathcal{R}_{\text{fuel}}]\cdot T\cdot\eta. \tag{3.14}$$

A schematic description of the differences between the flight models employed in this

Solo flight	Formation flight
$\mathcal{D}_{pq} \geq 20b$	$10b \leq \mathcal{D}_{pq} \leq 20b$
$\dot{\phi} = \dfrac{V\cos\chi + V_{W_N}}{R_E + h},$	$\dot{\phi} = \dfrac{V\cos\chi + V_{W_N}}{R_E + h},$
$\dot{\lambda} = \dfrac{V\sin\chi + V_{W_E}}{\cos\phi\cdot(R_E + h)},$	$\dot{\lambda} = \dfrac{V\sin\chi + V_{W_E}}{\cos\phi\cdot(R_E + h)},$
$\dot{V} = \dfrac{T - D}{m},$	$\dot{V} = \dfrac{T - D}{m},$
$\dot{\chi} = \dfrac{L\sin\mu}{mV},$	$\dot{\chi} = \dfrac{L\sin\mu}{mV},$
$\dot{m} = -T\eta,$	$\dot{m} = -[1 - \mathcal{R}_{\text{fuel}}]\cdot T\cdot\eta,$
$L = \dfrac{mg}{\cos\mu},$	$L = \dfrac{mg}{\cos\mu}$

Table 3.2: Longitudinal distance constraints and dynamic model in solo and formation flights.

thesis to describe the solo and formation flights is given in 3.2. The model is selected based on the longitudinal distance between aircraft.

It is quite difficult to model the drag reduction ϵ and, hence, the fuel burn reduction $\mathcal{R}_{\text{fuel}}$ achieved during a formation flight, since there are many factors to take into account. The number of aircraft involved in the formation, their type, size, and weight, the ability of the trailing aircraft to place itself in the optimum location of the wake, and the stresses and vibrations induced, among others, strongly influence the benefits of the formation.

It is important to point out that the full three degrees of freedom point variable-mass dynamic model described in the DAE system (3.3) with the induced drag reduction modeling described by Eq. (3.11) could have been employed in the formation mission planner presented in this thesis. However, using the full model makes the statement of the problem, its numerical resolution, and the analysis of the results more complicated. For this reason, the reduced model has been used in this thesis.

Taking into account the assumptions made in this section, the obtained results are slightly less accurate. In particular, taking Assumption M and Assumption N into consideration may lead to a loss of accuracy in the speed profile and flight altitude. In [Ning, 2011], the aerodynamic performance of extended formations is analyzed in detail. The results show that aircraft within a formation fly at a slower cruise speed than in their respective solo flights, as this helps to achieve a reduction in the penalties associated with viscosity and compressibility effects induced by the formation flight. Consequently, aircraft within the

formation would also need to fly at a lower altitude, at a higher lift coefficient, or a combination of both compared with solo flight. Therefore, aircraft in formation tend to cruise at a slightly lower speed than when flying solo, as shown in [Voskuijl, 2017], [Hartjes et al., 2018], and [Hartjes et al., 2019].

Other assumptions made in the formation mission design problem presented in this thesis regard the relative position of each aircraft, which is set in advance, and the type of formation allowed in three-aircraft formations, which is the in-line formation.

Finally, a maximum detour time from the solo flight time has been set in order to perform a more realistic formulation of the formation mission design problem, according to the usual operational requirements.

3.3 Wind model

ERA-Interim [Dee et al., 2011] is a third-generation global atmospheric reanalysis produced by the european centre for medium-range weather forecasts (ECMWF). Climate reanalysis consists in systematic and coherent assimilation of the global meteorological data constrained by the available observations obtained from different sources during the period of reanalysis, such as radiosondes or aircraft, and prior state estimates using an invariant consistent assimilation scheme and an integrated meteorological model. The third-generation reanalysis data refers to the last generation, which was developed in 2010s and significantly enhanced the spatiotemporal resolution of the former ones.

Gridded data products, which can be found in the ERA-Interim database, include a wide variety of atmospheric parameters relevant to the mission design problem such as air temperature, pressure, and wind at different altitudes and sea-surface temperatures. In this thesis, the components of the wind velocity in eastwards and northwards directions have been used.

ERA-Interim is presented as a regular latitude-longitude grid, with a spatial resolution from $0.25^\circ \times 0.25^\circ$ to $3^\circ \times 3^\circ$ for the deterministic reanalysis, at 37 atmospheric levels corresponding to different pressure levels from 1 to 1000 hPa. The temporal coverage is four times daily, returning six-hour data. In this study, the chosen pressure level was 200 hPa, corresponding to the cruise altitude. The selected spatial resolution was $0.5^\circ \times 0.5^\circ$. Finally, the selected day was April 30, 2019, at 12:00. To include atmospheric data in the hybrid optimal control problem used to solve the mission design problem, an analytic function that approximates the data must be determined. For this purpose, radial basis functions (RBF) [Buhmann, 2003] have been used.

The RBF technique approximates multivariate functions using the distance measure concept to obtain a function approximation from a set of known input data. In particular, given a set of known input data, a function approximation at any point is obtained constructing a linear space which depends on the relative position of the evaluated point with respect to the

known observations according to an arbitrary distance measure. RBF consider interpolating functions of the form

$$F(x) = c_0 + \sum_{i=0}^{N-1} c_c \varphi(\| x - R_i \|), \tag{3.15}$$

where $x \in \mathbb{R}^N$ is the input data vector and N is its dimension, $F(x)$ is the function approximation, φ is the basis function, and R_i is a vector containing the centers, which are the reference points of the basis functions. c_0 and c_c are constant coefficients calculated by the RBF method, in particular, c_0 is the bias term. The Euclidean norm is used to compute the distance between the input points and the centers. There are different options for the choice of the basis functions. In this thesis, Gaussian basis functions have been selected, expressed as follows:

$$\varphi(x) = e^{(-x^2/2\sigma)}, \tag{3.16}$$

where σ is a scaling parameter.

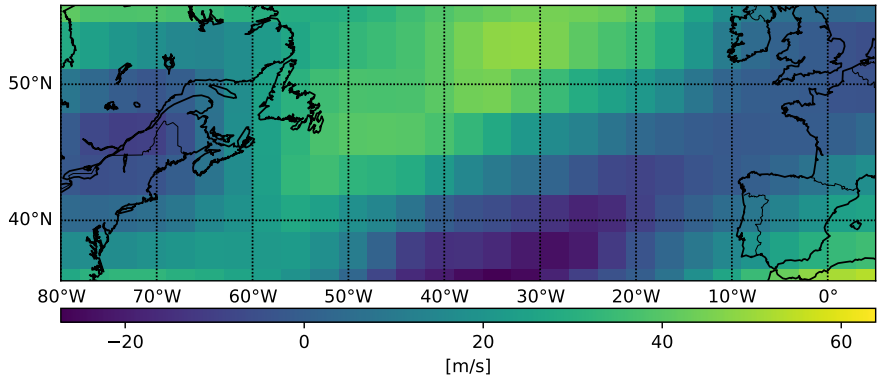

Fig. 3.2: Eastward wind speed on April 30, 2019 at 12:00.

Eastwards and northwards components of the wind speed taken from ERA-Interim and then approximated by the RBF method are represented in Fig. 3.2 and Fig. 3.3, respectively.

3.4 Model of the direct operating costs

According to the different operational functions within an airline, the costs can be classified into three major groups [Camilleri, 2018, ICAO, 2017]: flight operating costs, ground operating costs, and system operating costs. Any expense related to the operation of the aircraft is included in the flight operating costs, for example flight crew salaries, maintenance and fuel and oil expenses as well as aircraft ownership, depreciation and amortization. Passenger handling, cargo handling, and aircraft servicing belong to the ground operating costs. Landing fees together with reservation and ticketing services expenses are also included

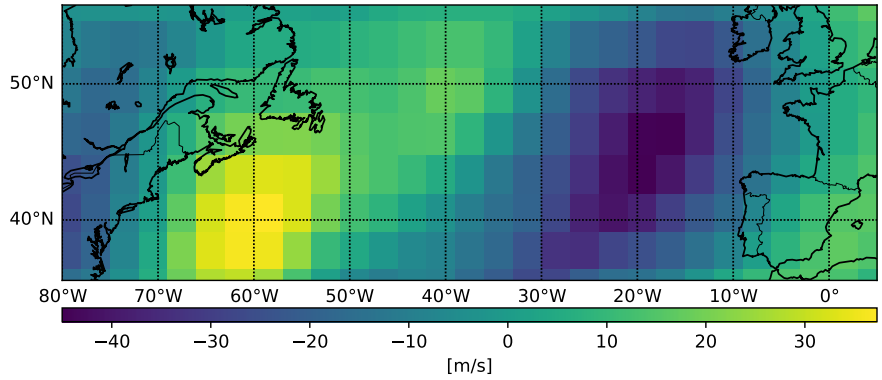

Fig. 3.3: Northward wind speed on April 30, 2019 at 12:00.

in this group. Finally, any corporate costs are included in the system operating costs. For instance, this applies to marketing and administrative costs, publicity costs, and on-board passenger services such as meals and entertainment. Fig. 3.4 gives a schematic categorization of the above costs. The historical percentage associated with flight operating costs is the

Flight operating costs	Ground operating costs	System operating costs
Flight crew	Aircraft servicing	Passenger services
Fuel & oil	Passenger handling	Advertising
Maintenance	Cargo handling	General
Aircraft ownership	Sales fees	Administrative

Fig. 3.4: Main functional expenses classified into flight, ground, and system operating costs.

greatest, amounting to half the total costs. Ground operating costs make up around 30% and, therefor esystem operating costs account for the lowest share of approximately 20%.

Direct operating costs, also known as DOC, are particularly important in trajectory optimization purposes, because not only do they represent a great rate of the whole costs of an airline, but they also depend critically on the performance of the flights. These expenses are usually divided into three different groups: flight operating costs such as flight crew salaries, fuel and oil, and airport and en-route charges; costs related to maintenance and overhaul; and aircraft depreciation. Fuel and oil consumption cost is of great importance since it represents about 20-30% of the total cost of an airline. Notice that several of the costs included in the DOC are indirectly time-related costs such as flight crew salaries, maintenance and overhaul, and aircraft depreciation.

The choice of the objective functional is decisive in any trajectory optimization problems in which the fuel consumption is, in general, minimized. However, two inherently competing

criteria must be considered in formation mission design problems: fuel consumption and flight time. Indeed, on the one hand, formation flight, in general, reduces the total fuel consumption and, on the other hand, it usually requires an increase in the total flight time to create the formation itself. Therefore, the need to get away from traditional fuel consumption minimization criteria is clearly evident in formation mission design problems. Although costs related to the duration of the flight and to fuel consumption are both included in the DOC, evaluating the DOC as a whole is quite challenging because it entails modeling all the costs associated with aircraft flying operations, which is beyond the scope of this thesis. Therefore, instead of using the DOC, the cost index (CI) has been employed in the objective functional. The CI is defined as the ratio between time-related and fuel-related operational costs, C_{time} and C_{fuel}, respectively, for a specific flight as follows:

$$CI = \frac{C_{time}}{C_{fuel}}. \tag{3.17}$$

Choosing the CI based on the interests of the airlines for the flights involved in a formation mission makes it possible to obtain a solution that represents the desired balance between flight time-related and fuel-related operational costs.

In this thesis, fuel consumption and flight time are combined in the objective functional using weighting coefficients based on typical CI values. No other costs have been considered.

The objective functional J for N_a aircraft, is defined as follows:

$$\min \quad J = \alpha_t \sum_{p=1}^{N_a} t_{flight_p} + \alpha_f \sum_{p=1}^{N_a} m_{f_p}, \tag{3.18}$$

where α_t and α_f are the time and the fuel burn weighting parameters, respectively, $t_{flight_p}, \forall p \in \{1, \ldots, N_a\}$, is the total flight time for aircraft p, and $m_{f_p}, \forall p \in \{1, \ldots, N_a\}$, is the fuel consumption for aircraft p.

It is worth mentioning that the initial fuel loaded into an aircraft that has good chances of benefitting from a formation flight could be considerably lower than the amount of fuel loaded into the same aircraft without good chances to benefit from a formation flight. Nevertheless, in this thesis, a more conservative approach has been adopted and all aircraft are loaded with the same amount of fuel as in solo flight, even if this factor will result in lower benefits in terms of DOC.

3.5 Conclusions

In this chapter, the model of the system that represents the formation flight has been introduced. It includes the wind model and the model of the direct operation costs of the flight based on typical cost index values, combining fuel consumption, and flight time. A detailed description of the modeling assumptions has been made. The main assumption is

that formation flight is allowed only in the cruise phase of the flight, and, therefore, only this phase of the flight has been considered in the formulation of the formation mission design problem. Considering only this phase of the flight, in which aircraft fly in the horizontal plane, leads to a reduction of their dynamic models. Another important assumption is that the benefits achieved by the trailing and the intermediate aircraft due to the formation flight can be directly modeled as a rate of reduction in the fuel consumption instead of in the induced drag. Although accuracy is lost due to these assumptions, they lead to a simplification in the statement of the problem, its numerical resolution, and the analysis of the results. However, it is important to point out that the methodology employed in this thesis to solve the formation mission design problem could have been applied to the full model without introducing any simplification.

Chapter 4

Deterministic Optimal Control Approach

In this chapter, the optimal control method employed to solve the deterministic formation mission design problem is introduced. First, the formulation of the formation mission design problem is presented. It is formulated as an optimal control problem for a switched dynamical system with logical constraints in disjunctive form. Switched dynamical systems, which are described by both a continuous and a discrete dynamics, are employed to represent the formation flight and logical constraints in disjunctive form are used to model the discrete dynamics of the switched system. In these constraints, binary or integer variables are used to model switching decisions. Finally, the embedding approach is described, which is used to convert the original switched optimal control problem into a smooth optimal control problem, in which the logical constraints in disjunctive form are converted into equality and inequality constraints without binary or integer variables.

4.1 The smooth optimal control problem

Consider a dynamical system described by a differential equation

$$\dot{x}(t) = f(t, x(t), u(t)), \tag{4.1}$$

in which variable t represents the time variable and the functions $x(t)$ and $u(t)$ represent the state and the control input of the system, respectively. Let

$$J(t, x(t), u(t)), \tag{4.2}$$

be a cost functional, which maps the time variable and the state and control functions into a single number.

An instance of a smooth OCP can be informally stated as follows: determine the control

input that steers the system from an initial state to a final state minimizing the cost functional J . In general, the time variable and the control and state functions are subject to constraints.

This simple instance of an OCP corresponds to a single-phase OCP. In general, optimal control models include more than one phase. Each phase in an OCP represents a portion of the trajectory of a dynamical system, and may be subject to different equations of motion, different time discretization, different control parameterizations, or different path constraints.

A different set of ODEs can be employed in each phase to reflect the switching behaviour of a dynamical system. A specific time discretization fitted to the dynamics of that portion of the trajectory can be used in every phase. For instance, if one part of a trajectory has slower dynamics and another part has faster dynamics, the time interval can be split into two phases with coarser time discretization for the first phase and a finer time discretization for the second phase. In the control parameterization method, the control space is discretized by approximating the control function using a linear combination of basis functions. In this way, the OCP is reduced to a NLP with a finite number of decision variables. Different control parameterizations such as piecewise constant and piecewise linear, can be employed in the same problem by defining different phases. Different path constraints, which are bound constraints on some performance parameter, can also be imposed within each phase. Phases are also necessary to impose intermediate constraints upon some variables. This can be done by imposing them as boundary constraints at the junction between two phases. Finally, linkage constraints should be enforced in order to assemble all the phases of the problem to get a unique trajectory for the system [Falck et al., 2021].

OCP can be formulated for continuous-time dynamical systems, as is the case in this thesis, and for discrete-time dynamical systems. OCP formulations may also include binary or integer variables to model decision-making processes.

As mentioned before, in general, optimal control problems include not only differential constraints but also algebraic constraints and path constraints. A more general formulation of a continuous smooth OCP is the following:

$$\min_{u \in \Omega} \quad J\left(t, x(t), u(t)\right) = \mathcal{M}(t_F, x_F) + \int_{t_I}^{t_F} \mathcal{L}(t, x(t), u(t)) dt, \tag{4.3a}$$

$$s.t. \quad \dot{x}(t) = f(t, x(t), u(t)), \tag{4.3b}$$

$$0 = g(t, x(t), u(t)), \tag{4.3c}$$

$$\eta_l(t) \leq \eta(t, x(t), u(t)) \leq \eta_u(t), \tag{4.3d}$$

$$x(t_I) = x_I \in \mathbb{R}^n, \tag{4.3e}$$

$$x(t_F) = x_F \in \mathbb{R}^n, \tag{4.3f}$$

where $u(t) \in \mathbb{R}^m$, $x(t) \in \mathbb{R}^n$, and Eq. (4.3a) represents the performance index of the OCP, in which J is a Bolza cost functional, consisting of two terms, the endpoint cost functional $\mathcal{M}$, also known as Mayer term, which is defined on a neighborhood of B, and the running

cost functional, $\mathcal{L}$, also known as Lagrange term, which is a continuously differentiable functional. The control input $u(t)$ is constrained to belong, at each time instant, to the bounded and convex set Ω. Eqs. (4.3b) and (4.3c) represent the set of algebraic-differential equations, where function f determines the dynamics of the system and function g describes the right-hand side of the algebraic constraints. The problem can be also constrained by path constraints represented by Eq. (4.3d), where η_l and η_u represent the lower and upper bound for each function η. Finally, Eqs. (4.3e) and (4.3f) represents the initial and final boundary conditions, respectively. The initial time t_I, the initial state $x(t_I)$, the final time t_F, and final state $x(t_F)$ are assumed to be restricted to a boundary set B as follows: $(t_I, x(t_I), t_F, x(t_F)) \in B = T_I \times B_I \times T_F \times B_F \subset \mathbb{R}^{2n+2}$.

In typical aerospace optimization problems the performance index of Eq. (4.3a) only contains the Mayer term. This is the case of this thesis, in which the objective functional in Eq. (3.18) is in Mayer form and represents a combination of fuel consumption and flight time of the aircraft.

Eqs. (4.3b) and (4.3c) correspond to the DAE systems given in Table 3.2, which describe the motion of each aircraft involved in a formation. In particular, the DAE system in the left column of the table describes the solo flight and the flight of the leader of a formation, and the DAE system in the right column of the table describes the flight of the intermediate and trailing aircraft of a formation.

The path constraints represented by Eq. (4.3d) correspond to the flight envelope given in Eq. (3.4). These constraints are usually given in terms of lower and upper bounds for several state and control variables such as flight altitude, load factor and airspeed. Notice that, Eqs.(4.3c) and (4.3d) also include logical constraints based on the stream-wise distance between aircraft, which are used in this thesis to model the switching between solo flight mode and formation flight mode for each aircraft. These constraints will be discussed later, in Section 4.2.4 of this chapter.

Eqs. (4.3e) and (4.3f) represent the initial and final conditions which are specified for each experiment in chapters 7 and 8.

For the sake of ease of exposition, in the formulation of the OCP for switched dynamical systems presented in the following section, neither algebraic equations nor path constraints have been included.

4.2 The switched optimal control problem

In this thesis, the formation mission design problem is formulated as an OCP for a switched dynamical system. Switched systems are described by both a continuous and a discrete dynamics in which the transitions among discrete states are not established in advance. In particular, each aircraft has different flight modes, namely solo flight and flight in different positions inside a formation, and their combination is represented by the discrete state of the

switched dynamical system, which models their joint dynamic behavior. Each flight mode will be represented by different dynamical equations which may include or not formation flight benefits in terms of fuel savings.

In this section, following [Bengea et al., 2011], the formulation of a simple OCP given in Section 4.1, is generalized for switched systems, introducing the switched optimal control problem (SOCP) for two-switched dynamical systems. Hereinafter, subindex "S" has been employed in the formulation of the OCP for switched dynamical systems for the sake of clarity. In particular, the dynamical model of a two-switched dynamical system can be represented by

$$\begin{aligned} \dot{x}_S(t) &= f_{v_S(t)}(t, x_S(t), u_S(t)), \\ x_S(t_I) &= x_I \in \mathbb{R}^n, \\ x_S(t_F) &= x_F \in \mathbb{R}^n, \\ v_S(t) &\in \{0,1\},\ t_I \le t \le t_F. \end{aligned} \tag{4.4}$$

In this model, the continuously differentiable vector fields, $f_0, f_1 : \mathbb{R} \times \mathbb{R}^n \times \mathbb{R}^m \to \mathbb{R}^n$, specify the dynamics of the two possible modes of the system. The control input $u_S(t) \in \Omega \subset \mathbb{R}^m$ is constrained to belong, at each time instant t, to the bounded and convex set Ω. The binary variable $v_S(t)$ is the mode selection variable that identifies which of the two possible system modes, f_0 or f_1, is active. Thus, both of them, $u_S(t)$ and $v_S(t)$, can be regarded as control variables. The initial time t_I, the initial state $x_S(t_I)$, the final time t_F, and final state $x_S(t_F)$ are assumed to be restricted to a boundary set B as follows: $(t_I, x_S(t_I), t_F, x_S(t_F)) \in B = T_I \times B_I \times T_F \times B_F \subset \mathbb{R}^{2n+2}$. The performance index of the SOCP has the following form

$$J_S\left(t, x_S(t), u_S(t), v_S(t)\right) = \mathcal{M}_S(t_F, x_F) + \int_{t_I}^{t_F} \mathcal{L}_{v_S(t)}(t, x_S(t), u_S(t))dt, \tag{4.5}$$

where the endpoint cost function $\mathcal{M}_S$ is defined on a neighborhood of B and formally coincide with function $\mathcal{M}$, and $\mathcal{L}_0$ and $\mathcal{L}_1$ are real-valued continuously differentiable functions that represent the running cost of operation of the system in each mode.

The SOCP is thus stated as follows

$$\min_{u_S \in \Omega, v_S \in \{0,1\}} J_S\left(t, x_S(t), u_S(t), v_S(t)\right), \tag{4.6}$$

subject to dynamical equations and endpoint constraints from the set of Eqs. (4.4).

Note that, although the statements of the OCP and the SOCP are quite similar, they are very different in their essence. The fact that the binary variable, $v_S(t) \in \{0,1\}$, appears within the SOCP formulation, requires an additional transformation of this kind of problems to enable the use of classical optimal control techniques to solve it. To do so, the embedding approach is introduced in the following section.

4.2.1 Specification of the switched optimal control problem

In the formation mission design problem posed in this thesis, each aircraft has different flight modes, namely solo flight and flight in different positions inside a formation, solo flight (SF) or formation flight (FF), respectively, and their combination is represented by the discrete state of the switched dynamical system, which models their joint dynamic behavior. Therefore, the problem will be formulated as an OCP for a switched dynamical system, following the SOCP formulation. Each flight mode will be represented by different dynamical equations which may include or not formation flight benefits in terms of fuel savings.

4.2.2 The embedding approach

In this section the embedding approach employed to transform a SOCP into an embedded optimal control problem (EOCP) is presented. In this way, a smooth OCP without binary variables is obtained, reducing the computational complexity of finding the solution.

Similarly to previous sections, subindex "E" has been employed in the formulation of the EOCP for sake of clarity. Following again [Bengea et al., 2011], the differential equation of the set of Eqs. (4.4) can be rewritten as follows

$$\dot{x}_E(t) = [1 - v_E(t)] f_0(t, x_E(t), u_{E_0}(t)) + v_E(t) f_1(t, x_E(t), u_{E_1}(t)). \tag{4.7}$$

The dynamical constraint from the set of Eqs. (4.4) and Eq. (4.7) formally coincide under the conditions $v_E(t) = v_S(t)$ and $u_{E_0}(t) = u_{E_1}(t) = u_S(t)$. However, in Eq. (4.7), $v_E(t) \in [0,1]$, while in Eq. (4.4), $v_S(t) \in \{0,1\}$, which is the key feature of the embedding approach [Bengea and DeCarlo, 2005, Bengea et al., 2011]. This method is based on solving the SOCP defined above, using only continuous control variables $v_E(t) \in [0,1]$, $u_{E_0}(t), u_{E_1}(t) \in \Omega$. In this way, the original switched system is embedded into a larger family of systems parameterized by $v_E(t) \in [0,1]$. The performance index of the SOCP from Eq.(4.5) is rewritten as

$$\begin{aligned} &J_E\left(t, x_E(t), u_{E_0}(t), u_{E_1}(t), v_E(t)\right) = \mathcal{M}(t_F, x_E(t_F)) \\ &+ \int_{t_I}^{t_F} \left([1 - v_E(t)] \mathcal{L}_0(t, x_E(t), u_{E_0}(t)) + v_E(t) \mathcal{L}_1(t, x_E(t), u_{E_1}(t))\right) dt. \end{aligned} \tag{4.8}$$

The EOCP is thus formulated as

$$\min_{u_{E_0}, u_{E_1} \in \Omega, v_E \in [0,1]} J_E\left(t, x_E(t), u_{E_0}(t), u_{E_1}(t), v_E(t)\right), \tag{4.9}$$

subject to dynamical equations and endpoint constraints from the set of Eqs. (4.7), which is an OCP without binary variables. Therefore, classical techniques from optimal control theory can be applied to solve it.

It has been shown in [Bengea and DeCarlo, 2005] and [Bengea et al., 2011] that, once a solution of the EOCP has been obtained, either the solution is of the switched type, that is, v_E takes only the values 0 and 1, or suboptimal trajectories of the SOCP can be constructed that can approach the value of the cost for the EOCP arbitrarily closely, and satisfy the boundary conditions within ϵ, with arbitrary $\epsilon > 0$. A thorough discussion about the relationship between the solutions of the SOCP and the EOCP can be found in [Bengea and DeCarlo, 2005] and [Bengea et al., 2011].

In Section 4.2.4, this approach is particularized to the formation mission design problem in which each aircraft can have different dynamic behavior depending on flying in solitaire, or in a different position within the formation.

4.2.3 Logical constraints modeling

The approach proposed in [Wei et al., 2008] has been employed to transform logical constraints in disjunctive form into inequality and equality constraints that involve only continuous auxiliary variables.

It has been shown in [Cavalier et al., 1990] that every Boolean expression can be transformed into conjunctive normal form (CNF). Hence, there is no loss of generality in considering that any logical constraint can be formulated as a CNF expression

$$Q_1 \wedge Q_2 \wedge \ldots \wedge Q_n, \tag{4.10}$$

in conjunctive form, where the symbol $\wedge$ denotes the "and" operator and

$$Q_i = P_i^1 \vee P_i^2 \vee \ldots \vee P_i^{m_i},\ \forall i \in \{1, 2, \ldots, n\}, \tag{4.11}$$

where Q_i is expressed in disjunctive form, in which the symbol $\vee$ denotes the "or" operator and the proposition P_i^j is either X_i^j or $\neg X_i^j$. The term X_i^j is a literal that can be either True or False and the symbol $\neg$ represents the "negation" operator.

Term X_i^j represents statements such as "$\mathcal{D}_{12}(t) \geq 20b$ ". Therefore, P_i^j takes the form

$$P_i^j \equiv \left\{ g_i^j\left(x(t)\right) \leq 0 \right\}, \tag{4.12}$$

$\forall i \in \{1, 2, \ldots, n\},\ \forall j \in \{1, 2, \ldots, m_i\}$, where $g_i^j : \mathbb{R}^{n_x} \to \mathbb{R}$ is assumed to be a $\mathcal{C}^1$ function.

To incorporate logical constraints in a OCP, they must be converted into a set of equality or inequality constraints. Additionally, if binary variables are not used, the combinatorial complexity of integer programming is avoided. Notice that, conjunctions from Eq. (4.10) can be easily included in a OCP are equivalent to $Q_i, \forall i \in \{1, 2, \ldots, n\}$. To be able to transform the disjunctions into a set of inequality constraints, a continuous variable $\alpha_i^j(t) \in [0, 1]$ is

defined and associated with each P_i^j in Eq. (4.12). Thus, Eq. (4.11) can be rewritten as

$$\begin{aligned} \forall i \in \{1,2,\ldots,n\}, \forall j \in \{1,2,\ldots,m_i\}: \quad & \alpha_i^j(t) \cdot g_i^j\left(x(t)\right) \leq 0, \\ \text{and} \quad & 0 \leq \alpha_i^j(t) \leq 1, \\ \text{and} \quad & \sum_{j=1}^{m_i} \alpha_i^j(t) = 1, \end{aligned} \tag{4.13}$$

The first constraint in (4.13) shows that when $\alpha_i^j(t) = 0$ the constraint $g_i^j\left(x(t)\right) \leq 0$ is not forced to be fulfilled. In contrast, if $0 < \alpha_i^j(t) \leq 1$, then $\alpha_i^j(t) \cdot g_i^j\left(x(t)\right) \leq 0$, and, consequently, the constraint $g_i^j\left(x(t)\right) \leq 0$ is forced to be fulfilled. The last equation in the system (4.13) guarantees that, at least, one of the propositions P_i^j holds.

In the next section, this approach will be applied to the formation mission design problem in which logical constraints involve the longitudinal distance between aircraft.

4.2.4 Specification of the embedded optimal control problem with equality and inequality constraints

In this section, the embedding approach is applied to the SOCP described in Section 4.2 and the logical constraints in disjunctive form based on the stream-wise distance between aircraft are converted into a set of inequality and equality constraints which will be added to the EOCP.

In the formation mission design problem posed in this thesis, not all the dynamic Eqs. (3.12) are subject to switches. More specifically, the equations of motion associated to the state variables ϕ, λ, χ, and V, do not switch whereas the aircraft's mass flow rate does when the aircraft p joins or leaves a formation as a trailing or an intermediate aircraft. To model this switching, mass flow rate equations considering fuel savings and not considering them, are combined using the selection variable $v_{E_p}(t)$, $p \in \{1,\ldots,N_a\}$ as follows

$$\begin{aligned} \forall p \in \{1,\ldots,N_a\}: & \\ \dot{\phi}_p = & \quad \frac{V_p \cdot \cos\chi_p + V_{W_N}}{R_E + h_p}, \\ \dot{\lambda}_p = & \quad \frac{V_p \cdot \sin\chi_p + V_{W_E}}{\cos\phi_p \cdot (R_E + h_p)}, \\ \dot{\chi}_p = & \quad \frac{L_p \cdot \sin\mu_p}{V_p \cdot m_p}, \\ \dot{V}_p = & \quad \frac{T_p - D_p}{m_p}, \\ \dot{m}_p = & \quad (1 - v_{E_p}) \cdot [-T_p \cdot \eta_p] + v_{E_p} \cdot [-(1 - \mathcal{R}_{\mathsf{fuel}_p}) \cdot T_p \cdot \eta_p], \end{aligned} \tag{4.14}$$

where $v_{E_p}(t) = 1$ corresponds to FF and $v_{E_p}(t) = 0$ to SF.

Thus, each aircraft has a different individual dynamic behavior which corresponds to SF or FF in a different position within the in-line formation. The combination of these behaviors represents the discrete states of the switched system that models the joint dynamic behavior of all the aircraft.

However, in mission design problems, the switching control variables $v_{E_p}(t),\ p \in \{1,\dots,N_a\}$ depend on the state variables, in particular on the geographical coordinates of the aircraft. Indeed, not all transitions between discrete states are possible at any time, since while the distance between aircraft is larger than 20 wingspans, FF can not take place. Furthermore, the switching control variables depend on one another. For instance, in a two-aircraft formation, if one aircraft is selected as the trailing aircraft the other one is forced to be the leader and vice versa. Similarly, in a three-aircraft formation, if one position in the formation is assigned to one aircraft, the other ones must fly in another position.

Thus, the switched system that represents the joint dynamic behavior of all the aircraft involved in the mission design problem should follow some rules that are specified using logical constraints. In particular, the switching logic among the discrete states of the system presented in the SOCP presented in this thesis, are modeled by logical constraints in disjunctive form, based on the stream-wise distance between aircraft. As stated in Eq. (3.7), it has been considered that the great-circle distance between aircraft in FF is between 10 and 20 wingspans, and is greater than 20 wingspans in case of SF. Hence, the distance between aircraft satisfies

$$\begin{aligned} \forall p,q \in \{1,\dots,N_a\},\ p<q: \quad & 10b \le \ \mathcal{D}_{pq}(t) \ \le 20b, \\ \text{or} \quad & \mathcal{D}_{pq}(t) \ \ge 20b. \end{aligned} \tag{4.15}$$

Using simple Boolean algebra, Eq.(4.15) can be rewritten as

$$\begin{aligned} \forall p,q \in \{1,\dots,N_a\},\ p<q: \quad & 10b \le \mathcal{D}_{pq}(t), \\ \text{and} \quad & \mathcal{D}_{pq}(t) \ \le 20b \quad \text{or} \quad \mathcal{D}_{pq}(t) \ \ge 20b. \end{aligned} \tag{4.16}$$

To transform the disjunctions into a set of equality and inequality constraints, a new variable is defined. Thus, in two-aircraft mission design problems, only a continuous variable related to the longitudinal distance $\mathcal{D}_{12}$ should be defined, whereas, in three-aircraft mission design problems three continuous variables must be introduced, which are related to the longitudinal distances $\mathcal{D}_{12}, \mathcal{D}_{13}, \mathcal{D}_{23}$. Thus, calling the new continuous variable $\alpha_{pq}(t) \in [0,1]$,

$\forall p, q \in \{1, \ldots, N_a\},\ p < q$, the logical constraints in Eq.(4.16) can be rewritten as

$$\begin{aligned} \forall p, q \in \{1, \ldots, N_a\},\ p < q: \quad & \alpha_{pq}(t)\,(\mathcal{D}_{pq}(t) - 20b) \leq 0, \\ \text{and} \quad & (1 - \alpha_{pq}(t))\,(20b - \mathcal{D}_{pq}(t)) \leq 0, \\ \text{and} \quad & 0 \leq \alpha_{pq}(t) \leq 1, \\ \text{and} \quad & \mathcal{D}_{pq}(t) \geq 10b. \end{aligned} \tag{4.17}$$

For aircraft p and q, if $\mathcal{D}_{pq}(t) > 20b$, $\alpha_{pq}(t)$ must be zero in order to satisfy the second constraint in (4.17). Otherwise, when $\mathcal{D}_{pq}(t) \leq 20b$, the variable $\alpha_{pq}(t) = 1$, to fulfill the second constraint in the above set of equations. Formation flight benefits will be achieved only when $\alpha_{pq}(t) = 1$. In any case, the last constraint in (4.17) ensures that the longitudinal distance between aircraft will always satisfy the safety minimum distance of $10b$.

It can be observed that nature of the variables $v_{E_p}(t)$, $\forall p \in \{1, \ldots, N_a\}$, and $\alpha_{pq}(t)$, $\forall p, q \in \{1, \ldots, N_a\},\ p < q$, is similar. The variable $v_{E_p}(t)$ selects equations of the dynamic model for aircraft p, whereas the variable $\alpha_{pq}(t)$ selects constraints. Therefore, although, for the sake of clarity, a different notation has been employed in the previous sections to describe them, the variables $\alpha_{pq}(t)$ and $v_{E_p}(t)$ are directly related by the following equivalence

$$\forall p, q \in \{1, \ldots, N_a\},\ p < q: \quad \alpha_{pq}(t) = v_{E_p}(t), \tag{4.18}$$

where aircraft p is supposed to be the trailing aircraft. Therefore, the variable $v_{E_q}(t)$, which selects equations of the dynamic model for aircraft q, must be zero regardless of the value of variable $\alpha_{pq}(t)$, as aircraft q will be the leader one and, hence, it will achieve no benefits from the formation.

It is important to notice that the equivalence in Eq. (4.18) between the continuous variables obtained from the embedding approach, used to model the switched dynamical system and transform the logical constraints in disjunctive form into inequality and equality constraints, need not necessarily be fulfilled in others EOCPs.

4.3 Conclusions

In this chapter, the optimal control method employed to solve the deterministic formation mission design problem has been presented. The problem is formulated as an optimal control of a switched dynamical system which has been converted into a smooth optimal control problem using the embedding approach. The embedding approach is a unifying technique able to efficiently tackle both the switching dynamics and the logical constrains of the optimal control problem, transforming it into a smooth optimal control problem, which can be solved using classical optimal control techniques. The main advantages of this approach are that the multiphase formulation is avoided, as well as the use of integer variables, decreasing

the computational time and effort in finding the solution. This approach has substantial advantages compared to multiphase approaches, which are based on exhaustively analyzing every possible formation mission individually and then, comparing the results. Additionally, it is easily scalable to design formation mission problems with an arbitrary number of flights.

Chapter 5

Numerical Optimal Control Methods

In this chapter, a general overview to numerical methods for optimal control is given. They can be classified in indirect and direct numerical methods based on whether they are based on optimality conditions or not. Direct methods can be classified into shooting and collocation methods. The latter, can be classified into local and global collocation methods. The main advantages and disadvantages of each class of methods is discussed.

5.1 Introduction: direct and indirect numerical optimal control methods

Two different numerical approaches have been traditionally followed to solve OCPs, indirect and direct methods.

The indirect methods follow the strategy of "*first optimize, then discretize*" and are based on the Pontryagin's Maximum Principle. By contrast, direct methods follow the strategy of "*first discretize, then optimize*" and transcribe an infinite-dimensional OCP into a finite-dimensional optimization problem, which, in general, is a nonlinear programming (NLP) problem [Betts, 2010].

Indirect methods are based on the necessary conditions of the Pontryagin's maximum principle. However, these conditions depend on the constraints of the OCP and change when some constraints become active, i.e., when the state or the control variables reach the boundary of their admissible sets. The main drawback of this setting is that it is not possible to know in advance when this occurs, and therefore, it is not easy to derive a general numerical method from these conditions. Moreover, accurate initial guesses are required, not only for state and control variables, as it is in many numerical methods, but also for the costate variables, which are non-intuitive and therefore, very difficult to be accurately established. For the same reasons, analytical solutions can be obtained only for the simplest OCPs.

Direct methods do not rely on the necessary conditions of the Pontryagin's maximum principle. They are numerical methods in which the process to obtain the optimal solution

of the OCP is quite easier than in indirect methods, because although, in general, large scale NLP problems are obtained with a great amount of variables and constraints, fast and reliable NLP solvers are available to solve them. In Fig. 5.1, a schematic overview of both advantages and disadvantages of each approach is given.

Since the advantages of direct methods outweigh their disadvantages compared to indirect approaches, in this thesis, a direct approach has been employed to solve OCPs.

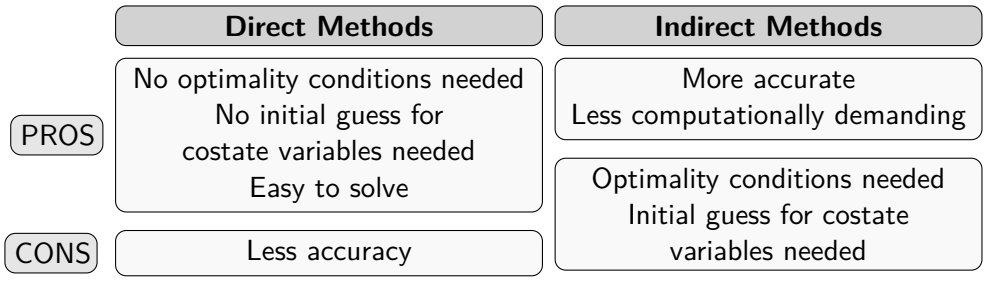

Fig. 5.1: Advantages and disadvantages of direct and indirect methods.

5.2 Direct methods

Direct methods can be divided in two main categories, direct shooting methods and direct collocation methods, as shown in Fig. 5.2.

Direct shooting methods can be further divided into two categories: single and multiple shooting methods. Single shooting methods are control parameterization methods in which a time grid is defined and the controls are discretized on that grid as a set of NLP variables, while the states are discretized using numerical integration. These methods are the simplest technique to numerically solve OCPs. The major advantage of them is that, although a high-dimensional state vector is involved in the problem, the transcribed problem will have few degrees of freedom. Additionally, only initial guesses for controls are required. However, the main disadvantage of single shooting is that this technique is quite sensitive to initial conditions.

These drawbacks make them poorly suitable for solving most OCPs [Betts, 2010]. To reduce the sensitivity to initial conditions of the single shooting method, the multiple shooting method has been devised, in which the time interval is split into shorter subintervals, and thereafter, the problem is transcribed as in the single shooting methods, where the initial state of each subinterval is a variable of the resulting NLP problem. In the multiple shooting method, although the sensitivity-related issues are fixed, the number of variables involved in the NLP problem increases.

Direct collocation methods do not rely only on parameterization of the control, they rely on parameterization of both state and control. Within collocation methods, there are two major groups: local collocation and global collocation methods. As its name suggests, in

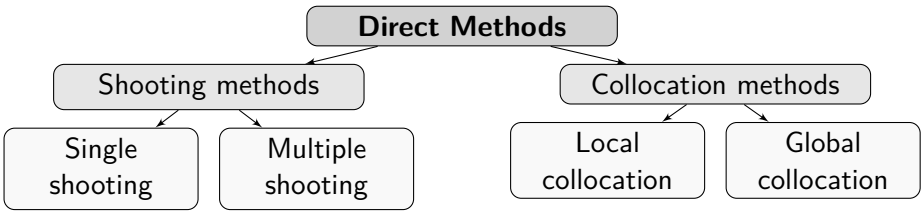

Fig. 5.2: Direct methods classification.

local collocation methods local approximations of states and controls are made, and local integration techniques are applied for the differential equations that represent the dynamic system. Local collocation methods are the simplest collocation methods and are less accurate than global collocation methods [Huntington and Rao, 2008]. Some of the best-known local collocation methods are the trapezoidal and the Hermite-Simpson collocation schemes. The main difference between them is the kind of functions that are employed to approximate the system dynamics in each of them, being piecewise linear functions in the trapezoidal scheme and piecewise quadratic functions in the Hermite-Simpson collocation scheme. Unlike local collocation methods, global ones use global polynomials to approximate the states across the whole time interval. The main family of global collocation methods are the pseudospectral methods (PSM). In this thesis, PSM have been used. They will be introduced in the next section.

5.3 Pseudospectral methods

PSM are a type of direct global collocation methods which use global polynomials to parameterize the state variables. The nodes are generally obtained from a Gaussian quadrature, which is employed to collocate the set of differential-algebraic equations. The use of global polynomials, instead of using piecewise-continuous polynomials as interpolant between prescribed subintervals, makes PSM more efficient and simpler than other direct methods [Fahroo and Ross, 2000].

The first step to introduce PSM is to transform the original time variable, $t \in I = [t_I, t_F]$, into a new time variable, $\tau \in [-1, +1]$. The transformation that relates both time variables is the following

$$t = \frac{(t_F - t_I)\,\tau \;+\; (t_F + t_I)}{2}. \tag{5.1}$$

From Eq. (5.1), it is easy to obtain the following relationship:

$$dt = \frac{t_F - t_I}{2} d\tau. \tag{5.2}$$

In trajectory optimization problems, the four most commonly used sets of collocation points are the Legendre-Gauss (LG), Legendre-Gauss-Radau (LGR), also known as direct LGR,

Flipped Legendre-Gauss-Radau (f-LGR), and Legendre-Gauss-Lobatto (LGL) points. Notice that, although in all these methods the discretization points employed in the problem must lie in the $[-1, +1]$ interval, this is not required for the collocation points. Indeed, although the position of the points changes from one set of collocation points to another, as described in detail below, the major difference between the methods is that, depending on the set of collocation points chosen, both, one, or none endpoints of the interval $[-1, +1]$ will be excluded in the approximation of the control variables [Garg et al., 2011].

Collocation points are roots of orthogonal polynomials, or linear combinations of them and its derivatives [Huntington, 2007, Garg et al., 2009]. In particular, the four sets of collocations points seen above are based on Legendre polynomials. Denoting the Legendre polynomial of *k-th* degree as P_K, where K represents the total number of discretization points, the particular relationship between the different sets of collocation points and the Legendre polynomial is specified in Fig. 5.3.

	Roots from
LG	$P_K(\tau)$
LGL	$\dot{P}_{K-1}(\tau)$ including endpoints -1 and $+1$
LGR	$P_{K-1}(\tau) + P_K(\tau)$
f-LGR	$P_K(\tau) - P_{K-1}(\tau)$

Fig. 5.3: Roots of the Legendre polynomials, or combinations of them, for different sets of collocation points.

In Fig. 5.4 a schematic overview of the positioning of the points for the different collocation schemes is given. In particular, it can be seen that both endpoints are included in the LGL points, i.e. $\tau \in [-1, 1]$, neither of them are included in the LG points, i.e. $\tau \in (-1, 1)$ and just one of the endpoints is included in the LGR points. If the initial point -1 is included, i.e. $\tau \in [-1, 1)$, the set of collocation points are usually called just LGR points or direct LGR points, whereas, when the terminal endpoint $+1$ is included, i.e. $\tau \in (-1, 1]$, the resulting set of points is known as the f-LGR points. Notice that, while the LG and LGL points located symmetrically with respect to the origin, the direct LGR and f-LGR points are not.

Since in the LG points, the endpoints are not included, additional quadrature constraints are necessary in order to force collocation at initial and terminal endpoints. These additional constraints make the problem resolution unnecessarily more complicated. This drawback can be overcome using the LGL points. However, the use of the LGL points has some additional drawbacks such as the slow convergence of the costate variables. Finally, due to their asymmetric positioning with respect to the origin, both direct LGR and f-LGR collocation points, are good candidates, because they permit collocation at endpoints without significant convergence issues for the costate variables [Fahroo and Ross, 2008, Garg, 2011].

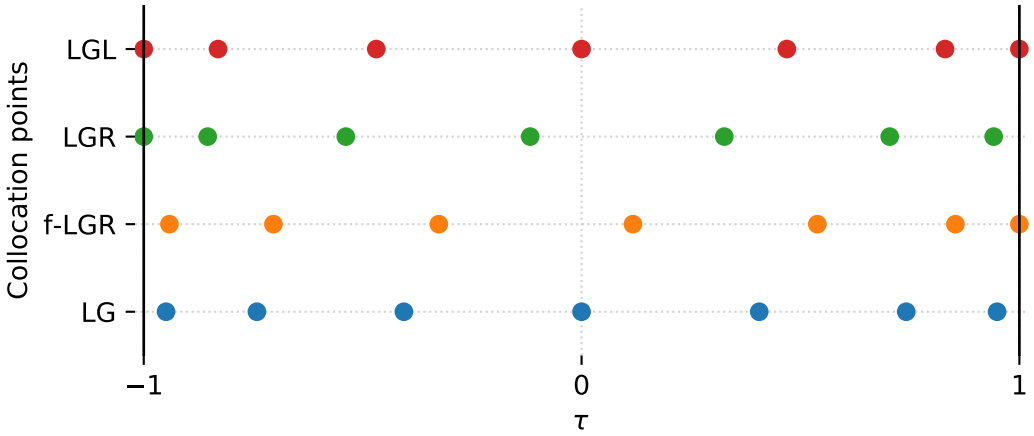

Fig. 5.4: Schematic comparison between the LG, LGR, f-LGR, and LGL collocation points.

In [Garg et al., 2009], it is stated that direct LGR and f-LGR collocation points are useful in infinite-horizon problems and in finite-horizon problems in which endpoints constraints are involved or the state at the terminal time is included in the objective function.Therefore, PSM based on f-LGR points have been employed in this thesis, which will be introduced in the next section.

5.3.1 Pseudospectral method using f-LGR points

In this section, following [Garg et al., 2011, Garg et al., 2009], the PSM using the f-LGR collocation points will be presented. Consider K flipped Radau collocation points lying on the interval $\tau \in (-1, 1]$ and N discretization points lying on the interval $\tau \in [-1, 1]$, which include the mentioned K collocation points together with the initial endpoint -1. In this case, $K = N - 1$. For a better understanding of their position, a schematic representation of the position of the f-LGR collocation points and the corresponding discretization points, is given in Fig. 5.5.

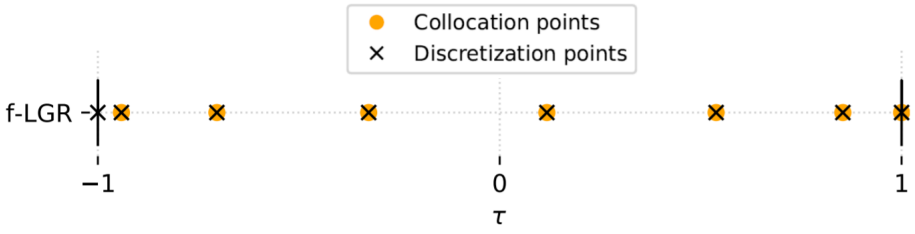

Fig. 5.5: Schematic representation of the position of the f-LGR collocation points and the corresponding discretization points.

Thus, considering the time transformation defined in Eq. (5.1), each component *j-th* of the state variable evaluated at the *k-th* collocation point, $x_j(\tau_k)$, can be approximated using

a basis of N Lagrange polynomials $L_i, i = 1, \ldots, N$, by the following expression:

$$x_j(\tau_k) \approx \sum_{i=1}^{N} x_j(\tau_i) L_i(\tau_k), \quad \text{for } k = 1, \ldots, K, \tag{5.3}$$

where the nodes $\tau_i, i = 1, \ldots, N$ are the discretization points, $\tau_k, k = 1, \ldots, K$ are the collocation points, and $L_i(\tau_k)$ is a Lagrange polynomials basis particularized for each collocation point k, given by the Lagrange polynomial interpolation:

$$L_i(\tau) = \prod_{\substack{j=1 \\ j \neq i}}^{N} \frac{\tau - \tau_j}{\tau_i - \tau_j}. \tag{5.4}$$

Differentiating Eq. (5.3), and defining a new matrix D_{ki}, which satisfies $D_{ki} = \dot{L}_i(\tau_k)$, yields

$$\dot{x_j}(\tau_k) \approx \sum_{i=1}^{N} x_j(\tau_i) \dot{L}_i(\tau_k) = \sum_{i=1}^{N} D_{ki} x_j(\tau_i), \quad \text{for } k = 1, \ldots, K. \tag{5.5}$$

PSM are characterized by the differentiation matrix $D \in \mathbb{R}^{K \times N}$, which is used to approximate the derivative of the state at the collocation points. The differentiation matrix for the f-LGR collocation points is defined as follows:

$$D_{ki} = \begin{cases} \dfrac{\dot{g}(\tau_k)}{(\tau_k - \tau_i)\dot{g}(\tau_i)}, & \text{for } k \neq i, \\ \dfrac{\ddot{g}(\tau_i)}{2\dot{g}(\tau_i)}, & \text{for } k = i, \end{cases} \tag{5.6}$$

where the function $g(\tau_i) = (1+\tau_i)[P_K(\tau_i) - P_{K-1}(\tau_i)]$, based on the roots of the combination of Legendre polynomials for the f-LGR points, shown in Fig. 5.3.

Notice that, with the method explained here, increasing the degree of the Lagrange polynomials allows the state variables to be approximated at every discretization point, including both endpoints.

However, the control variables are only discretized and approximated at the f-LGR collocation points using $N - 1$ Lagrange polynomials. Therefore, the *j-th* component of the control can be approximated as follows:

$$u_j(\tau_k) \approx \sum_{i=2}^{N} u_j(\tau_i) L_i(\tau_k), \quad \text{for } k = 1, \ldots, K. \tag{5.7}$$

Using Eq. (5.2), the first time derivative of the *j-th* of the state variable, with respect to $t \in I = [t_I, t_F]$, $\dot{x_j}(t)$, can be expressed as follows:

$$\dot{x_j}(t) = \frac{2}{t_F - t_I} \sum_{i=1}^{N} D_{ki} x_j(\tau_i), \quad \text{for } k = 1, \ldots, K. \tag{5.8}$$

Thus, the differential equation (4.1) of the OCP, $\dot{x}(t) = f(t, x(t), u(t))$, will be incorporated in the NLP problem as:

$$\sum_{i=1}^{N} D_{ki} x_j(\tau_i) - \frac{t_F - t_I}{2} f(\tau_k, x(\tau_k), u(\tau_k)) = 0. \tag{5.9}$$

As mentioned before, global polynomials are used in PSM. Discontinuities in the time derivatives of the state or control variables can not be accurately approximated using this type of polynomials. The EOCP described in Section 4.2.2, which arises in solving the formation mission design problem, is a nonsmooth OCP with discontinuities in the time derivatives of the state and control variables caused by the switches in the dynamic constraints of the problem. Additionally, in the EOCP, the initial and final times of each flight are, in general, different and, consequently, the collocation nodes of each flight do not match. However, to model the logical constraints from Eq. (4.16) that describe the switching logic among discrete states of the switched dynamical system that represent the formation flight, it is necessary to have the same set nodes for all the flights involved, at least during the flight phases in which aircraft fly in formation. These reasons make PSM not very suitable in dealing with the non-smooth EOCP. Therefore, an extension of the PSM, called pseudospectral knotting method has been employed in this thesis, which is outlined in the next section.

5.3.2 Pseudospectral knotting method

Pseudospectral knotting methods generalize the spectral patching method by the exchange of information across the different patches among standard PSM in the form of switching conditions [Ross and Fahroo, 2004]. These constraints are localized at the so-called knots of the problem. The knots are some special nodes which enable the global time interval to be divided into several time subintervals to apply PSM over each subinterval. So, the knots represent double nodes, coinciding with the last node of one subinterval or patch and with the first node of the following subinterval. Different kind of knots can be defined such as soft or hard knots, or free or fixed knots.

In relation to the numerical difficulties associated to the nonsmoothness of the mission design problem, the Gibbs phenomenon should also be mentioned. This phenomenon appears when a nonsmooth function is approximated with some smooth functions [Ross and Fahroo, 2004], and the pseudospectral knotting method allows this phenomenon to be prevented.

5.4 Solution of the embedded optimal control problem

In this section, the specification of the PSM employed to solve the formation mission design problem studied in this thesis is given. The peculiarities of the problem that make

it to be solved using the knotting PSM are discussed and the solver employed to solve the resulting NLP problem is described.

The deterministic formation mission design problem presented in Chapter 4 is formulated as a SOCP, which has been transcribed into an EOCP using the embedding approach. Finally, the knotting PSM is applied to solve the EOCP.

Following [Ross and Fahroo, 2004], in the formation mission design problems solved in this thesis, only two interior soft knots are considered, independently of the number of aircraft involved in the formation. Additionally, initial-time and final-time conditions are considered as part of the general framework of knots. In particular, the knots corresponding with the initial-time and final-time are defined as hard knots because they are intrinsic to the formulation of the problem.

The interior knots are defined as free knots but constrained by the condition that the time position of the first interior knot, t_{k_1}, should be greater than the initial times of all flights, max$(t_{I,p})$, and the time position of the second one, t_{k_2}, should be smaller than the final times of all flights, min$(t_{F,p})$, as schematically shown in Fig. 5.6. On this basis, three different time intervals, I^1, I^2, and I^3, have been considered for each flight:

- I^1: before the first interior knot: $t_p \in [t_{I,p},\ t_{k_1}), \forall p \in \{1,\ldots,N_a\}$, formation is not allowed.
- I^2: between the two interior knots: $t_p \in [t_{k_1},\ t_{k_2}],\ \forall p \in \{1,\ldots,N_a\}$, formation is allowed.
- I^3: after the second interior knot: $t_p \in (t_{k_2},\ t_{F,p}], \forall p \in \{1,\ldots,N_a\}$, formation is not allowed.

In Fig. 5.7 a schematic representation of the three different time intervals, I^1, I^2, and I^3, and the knots and nodes of the problem are presented. The vertical lines correspond to the times of each node, and the big points represent the knots.

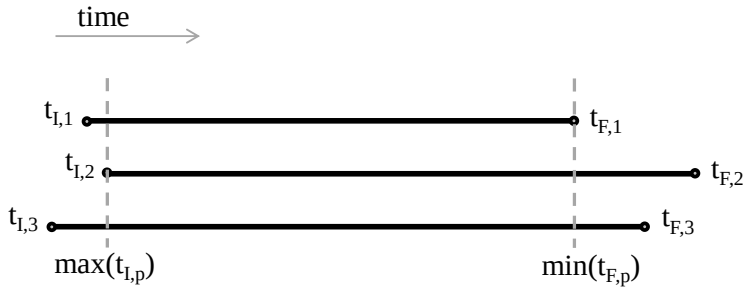

Fig. 5.6: Schematic flight times representation in a three-aircraft mission design problem.

It is easy to see that, in two-aircraft formation design problems, the formation can only happen if both aircraft are flying, in other words, during the overlapped flight time

[Xu et al., 2014]. Thus, the formation is only allowed during the second time interval, I^2, and the collocation points of all the aircraft are forced to be the same in this interval. Notice that, as mentioned before, the two interior knots of the problem should be greater than $max(t_{I,p})$ and lower than $min(t_{F,p})$, but are not fixed to be equal to those values. Thus, the time value of the interior knots should be also determined in the solution. The same assumption has been taken for three-aircraft formations.

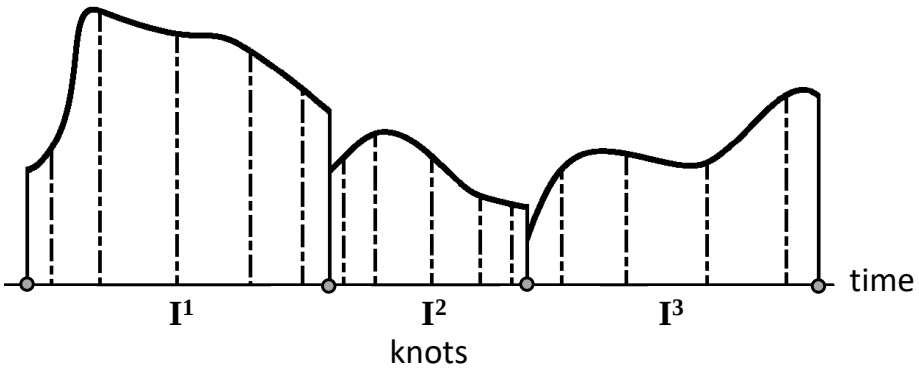

Fig. 5.7: Knots and nodes. Figure adapted from [Ross and Fahroo, 2004].

In short, the resulting EOCP together with the inequality and equality constraints given in Section 4.2.4 can be solved using traditional optimal control techniques.

There are several integrated software packages available to solve OCPs using direct collocation methods such as DIDO [Ross, 2020], GPOPS [Rao et al., 2009] and GPOPS-II [Patterson and Rao, 2014]. All of them implement PSM and are user-friendly, in the sense that they allow people with no knowledge of the underlying pseudospectral theory to use them. However, they are commercial software packages for the commercial Matlab environment. To gain a deeper insight into knotting PSM and to avoid dependance from commercial software, the knotting pseudospectral method has been implemented from scratch in this thesis. The four different collocation points schemes have been implemented and tested, obtaining that f-LGR points show the best convergence for the formation mission design problem. Therefore, the Radau knotting PSM have been selected to transcribe the EOCP into a NLP problem.

The resulting NLP problem has been modeled using Pyomo [Hart et al., 2012], an open-source Python-based software package for modeling complex optimization problems, and solved using interior point optimizer (IPOPT) solver, an open-source software package suitable for large-scale nonlinear optimization. It implements an interior-point line-search filter method and can be employed to solve general NLP problems [Wächter and Biegler, 2006].

5.5 Conclusions

In this chapter, the main numerical methods for optimal control have been described. The accuracy of global collocation methods has led to choose in this thesis a pseudospectral method to solve optimal control problems, namely the pseudospectral method based on the Flipped Legendre-Gauss-Radau collocation points, which is especially suitable due to the presence of endpoints constraints in the optimal control problem and the state at the terminal time in the objective functional. The peculiarities of the formation mission design problem studied in this thesis, has made it necessary to use a special pseudospectral method, the knotting pseudospectral method. To gain a deeper insight into these methods and to avoid dependance from commercial software, the knotting pseudospectral method has been implemented from scratch in this thesis.

Chapter 6

Stochastic Optimal Control Approach

In this chapter, the stochastic optimal control method employed to solve the stochastic formation mission design problem is introduced. First, the main sources of uncertainty in air traffic management are described. Later, the formulation of the stochastic switched optimal control problem is introduced. After that, the methodology to convert the stochastic constraints into deterministic constraints and the stochastic objective functional into a deterministic objective functional is described. This methodology is based on nonintrusive generalized polynomial chaos stochastic collocation. Finally, the method employed to conduct the sensitivity analysis is described, the aim of which is to identify the random variables that have more influence on the variability of a component of the solution of the stochastic formation mission design problem.

6.1 Introduction

An OCP of a stochastic switched dynamical system is an OCP in which the continuous dynamics of the system is represented by stochastic differential equations, the objective functional is a stochastic functional, and the constraints, which are defined by means of stochastic functions, must be satisfied almost surely, i.e., with probability 1. The set of possible exceptions in which the constraints are not satisfied may be non-empty but must have probability 0. Therefore, in this thesis, the adjective stochastic means that the functions and the solutions of the differential equations depend on a vector of random variables. This problem is referred to as the stochastic switched optimal control problem (SSOCP).

Modeling, control, and optimal control of stochastic switched systems are addressed in [Alwan and Liu, 2018, Zhu, 2019], in which the random factors acting on the continuous dynamic models of the switched system in each discrete state are represented by some idealized processes such as the Wiener process, and tools such as stochastic calculus have been employed to obtain solutions.

Another approach to model uncertainties in switched dynamical systems is to treat uncertainties as random variables or random processes and recast the original deterministic switched dynamical system as a stochastic switched dynamical system. This type of stochastic systems are different from those represented by classical stochastic differential equations, where the random inputs are idealized processes. Consider a stochastic optimal control problem in which only random variables are present in its formulation like in the formation mission design problem studied in this thesis. One of the most commonly used methods to solve OCPs of stochastic dynamical systems of this type is the Monte Carlo sampling [Shapiro, 2003], in which independent realizations of the random variables are generated based on their probability distributions. For each realization, the OCP becomes deterministic. After solving the deterministic instances of the problem that correspond to these realizations of the random variables, an ensemble of solutions is obtained, from which statistical information can be extracted. Although Monte Carlo sampling is straightforward to apply as it only requires iterative resolutions of deterministic instances of the OCP, it requires a large number of solutions, because the solution statistics converge relatively slowly. For example, the mean value typically converges as $1/\sqrt{N}$, where N is the number of realizations. The need for large number of solutions for accurate results can lead to an excessive computational cost, especially for OCPs that are already computationally intensive in the deterministic settings, as the mission design problem considered in this thesis. The Generalized Polynomial Chaos (gPC) expansion can contribute to alleviating this drawback.

A systematic and coherent presentation of numerical strategies for uncertainty quantification and stochastic computing is given in [Xiu, 2010], with a focus on the methods based on the gPC approach. Both the intrusive stochastic Galerkin and the nonintrusive stochastic collocation approaches to gPC are illustrated in detail. The nonintrusive stochastic collocation approach based on regression is described in [Sudret, 2008] and [Blatman and Sudret, 2010].

In this thesis, a stochastic collocation method has been selected. With this approach, a small number of sample points of the random variables are used to jointly solve particular instances of the SSOCP. The obtained solutions are then expressed as orthogonal polynomial expansions in terms of the random variables using these sample points. This is a nonintrusive methodology because the model equations are not altered. Depending on the distributions of the random variables, different types of orthogonal polynomials can be chosen to achieve better numerical precision. This technique allows statistical and sensitivity analysis of the stochastic solutions to be conducted at a low computational cost. Thus, the gPC method converts the SSOCP into an augmented deterministic SOCP, in which particular instances of the SSOCP are solved together as a single deterministic OCP. It is important to point out that the gPC method is applicable to solve the SSOCP when the solution depends smoothly on the random variables. This means that the solutions obtained for each combination of sample points of the random variables must give rise to the same discrete solution, i.e., to the same sequence of discrete states of the switched dynamical system that represents the

formation mission.

Sources of uncertainty in ATM

In [Cook et al., 2015], the different sources of uncertainty that affect ATM have been classified according to the following five major groups:

- Data uncertainty. This type of uncertainty is due to the presence of some level of uncertainty in the data or some degree of inaccuracy in the models.
- Data unavailability. In this case, there is lack of information due to managerial or technological barriers.
- Operational uncertainty. In this case, uncertainty is due to decisions taken by humans, e.g. air traffic controllers, flight dispatchers, and pilots.
- Equipment uncertainty. This type of uncertainty is due to problems with aircraft or with the communications, navigation and surveillance equipment.
- Weather uncertainty. This type of uncertainty is due to the presence of winds, thunderstorms, snowfalls, and fog.

From all this sources of uncertainty, it is well known that uncertainty in flight departure times is among the main causes of trajectory uncertainty, which generates inefficiency in the ATM system [Rivas and Vazquez, 2016]. Timing is not only crucial in general ATM operations, but also in formation missions. Indeed, considering the usual cruise speed of most long-haul commercial aircraft, missing the rendezvous location by, for instance, ten minutes means spatially missing the partner aircraft by 150 km. Such cases require catch-up maneuvers, which result in a loss of performance compared to the planned formation mission.

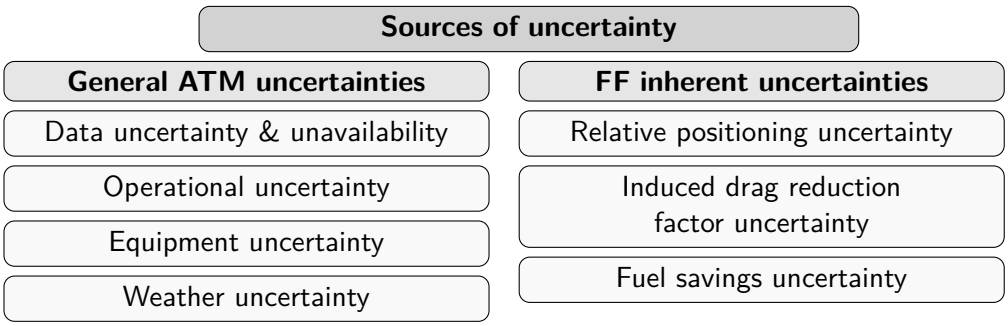

Fig. 6.1: Sources of uncertainty affecting formation flight.

Additionally to the former general ATM-related uncertainties, there are uncertainties inherent to formation flight.

As seen in Chapter 2, in extended formations, due to the great distance between the leader and the follower aircraft, instabilities such as meandering and external factors, may affect the

motion of the vortices. It is therefore important to maintain the relative position between the follower aircraft and the leader's wake vortices precisely, as the potential formation benefits are very sensitive to that relative positioning. However, the relative positioning between the follower aircraft and the leader's wake vortices can not be kept precisely. Therefore, the induced drag reduction factor and the fuel savings achieved in formation flight are actually uncertainties of the formation mission design problem. Fig. 6.1 gives a schematic overview of both, general uncertainties related to ATM and uncertainties inherent to formation flight.

A great number of research studies focused on stochastic modeling. In [Shone et al., 2021] a review of the literature on stochastic modeling with applications to ATM is provided, include literature on stochastic optimal control.

Most of these studies focused on the conflict detection and resolution problem. In [Hu et al., 2005], the problem of aircraft conflict prediction is studied for two-aircraft midair encounters. First, a model is presented for prediction of the aircraft positions along a time horizon, during which each aircraft is following a prescribed flight plan in the presence of additive wind perturbations on its velocity. Then, a method for estimating the probability of conflict is proposed. This method is based on a Markov chain approximation of the stochastic processes that models the aircraft flight. In [Prandini and Hu, 2009], the aircraft conflict prediction problem is formulated as a reachability problem in a stochastic hybrid system framework. Specifically, a switching diffusion model is employed to predict the future positions of an aircraft following a given flight plan, and the probability that the aircraft enters an unsafe region of the airspace is estimated using a numerical algorithm for reachability computation.

In [Li et al., 2014], an approach to aircraft trajectory optimization in the presence of uncertainties based on gPC is presented, where only one random variable has been considered, which represents an uncertain aerodynamic parameter of the dynamic model of the aircraft. This random variable has been modeled as a uniformly distributed random variable. In [Matsuno et al., 2015], a stochastic optimal control method based on gPC is developed for determining conflict-free aircraft trajectories under wind uncertainty. The random processes that represent the components of the wind speed are approximated as a linear combination of deterministic functions multiplied by independent random variables using the Karhunen-Loève expansion.

Although there is a growing interest in addressing uncertainties in the field of ATM, there are very few studies that study formation flight for commercial aircraft in the presence of uncertainties. One of these few research studies is [Kent and Richards, 2014], in which the impact of ground delays on formation flight is studied using stochastic dynamic programming.

Specification of the stochastic formation mission design problem

In this thesis, the formation mission design problem for commercial aircraft in the presence of uncertainties in some of the parameters and boundary conditions of the problem is studied.

Given several commercial flights, the stochastic formation mission design problem consists in establishing how to organize them in formation or solo flights and in finding the trajectories that minimize the expected value of the DOC of the formation mission in the presence of uncertainties. Since each aircraft can fly solo or in various positions within a formation, the mission is modeled as a stochastic switched dynamical system, in which the flight modes of the aircraft are described by sets of stochastic ordinary differential equations, the discrete state describes the combination of flight modes of the individual aircraft, and logical constraints establish the switching logic among the discrete states of the system. Stochastic switched dynamical systems inherit all the features of the deterministic switched dynamical systems seen in Chapter 4.

Both the discrete and the continuous dynamics are affected by uncertainties. This general definition can encompass a wide range of stochastic phenomena. In this thesis, only the stochastic hybrid systems in which random variables only affect the continuous dynamics have been considered. Specifically, random variables represent uncertain in the departure times of the aircraft and in the fuel burn savings for the trailing aircraft. The probability distribution functions of these random variables are assumed to be known.

In the following section, the formulation of an OCP of a stochastic switched dynamical system is introduced.

6.2 The stochastic switched optimal control problem

The presence of random variables in the SOCP converts it into an SSOCP. In the formation mission design problem studied in this thesis, not all the elements of the SSOCP contain random variables. Specifically, the fuel consumption reduction factor $\mathcal{R}_{\text{fuel}}$ in the mass flow rate equation (3.14) of the aircraft flying in formation as a trailing or an intermediate aircraft is a random variable. In contrast, the equations of motion associated with the state variables ϕ, λ, χ, and V do not contain random variables. The departure times of the aircraft are also assumed to be random variables of the SSOCP. One of these departure times coincides with t_I, the initial time of the formation mission. These random variables are assumed to be independent and characterized by probability density functions.

Let $\theta = (\theta_1, \theta_2, \ldots, \theta_N)$ be the vector of random variables that represent the random parameters of the SOCP. For sake of clarity, hereinafter the subindex "SS" will be employed in the formulation of the OCP for stochastic switched dynamical systems. It is assumed that the control vector $u_{SS}(t)$ is deterministic and, therefore, it is a function of time only, whereas the state vector $x_{SS}(t, \theta)$ is stochastic and, therefore, it is a function of both time and the vector of random variables, θ [Li et al., 2014].

The continuous-time SSOCP has been formulated as in [Li et al., 2014], namely all the elements of the problem depend on θ and the dynamic equations, the path constraints, and the boundary conditions must be satisfied almost surely. In the formulation of the SSOCP,

the dynamical equations and endpoint constraints are:

$$\begin{aligned} \dot{x}_{SS}(t,\theta) &= f_{SS,v_{SS}(t)}(t, x_{SS}(t,\theta), u_{SS}(t), \theta) \text{ a.s.}, \\ x_{SS}(t_I,\theta) &= x_I \in \mathbb{R}^n \text{ a.s.}, \\ x_{SS}(t_F,\theta) &= x_F \in \mathbb{R}^n \text{ a.s.}, \\ v_{SS}(t) &\in \{0,1\},\ t_I \le t \le t_F. \end{aligned} \tag{6.1}$$

The performance index of the SSOCP has the following form:

$$\begin{aligned} &J_{SS}\left(t, x_{SS}(t,\theta), u_{SS}(t), v_{SS}(t), \theta\right) = \\ &\mathcal{M}_{SS}(t_F, x_F, \theta) + \int_{t_I}^{t_F} \mathcal{L}_{SS,v_{SS}(t)}(t, x_{SS}(t,\theta), u_{SS}(t), \theta) dt. \end{aligned} \tag{6.2}$$

The SSOCP is thus stated as follows

$$\min_{u_{SS}\in\Omega, v_{SS}\in\{0,1\}} J_{SS}\left(t, x_{SS}(t,\theta), u_{SS}(t), v_{SS}(t), \theta\right), \tag{6.3}$$

subject to dynamical equations and endpoint constraints from the set of Eqs. (6.1). It can be seen that the difference between the formulations of the deterministic SOCP and the SSOCP is that the vector random variables θ is included in the latter.

It is important to point out that probabilistic constraints, also known as chance constraints, could be introduced in the formulation of the SSOCP [Matsuno et al., 2015]. However, in this thesis, chance constraints have not been considered in the formulation of the SSOCP employed to solve the stochastic formation mission design problem.

6.2.1 The generalized polynomial chaos expansion

In this section, following [Li et al., 2014, Matsuno et al., 2015], the gPC expansion is introduced and the method for determining the stochastic solution of the SSOCP and computing its statistical information is described.

Using the gPC expansion, the stochastic solution of the SSOCP can be approximated by a finite sum of orthogonal polynomials. The P-th order gPC approximation of the stochastic solution of the SSOCP, $z(t,\theta)$, can be expressed as

$$z_P(t,\theta) = \sum_{m=1}^{M} C_m(t)\Phi_m(\theta), \tag{6.4}$$

where $\theta = (\theta_1, \theta_2, \ldots, \theta_N)$ is a vector of independent random variables, $C_m(t)$ are the corresponding coefficients of the expansion, which can be obtained using either a nonintrusive or an intrusive approach, and $\Phi_m(\theta)$ are the multivariate orthogonal polynomial basis functions, which are calculated from the l_i-th order one-dimensional polynomial basis function

$\phi^{(l_i)}(\theta_i)$ of the random variable θ_i by means of the tensor product rule as follows:

$$\Phi_m(\theta) = \prod_{i=1}^{N} \phi_i^{(l_i)}(\theta_i). \tag{6.5}$$

Notice that, in Eq. (6.5), a unique combination of $l_i, i = 1, 2, \ldots, N$, corresponds to each subscript m, which satisfy the condition $\sum_{i=1}^{N} l_i \leq P$. The number of tensor product basis functions is $M = \binom{N+P}{N}$.

Orthogonal polynomials basis functions

The orthonormal polynomials in Eq. (6.5) satisfy the following orthogonality condition

$$E[\phi_i^{(j)}(\theta_i)\ \phi_i^{(k)}(\theta_i)] = \int \phi_i^{(j)}(\theta_i)\ \phi_i^{(k)}(\theta_i)\rho_i(\theta_i)d\theta_i = \delta_{jk}, \tag{6.6}$$

where E is the expected value operator, $\rho_i(\theta_i)$ is the probability density function (PDF) of the random variable θ_i, and δ_{jk} is the Kronecker delta function.

To improve convergence, the choice of the orthogonal polynomials should be made on the basis PDF $\rho_i(\theta_i)$. For instance, the Legendre polynomials are the best choice for uniform random variables, whereas Hermite polynomials are the best option for Gaussian random variables. Some relationships between continuous and discrete probability distributions and their correspondent gPC basis polynomials are shown in Tables 6.1 and 6.2, respectively.

Distribution	gPC basis polynomial
Gaussian	Hermite
Uniform	Legendre
Gamma	Laguerre

Table 6.1: Correspondence between continuous random variables type and the gPC basis polynomial.

Distribution	gPC basis polynomial
Poisson	Charlier
Binomial	Krawtchouk
Hypergeometric	Hahn

Table 6.2: Correspondence between discrete random variables type and the gPC basis polynomial.

6.2.2 The stochastic collocation approach

The expansion coefficientes, $C_m(t)$, can be obtained using intrusive or nonintrusive

approaches.

In the stochastic Galerkin method, the gPC expansions in terms of the random variables that represent the sources of uncertainty such as parameters and boundary conditions, are first determined and then the gPC expansions are substituted into the model equations. The Galerkin projection is then performed to project the model equations onto the random space spanned by the polynomial basis. This projection transforms each stochastic equation of the model into a set of coupled deterministic equations. Finally, the resulting system of equations is solved with a suitable numerical method. This is an intrusive methodology in the sense that the model equations are altered. The stochastic Galerkin method can be challenging when the stochastic model equations take complicated forms. In this case, the derivation of the set of deterministic equations can be very difficult or even impossible [Li et al., 2014].

Within the nonintrusive methods, the regression approach and the stochastic collocation method can be employed. The nonintrusive stochastic collocation approach based on regression is described in [Sudret, 2008] and [Blatman and Sudret, 2010]. This method is specially appropriate when the number of random variables considered is high, in general, larger than 10 variables [Matsuno et al., 2015]. In stochastic collocation methods the stochastic model equations are satisfied at a discrete set of points, called nodes, in the corresponding random space. From this point of view, all classical sampling methods like Monte Carlo sampling are collocation methods. However, in stochastic collocation, polynomial approximation theory is employed to locate the nodes, known as collocation points, strategically to increase the numerical accuracy and significantly reduce the sample points.

In this thesis, the coefficients $C_m(t)$ of the expansion (6.4) are calculated using a nonintrusive gPC based stochastic collocation method as follows

$$C_m = E[z(t,\theta)\Phi_m(\theta)] = \int z(t,\theta)\Phi_m(\theta)\rho(\theta)d\theta, \tag{6.7}$$

where $\rho(\theta) = \prod_{i=1}^{N} \rho_i(\theta_i)$ is the joint probability density function of the vector of random variables θ.

A Gaussian quadrature can be employed to approximate the integral in Eq. (6.7) using a set of q collocation points $\theta_i^{(j)}$ for each random variable θ_i and calculating the corresponding set of quadrature weights $\alpha_i^{(j)}$, $j = 1, 2, \ldots, q$.

Higher precision in the quadrature can be achieved by increasing the number of collocation points q. Using the tensor product rule, the total number of collocation points is q^N. This number, which could become large when N, the number of random variables in θ, grows, can be reduced to Q using the sparse grid quadrature based on the Smolyak rule [Xiu, 2010].

Let $\theta^{(j)}$ be the collocation points and $\alpha^{(j)}$, $j = 1, \ldots, Q$, the corresponding weights.

Then, the coefficients of the expansion C_m in Eq. (6.7) are approximated by:

$$C_m \approx \sum_{j=1}^{Q} z(t, \theta^{(j)}) \Phi_m(\theta^{(j)}) \alpha^{(j)}, \tag{6.8}$$

where $z(t, \theta^{(j)})$ denotes the solution of the augmented SOCP obtained using the j-th collocation point $\theta^{(j)}$ and $\Phi_m(\theta^{(j)})$ represents the multivariate orthogonal polynomial basis function evaluated at the j-th collocation point $\theta^{(j)}$. Thus, the SSOCP is converted into an augmented deterministic SOCP, in which particular instances of the SSOCP, which correspond to the collocation points of the random variables, are combined into a single optimal control problem. The resulting augmented SOCP is solved by means of the numerical methods described in chapters 4 and 5. The expected value and variance of the stochastic solution $z_P(t, \theta)$ are calculated using the coefficients of the expansion as follows:

$$E[z_P(t, \theta)] = C_1(t), \tag{6.9}$$

$$\text{VAR}[z_P(t, \theta)] = \sum_{m=2}^{M} C_m^2(t), \tag{6.10}$$

where VAR denotes the variance operator. As stated in Eqs. (6.9) and (6.10), the expected value coincides with the first coefficient, whereas the variance is the sum of the squares of the other coefficients of the gPC expansion. Using the former expressions, statistical information of the solutions of the SSOCP can be easily computed. Additionally, the mean and the standard deviation of some component of the stochastic solution can be expressed as a function of the variables of the SSOCP and included in the objective functional and the constraints of the problem.

A complete treatment of the gPC expansion can be found in the monography [Xiu, 2010], whereas the procedure followed to determine the stochastic solution of the SSOCP and to compute its statistical information is schematically represented in Fig. 6.2. Further details can be found in [Li et al., 2014, Matsuno et al., 2015].

6.2.3 Specification of the stochastic switched optimal control problem

Following the technique described in [Li et al., 2014], the stochastic constraints from Eqs. (6.1) have been converted into deterministic constraints. Likewise, the stochastic objective functional of the SSOCP from Eq. (6.2) has been converted into a deterministic functional by taking its expected value. The new formulation of the SSOCP can be expressed

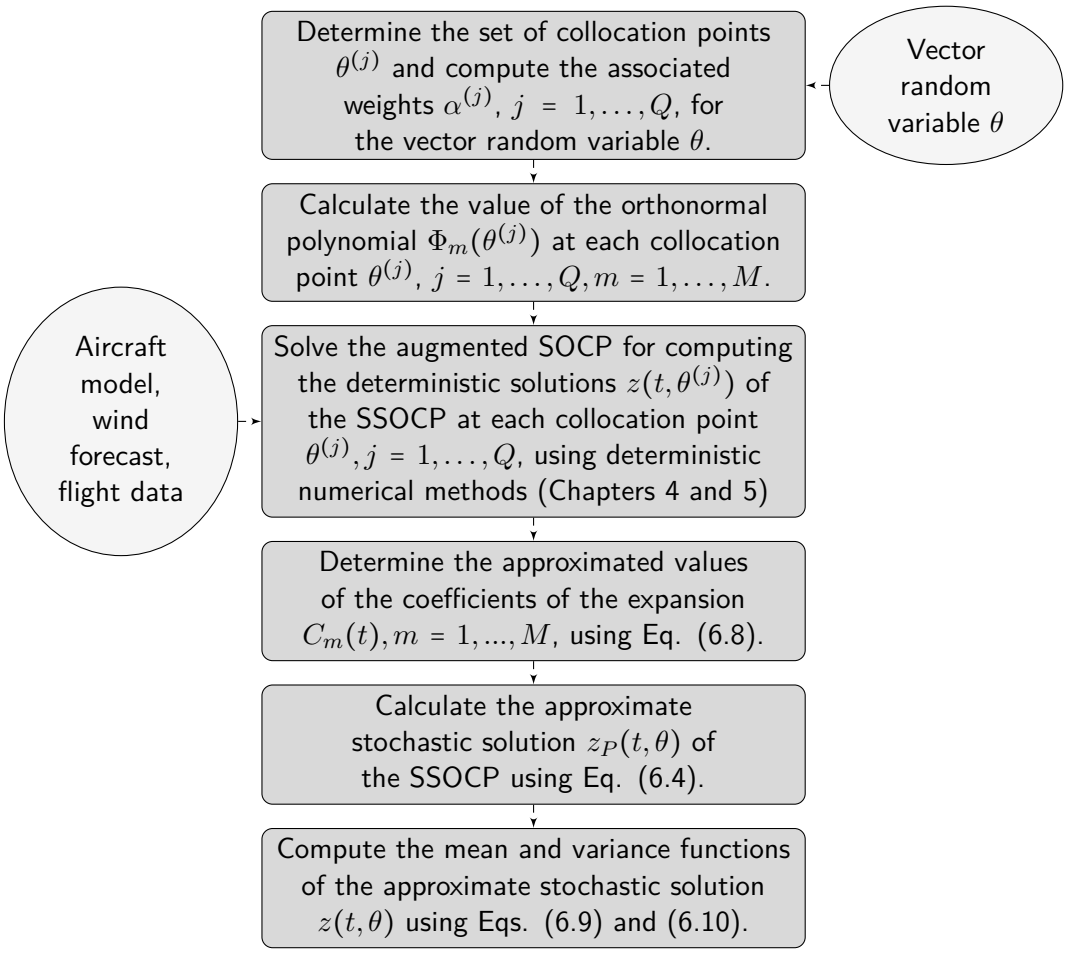

Fig. 6.2: Schematic diagram of the procedure for determining the stochastic solution of the SSOCP and computing its statistical information.

as follows

$$
\begin{aligned}
\min_{\substack{u_{SS}\in\Omega,\\ v_{SS}\in\{0,1\}}} \; & J_{SS} = E\left[\mathcal{M}_{SS}(t_F,x_F,\theta) + \int_{t_I}^{t_F} \mathcal{L}_{SS,v_{SS}(t)}(t,x_{SS}(t,\theta),u_{SS}(t),\theta)dt\right] \\
& s.t. \\
& \dot{x}_{1_{SS}}(t,\theta_1) = f_{SS,v_{SS}(t)}(t,x_{SS}(t,\theta_1),u_{SS}(t),\theta^{(1)}), \\
& \dot{x}_{2_{SS}}(t,\theta_2) = f_{SS,v_{SS}(t)}(t,x_{SS}(t,\theta_2),u_{SS}(t),\theta^{(2)}), \\
& \qquad\qquad \vdots \\
& \dot{x}_{N_{SS}}(t,\theta_N) = f_{SS,v_{SS}(t)}(t,x_{SS}(t,\theta_N),u_{SS}(t),\theta^{(Q)}), \\
& E\left[x_{SS}(t_I,\theta)\right] = x_I \in \mathbb{R}^n, \\
& E\left[x_{SS}(t_F,\theta)\right] = x_F \in \mathbb{R}^n, \\
& v_{SS}(t) \in \{0,1\},\ t_I \le t \le t_F,
\end{aligned}
\tag{6.11}
$$

where $\theta^{(1)}, \theta^{(2)}, \ldots, \theta^{(Q)}$ are the Q collocation points of the vector random variable θ.

Solution of the stochastic switched optimal control problem

As already seen in Chapter 4, deterministic switched dynamical systems are described by both a continuous and a discrete dynamics, in which the transitions among discrete states are not established in advance. Stochastic switched dynamical systems inherit all the features of the deterministic switched dynamical systems.

The stochastic collocation method converts the SSOCP into an augmented deterministic SOCP. With this approach, a small number of sample points of the random parameters are employed to jointly solve particular instances of the SOCP. The same methodology as the one explained in Chapter 4 for deterministic SOCP can be followed, obtaining an augmented deterministic EOCP with inequality and equality constraints which can be solved using the optimal control techniques explained in Chapter 5.

The solution of the SSOCP includes both the state and control variables of the system that represent the formation mission. Due to the presence of the vector of random variables in the SSOCP, the solution is stochastic, i.e., it depends on the actual realization of the vector random variable. In particular, it is a random function of state or time. Therefore, the solution is actually a random process, characterized by the mean function and the corresponding 95% confidence envelope. Specifically, the observed values of a state variable at a given time t is a random variable. In this case, the random process is a random function of time. Likewise, the time at which a given value of the state variable is reached is a random variable. This means that the timing of the trajectories, which is defined as the time at which a state is reached, is also a random process. In this case, the random process is a random function of the state. In this paper, the timing of the trajectories is represented as a random function of the orthodromic distance from the departure location. For the sake of ease of exposition, the stochastic solution of the SSOCP is denoted in the following sections as a random function of time. All the random variables observed at specific time instants or states are characterized by their expected values and by the corresponding 95% confidence intervals, including the arrival times and the fuel consumption of the aircraft of the formation mission.

6.3 Sensitivity analysis of the solution

The purpose of the sensitivity analysis is to identify the random variables that have more influence on the variability of a component of the stochastic solution with the aim of reducing its variability acting on the source. Therefore, in this thesis, a global sensitivity analysis of the stochastic solution is also conducted [Saltelli et al., 2008] in the numerical experiment that involves two random variables such as Experiment B presented in Chapter 8, in which a two-aircraft transoceanic mission design problem with uncertainty in the departure times of both flights is addressed.

In particular, the aim of the variance-based sensitivity analysis is to quantify what proportion of the variance of each component of the solution $z(t, \theta)$ of the formation mission design problem is due to the variance of each component $\theta_j, j = 1, 2, \ldots, N$ of the random vector θ.

In this thesis, this analysis relies on the computation of the so-called Sobol' indices, under the assumption that the random variables in θ are independent [Saltelli et al., 2008]. Sobol' indices can be directly derived from the coefficients $C_m(t)$ of the gPC expansion (6.4) as explained in [Trucchia et al., 2019].

Following [Trucchia et al., 2019], the Sobol' index $S_{i,j}(t)$ for the i-th component of the solution $z(t, \theta)$ and the j-th component of the random variable θ can be expressed as

$$S_{i,j}(t) = \frac{1}{\mathrm{VAR}_i} \sum_{m \in I} C_m^2(t), \tag{6.12}$$

where VAR_i is the variance calculated in Eq.(6.10) for the i-th component of the solution and I is the set of multi-indices such that the computation of $S_{i,j}(t)$ only includes terms that depend on the random variable θ_j, $j = 1, 2, \ldots, N$.

6.4 Conclusions

In this chapter, the formulation of the stochastic optimal control problem employed to model the stochastic formation mission design problem is presented and the approach followed to solve it is described. It is a nonintrusive polynomial chaos based stochastic collocation method, which converts the stochastic switched optimal control problem into an augmented deterministic switched optimal control problem. With this approach, a small number of sample points of the random parameters are used to jointly solve particular instances of the switched optimal control problem. The obtained solutions are then expressed as orthogonal polynomial expansions in terms of the random parameters using these sample points. The technique allows statistical and global sensitivity analysis of the stochastic solutions to be conducted at a low computational cost.

Chapter 7

Deterministic Formation Mission Design Problem

In this chapter, to show the effectiveness of the methodology described in Chapter 4 in solving the formation mission design problem in the absence of uncertainties, the results of three different numerical experiments will be described. All the experiments involve transoceanic eastbound flights operated by Airbus 330-200 aircraft. In the first experiment, a two-aircraft formation mission design problem is solved, in which one flight's departure time is free. Then, the optimal solution of this problem has been assumed as the baseline case for the next experiment, in which different delays in the departure times of both flights have been considered. Finally, a three-aircraft formation mission design problem is solved, in which different fuel savings schemes have been considered. For each experiment, a detailed description of the results is given together with a comparison with the results obtained in solo flights.

7.1 General description of the experiments

The following numerical experiments have been carried out:

- Experiment A: Two-aircraft transoceanic mission design with one flight's departure time free.
- Experiment B: Two-aircraft transoceanic mission design with delays in the departure times.
- Experiment C: Three-aircraft transoceanic mission design with different fuel savings schemes.

All the experiments involve transoceanic eastbound flights. Wind data from the ERA-INTERIM reanalysis database has been used. As mentioned above, in this study only the cruise phase has been modeled, the rest of the flight phases are neglected. Thus, the initial

and final cruise phase locations of the cruise phase of the flights have been assumed to be the latitudes and longitudes of the departure and arrival airports of each flight at cruise altitude. Airbus A330-200 aircraft BADA models have been considered for each flight. The initial mass of each aircraft is assigned as well as the initial and final velocities, which have been set at typical cruise values for the selected aircraft models. The initial heading angle is set to the initial heading angle of the orthodromic path between the initial and final locations of each flight. Arrival times are left free and a constraint on the maximum temporal deviation from the scheduled arrival time of 45 minutes has been introduced for each flight. The time and fuel burn weighting parameters, α_t and α_f, in the objective functional have been set to 0.3 and 0.7, respectively, based on the CI definition, as explained in Section 3.4.

The numerical experiments have been conducted on a 3.6 GHz Intel Core i9 computer with 32 GB RAM. The computational times reported in this section include both the time required to generate the warm-start solution and the time to find the optimal solution of the problem. The warm-start solution is a feasible solution of the problem generated by the NLP solver from initial guesses of the solution. The initial guesses for the latitude, the longitude and the heading angle have been generated using the orthodromic between departure and arrival locations of each flight. Typical cruise velocity and fuel consumption of the aircraft model selected have been used to generate the initial guesses of the velocity and the mass of each aircraft during the flight, respectively.

7.2 Experiment A: Two-aircraft transoceanic mission design with one flight's departure time free

7.2.1 Description of the experiment

Experiment A involves two transoceanic eastbound flights, Flight 1 and Flight 2, with given fuel savings for the trailing aircraft and boundary values of the state variables. Flight 1 and Flight 2 are operated by Aircraft 1 and Aircraft 2, respectively. In the SOCP stated to solve the mission design problem, the departure time of Flight 1 is fixed, whereas the departure time of Flight 2 is left free. In case of formation, Aircraft 1 will be the trailing one and Aircraft 2 will be the leader. Solving this problem entails to decide which mode of flight, i.e. formation or solo flight, is optimal, the optimal trajectories of the aircraft and the optimal departure time of Flight 2. Additionally, in case of formation flight, the rendezvous and splitting locations and times must also be determined. To check the optimality of the obtained solution, a comparison between formation flight and solo flight results has been carried out.

The two transoceanic flights considered in this experiment have the following departure and arrival locations:

- Flight 1: New York (`JFK`) - Madrid (`MAD`).

- Flight 2: Montreal (YUL) - London (LHR).

The fuel burn savings for the trailing aircraft is set to 10%. The departure time of Flight 1 has been set to 10:15. The boundary conditions for the state variables of each aircraft are listed in Table 7.1.

Symbol	Units	Flight 1	Flight 2
ϕ_I	[deg]	40.64	45.47
ϕ_F	[deg]	40.48	51.47
λ_I	[deg]	-73.78	-73.74
λ_F	[deg]	-3.57	-0.45
χ_I	[deg]	66.51	55.70
V_I	[m/s]	240	240
V_F	[m/s]	220	220
m_I	[kg]	$220\,000$	$215\,000$

Table 7.1: Experiment A: Boundary conditions.

As mentioned above, the formation configuration is selected in advance. In case of formation flight, Aircraft 1, associated to Flight 1, is forced to be the trailing aircraft. Hence, Aircraft 2, associated to Flight 2, will be the leader one.

7.2.2 Results

Optimal routes

In the optimal solution, formation flight has been selected as the optimal solution and the obtained optimal departure time for Flight 2 has been 10:50, 35 minutes after the departure of Flight 1. The obtained optimal formation flight routes are represented in Fig. 7.1, together with the solo flight routes and the wind field. In this figure, dashed lines are used to plot solo flight routes and solid lines are used to represent formation flight routes. Green and blue lines represent Flight 1 and Flight 2, respectively.

Flight 1 starts 35 minutes before Flight 2, and due to this difference in the departure times, the optimal solution implies a large initial detour of Flight 1 with respect to solo flight, in order to join Flight 2 as soon as possible, thereby, the rendezvous point is very close to the departure location of Flight 2.

Optimal state and control variables

The corresponding state and control variables are represented in Fig. 7.2 and Fig. 7.3, respectively. For a better understanding of these figures, the portions of the plots of the variables that correspond to formation flight have been represented on a grey background. It can be observed that the heading angle and the Mach number of both aircraft are the same during the formation, as opposed to the mass flow rate which is different for each aircraft.

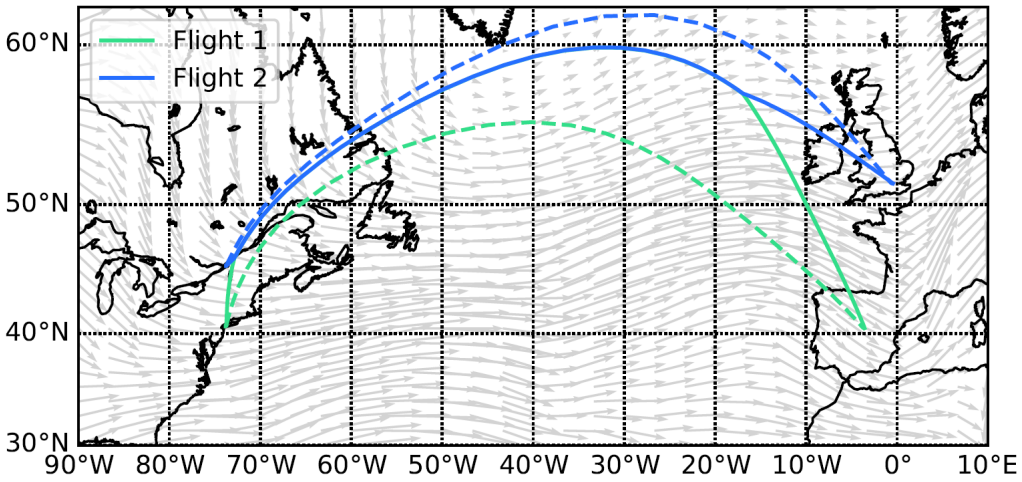

Fig. 7.1: Experiment A: Solo and formation flight routes.

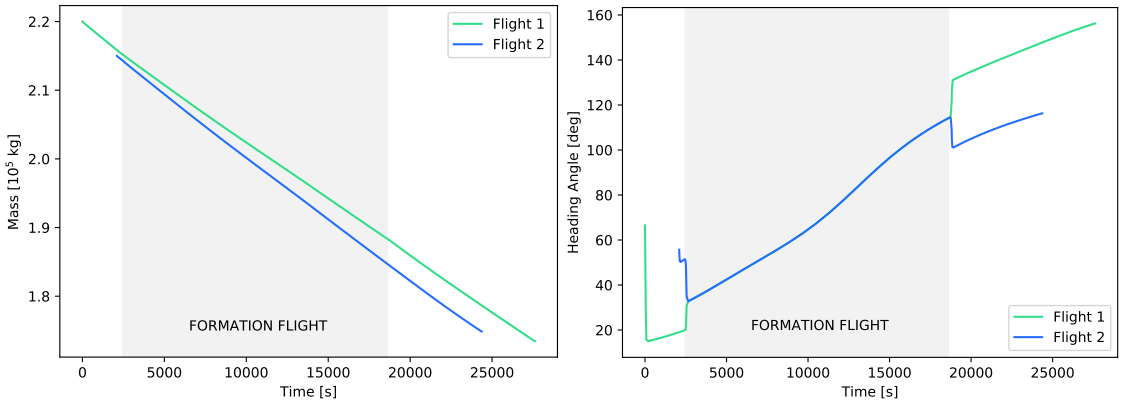

(a) Mass

(b) Heading angle

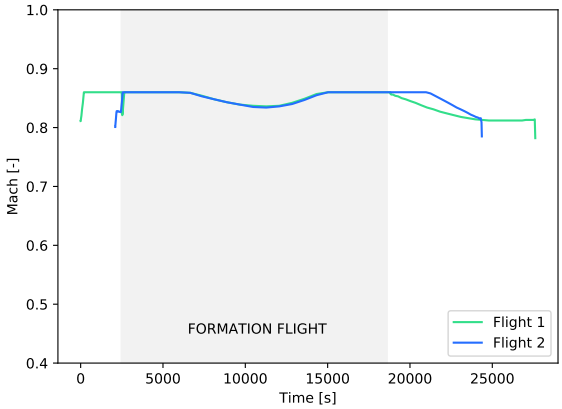

(c) Mach number

Fig. 7.2: Experiment A: State variables.

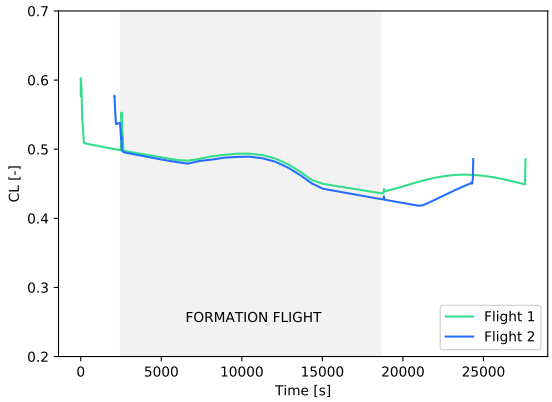

(a) Lift coefficient

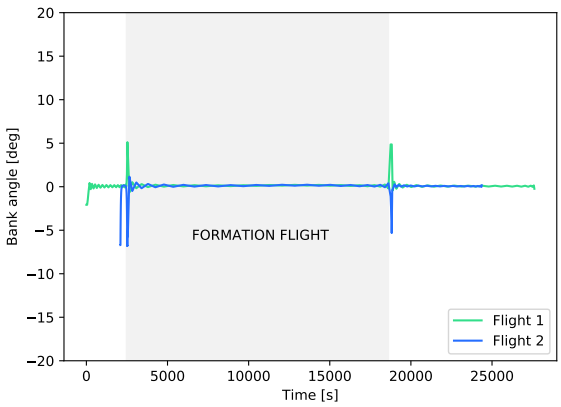

(b) Bank angle

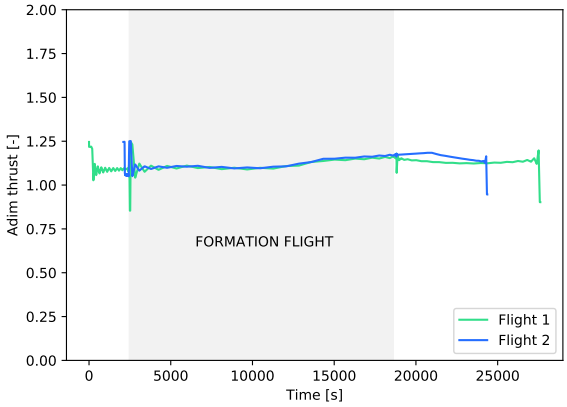

(c) Adimensional thrust

Fig. 7.3: Experiment A: Control variables.

All the state variables vary smoothly, except the heading angle and the Mach number at the beginning and at the end of the flight. This behavior of the state variables is typical in boundary value problems, in which a quick maneuver is necessary to steer each aircraft from its initial state to its optimal route and from the optimal route to the final state. On the other hand, the control variables vary in a quite smooth way except around the switching instants. Notice that, the Gibbs phenomenon, described in Section 5.3.2, is present near the rendezvous and the splitting locations. However, this non-smooth behavior at the switching times lasts for a very short period of time compared with the total flight time.

	Flight Time $[h]$	**Fuel Burn $[kg]$**	**Covered Distance $[km]$**	**DOC $[mu]$**
Formation F.	7.68	46543.93	6716.44	40875.15
Solo F.	7.47	48596.82	6205.81	42085.37

Table 7.2: Experiment A: Solo and formation flight results for Flight 1.

	Flight Time [h]	Fuel Burn [kg]	Covered Distance [km]	DOC [mu]
Formation F.	6.19	40130.77	5348.58	34776.74
Solo F.	6.18	39683.14	5462.84	34452.60

Table 7.3: Experiment A: Solo and formation flight results for Flight 2.

In this experiment, the great circle distance between departure and arrival locations of Flight 1 is 5761.08 km and the great circle distance between departure and arrival locations of Flight 2 is 5214.72 km. For these flights, the great circle distance between departure locations is 537.00 km and the great circle distance between arrival locations is 1244.77 km. Thus, this scenario and the selected fuel burn saving for the trailing aircraft can be considered not optimistic for formation flight.

Comparison with the results obtained in solo flight

Tables 7.2 and 7.3 summarize the results obtained in formation and solo flights for Flight 1 and Flight 2, respectively. As expected, the flight times increase for both aircraft in formation flight with respect to solo flight, although for Flight 2 this flight time increment is negligible. Moreover, the fuel consumption of Aircraft 2, the leader aircraft, increases whereas the fuel consumption of Aircraft 1, the trailing one, decreases. The DOC is expressed in generic monetary units, mu. The total DOC of formation flight is almost one thousand generic monetary units lower than that of the solo flight, which amounts to more than one percent of reduction. For Flight 1, the total flight distance covered in formation flight is more than 500 km larger than in solo flight. Surprisingly, for Flight 2, the total flight distance covered in formation flight is smaller than the distance covered in solo flight. Obviously, both of them are higher than the great circle distance. The reason behind this unexpected result for Flight 2 is the Jet Stream. Indeed, in order to get the greatest benefits from the wind field, Aircraft 2 in solo flight takes a route more than 200 km longer than the orthodromic route. In case of formation, this large detour, which would involve both aircraft, becomes less advantageous and therefore it does not appear in the optimal solution.

7.3 Experiment B: Two-aircraft transoceanic mission design with delays in the departure times

7.3.1 Description of the experiment

The flights considered in Experiment B, Flight 1 and Flight 2, have the same departure and arrival locations, the same boundary values for the state variables of each aircraft, and the same fuel burn savings for the trailing aircraft as in Experiment A. As before, in case of formation flight, Aircraft 1, associated to Flight 1, is forced to be the trailing aircraft and Aircraft 2, associated to Flight 2, is the leader one. The difference with respect to Experiment

A is that several delays in the departure times of both flights have been considered.

This experiment has been carried out to determine how delays in the departure times of both flights affect the formation flight, in terms of routes, rendezvous and splitting locations and times, until formation flight becomes non-optimal and, as a consequence, solo flights are selected by the algorithm.

	Delays [min]	
Cases	**Flight 1**	**Flight 2**
B_1	20	0
B_2	15	0
B_3	10	0
B_4	5	0
$\boldsymbol{B_5}$	-	-
B_6	0	5
B_7	0	10
B_8	0	15
B_9	0	20
B_{10}	0	25

Table 7.4: Experiment B: Delays in the departure time with respect to the baseline scenario for the different cases.

For this analysis, several numerical simulations have been conducted introducing delays in the departure times of both flights in Experiment A, namely, 10:15 for Flight 1 and 10:50 for Flight 2, which represents the baseline case. In particular, five-minute increments in the delays have been considered for each flight. The actual values of the delays are listed in Table 7.4, in which each case is identified by a different symbol $B_1, \ldots, B_{10}$, being B_5 the baseline case.

7.3.2 Results

Optimal routes

For a better understanding of the results, the optimal aircraft routes obtained for different delays in the departure times are represented together in Fig. 7.4, in which the green and blue lines represent the optimal routes of Flight 1 and Flight 2, respectively. The optimal route obtained in the baseline case, B_5, is represented with a thicker line. Notice that, in this figure, the scale is not the same for latitude and longitude axes, and the symbols on the third axis denote the different cases.

Optimal rendezvous and splitting locations and times

In particular, Fig. 7.4 shows the rendezvous and splitting locations for each case, which are represented with small black stars and triangles, respectively. It can be observed that there is a great dependency of the location of the rendezvous points on the delay. For instance, in cases

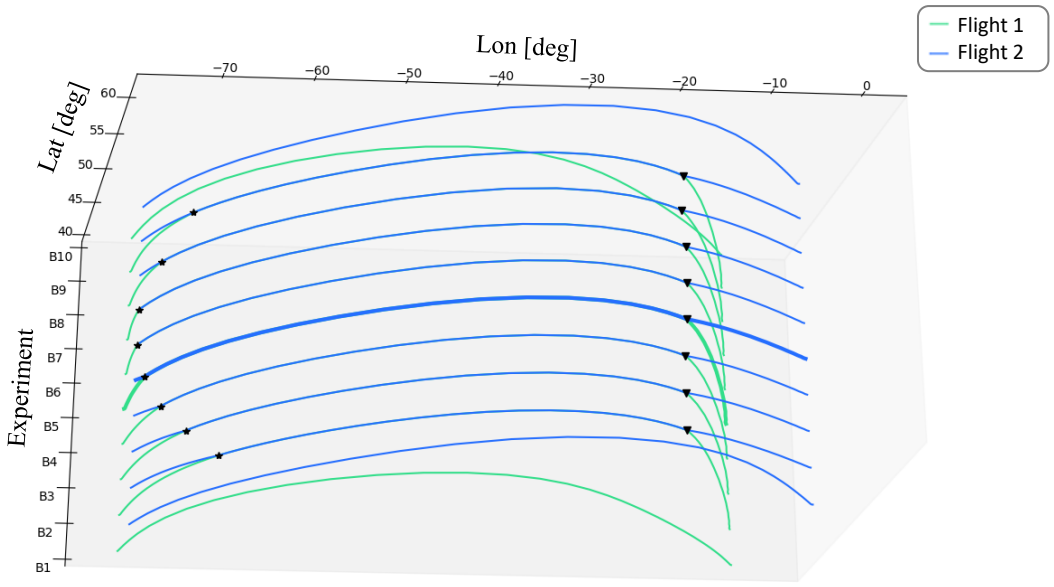

Fig. 7.4: Experiment B: Routes obtained in the different cases considered.

B_6 and B_7, the rendezvous location is very close to the departure location of Flight 2. On the contrary, the splitting locations barely change with delay. When the delay on one departure time increases, since it takes more time for the delayed aircraft to reach the other one, the rendezvous point changes. However, once the formation is created, both aircraft follow a very similar route for all the cases regardless of the delay in the departure time, and therefore, the optimal splitting locations do not change significantly. In Table 7.5, the rendezvous and splitting locations and the distance covered flying in formation obtained in cases $B_2, \ldots, B_9$ are displayed. Notice the proximity of the splitting locations in all the cases and the closeness among the rendezvous locations in cases B_6 and B_7 and the departure location of Flight 2. On the contrary, the individual flight times and the duration of the formation flight, as well

	Rendezvous (Lat, Lon) [deg]	**Splitting (Lat, Lon) [deg]**	**FF Distance [km]**
$\boldsymbol{B_2}$	(51.26, -65.69)	(57.05, -17.13)	3208.86
$\boldsymbol{B_3}$	(49.15, -68.85)	(57.04, -17.11)	3536.29
$\boldsymbol{B_4}$	(47.10,-71.22)	(57.04, -17.06)	3829.61
$\boldsymbol{B_5}$	**(46.04, -72.86)**	**(57.05, -16.83)**	**4024.45**
$\boldsymbol{B_6}$	(45.48, -73.71)	(57.06, -16.71)	4130.80
$\boldsymbol{B_7}$	(45.49, -73.72)	(57.06, -16.71)	4130.68
$\boldsymbol{B_8}$	(47.59, -71.91)	(57.06, -16.69)	3823.66
$\boldsymbol{B_9}$	(49.92, -69.09)	(57.06, -16.73)	3523.89

Table 7.5: Experiment B: Rendezvous and splitting locations and formation flight distance.

as the rendezvous and splitting times significantly change due to the initial detour made by both aircraft to create the formation. In Table 7.6, the rendezvous and splitting times and the duration of the formation flight for each case are listed. Notice that in cases B_1 and B_{10} solo flight is the optimal option. Therefore, the corresponding results have not been reported in tables and figures, where only the results obtained in formation flight are given. Further information on the results of cases B_1 and B_{10} can be found in the results of Experiment A.

	Time [h]		
	Rendezvous	**Splitting**	**FF duration**
$\boldsymbol{B_2}$	1.58	5.21	3.63
$\boldsymbol{B_3}$	1.22	5.21	3.99
$\boldsymbol{B_4}$	0.90	5.22	4.33
$\boldsymbol{B_5}$	**0.70**	**5.24**	**4.54**
$\boldsymbol{B_6}$	0.67	5.32	4.66
$\boldsymbol{B_7}$	0.75	5.40	4.66
$\boldsymbol{B_8}$	1.15	5.45	4.30
$\boldsymbol{B_9}$	1.61	5.58	3.96

Table 7.6: Experiment B: Rendezvous and splitting times and formation flight duration.

Direct operating costs

The main results in terms of the objective functional are reported in Table 7.7. In particular, the variations in the flight time and in the fuel consumption for each flight and the reduction in the DOC obtained in cases $B_2, \ldots, B_9$, all of them compared to solo flights results, are reported. It can be observed that, in general, the more the flight time of Flight 1 increases, the less the flight time of Flight 2 does and vice versa. Additionally, for those cases in which Flight 2 is delayed, the flight time increment of Flight 2 is very small. About the fuel burn, it can be seen that the greatest benefits for the trailing aircraft are achieved in the baseline case, which is the optimal one, as established in Experiment A. Notice the similarity among increments in fuel burn for Flight 2 in the results of cases B_6, B_7, B_8, and B_9, in which Flight 2 has a delay in the departure time. The greatest DOC reduction is 1.17% and the smallest is 0.02%. This tiny DOC reduction implies that flying in formation in case B_9 has negligible benefits, which could be further reduced by any contingency during the flight.

In general, one may conclude that the greatest flight distances covered in formation flight correspond to the highest total benefits in the fuel burn reduction. However, comparing the results displayed in tables 7.5 and 7.7, it is easy to check that longer distances covered in formation flight and greater duration of formation flight do not always imply more benefits in terms of reduction of DOC. It can be seen in tables 7.5 and 7.6, that in the results of cases B_6 and B_7, aircraft are flying 4.66 hours and about 4130 km in formation, being the greatest duration of formation flights and the greatest distance covered in formation flights,

	Δ Time [%]		Δ Fuel burn [%]		
	Flight 1	**Flight 2**	**Flight 1**	**Flight 2**	**Δ DOC [%]**
B_2	+2.56	+ 3.96	-3.30	+ 1.97	-0.14
B_3	+2.56	+ 2.60	-3.74	+ 1.80	-0.51
B_4	+2.57	+ 1.26	-4.13	+ 1.55	-0.89
B_5	**+2.79**	**+ 0.05**	**-4.22**	**+ 1.13**	**-1.17**
B_6	+3.79	+ 0.14	-4.15	+ 1.01	-1.09
B_7	+4.94	+ 0.13	-3.74	+ 1.01	-0.79
B_8	+6.07	+ 0.08	-3.06	+ 1.01	-0.36
B_9	+7.25	+ 0.07	-2.54	+ 1.00	-0.02

Table 7.7: Experiment B: Flight times, fuel burn and DOC variations compared to solo flights.

respectively. Nevertheless, as it can be observed in Table 7.7, the corresponding reductions in the DOC with respect to solo flights are 1.09% and 0.79%, respectively. The reduction of the DOC is slightly smaller than the one obtained in the baseline case, which amounts to 1.17%.

Table 7.8 has been added to give information about the total detour done by each flight. As in Experiment A, in all the cases considered in Experiment B there is a reduction in the distance covered by Flight 2 in formation flight compared to solo flight. Noteworthy is the great detour made by Flight 1 in the formation flight solution: about 500 kilometers of diversion from the solo flight route.

	Δ Distance [km]	
	Flight 1	Flight 2
B_2	451.21	-123.32
B_3	455.03	-127.23
B_4	467.05	-123.25
B_5	**510.62**	**-114.26**
B_6	543.56	-108.73
B_7	544.79	-111.76
B_8	516.48	-110.18
B_9	507.60	-109.73

Table 7.8: Experiment B: Extra distance covered compared to solo flight distance.

Computational time

Computational times have been quantified in order to show the advantages in terms of computational time to solve the formation mission design problem given by the method presented in this thesis with respect the multiphase approach. The same instances of the problem have been solved with both techniques.

The average computational time to find the solution has been 4.234 s. For the

sake of comparison, the same problem has been solved using a multiphase method [Hartjes et al., 2019]. In this case, two different OCP have been solved, namely, one in which aircraft flight solo and another one in which they are forced to fly in formation. The average computational time has been 7.784 s.

7.4 Experiment C: Three-aircraft transoceanic mission design with different fuel savings schemes

7.4.1 Description of the experiment

Experiment C involves three transoceanic eastbound flights, Flight 1, Flight 2 and Flight 3, with given fuel savings scheme and boundary values of the state variables. Flight 1, Flight 2, and Flight 3 are operated by Aircraft 1, Aircraft 2, and Aircraft 3, respectively. The three flights considered in this experiment have the following departure and arrival locations, the first two of them being the same as in Experiment A:

- Flight 1: New York (`JFK`) - Madrid (`MAD`).
- Flight 2: Montreal (`YUL`) - London (`LHR`).
- Flight 3: Boston (`BOS`) - Paris (`CDG`).

The departure times of Flights 1,2, and 3, are set to 10:15, 10:50, and 10:30, respectively. The first two of them are the same as in Experiment A. The boundary conditions for the state variables of the three aircraft are given in Table 7.9. The boundary conditions for the state variables of Aircraft 1 and Aircraft 2 are the same as in Experiment A.

Symbol	Units	Flight 1	Flight 2	Flight 3
ϕ_I	[deg]	40.64	45.47	42.36
ϕ_F	[deg]	40.48	51.47	48.85
λ_I	[deg]	-73.78	-73.74	-71.06
λ_F	[deg]	-3.57	-0.45	2.35
χ_I	[deg]	66.51	55.70	56.46
V_I	[m/s]	240	240	240
V_F	[m/s]	220	220	220
m_I	[kg]	$220\,000$	$215\,000$	$210\,000$

Table 7.9: Experiment C: Boundary conditions for the three flights.

The relative position of each aircraft in the formation is selected in advance. In case of two-aircraft formation flights that include Aircraft 3, Aircraft 3 will be the leader aircraft and Aircraft 1 or Aircraft 2 will be the trailing. In case of two-aircraft formation flights that do not include Aircraft 3, Aircraft 2 will be the leader aircraft and Aircraft 1 will be the trailing.

In case of three-aircraft formation flights, Aircraft 3 will be the leader aircraft, Aircraft 2 the intermediate, and Aircraft 1 the trailing.

Table 7.10 summarizes the results obtained assuming that each flight is performed as a solo flight. It can be observed that the flight times, the fuel consumption, the covered distance, and the DOC of each flight are quite different.

	Flight 1	**Flight 2**	**Flight 3**
Flight Time [h]	7.47	6.19	6.90
Fuel burn [kg]	48596.82	39683.14	42877.40
Covered Distance [km]	6205.81	5462.84	5945.89
DOC [mu]	42087.53	34462.32	37466.18

Table 7.10: Experiment C: Results for the three solo flights.

An analysis is performed to determine how the fuel savings scheme affects the formation flight, in terms of routes, rendezvous and splitting locations and times, and flight times.

As already mentioned, the only formation configuration allowed is the in-line formation and the relative position of the aircraft in the formation is fixed. The considered benefits for the intermediate and the trailing aircraft range from 6% to 14%. Several numerical simulations have been conducted introducing changes in the fuel savings for the intermediate and trailing aircraft, in which each case is identified by a different symbol $C_1, \ldots, C_5$. The fuel savings considered in the different cases for the intermediate and trailing aircraft have been listed in Table 7.11.

	Fuel savings [%]
$\boldsymbol{C_1}$	6
$\boldsymbol{C_2}$	8
$\boldsymbol{C_3}$	10
$\boldsymbol{C_4}$	12
$\boldsymbol{C_5}$	14

Table 7.11: Experiment C: Fuel savings for the intermediate and the trailing aircraft, in the different cases.

7.4.2 Results

Optimal routes

The optimal formation flight routes obtained in case C_3 are represented in Fig. 7.5, together with the solo flight routes and the wind field. In this figure, dashed lines are used to plot solo flight routes and solid lines are used to represent formation flight routes. Green, blue, and red lines represent Flight 1, Flight 2, and Flight 3, respectively. For the sake of brevity, the routes obtained in the other cases have been omitted.

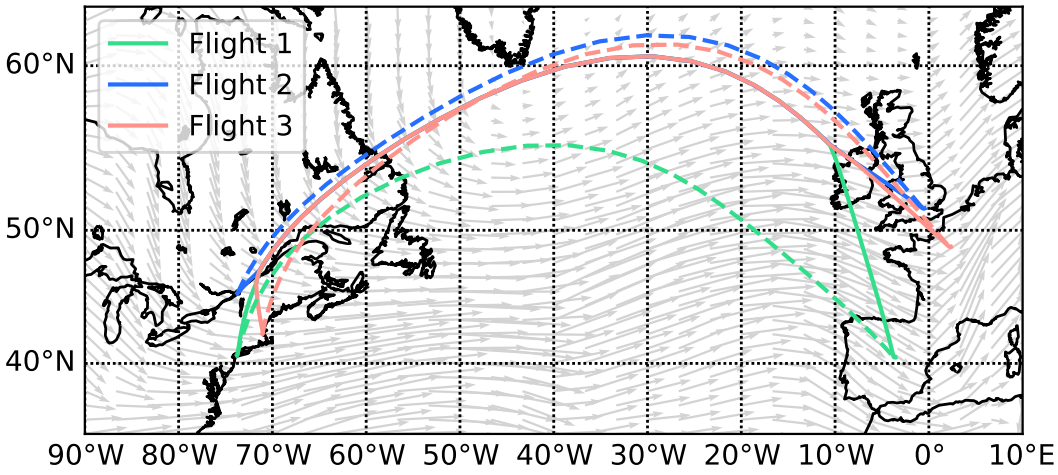

Fig. 7.5: Experiment C: Solo and formation flight routes.

In the optimal solutions of all the cases considered, there are five discrete states of the switched dynamical system that represent the joint behavior of the aircraft. In Fig. 7.6 a schematic representation of these five discrete states, from State I to State V, is given. In particular, each discrete state is characterized by the following modes

- State I: all the aircraft fly in solo mode.
- State II: two aircraft fly in formation and one in solo mode.
- State III: all the aircraft fly in formation.
- State IV: two aircraft fly in formation and one in solo mode.
- State V: all the aircraft fly in solo mode.

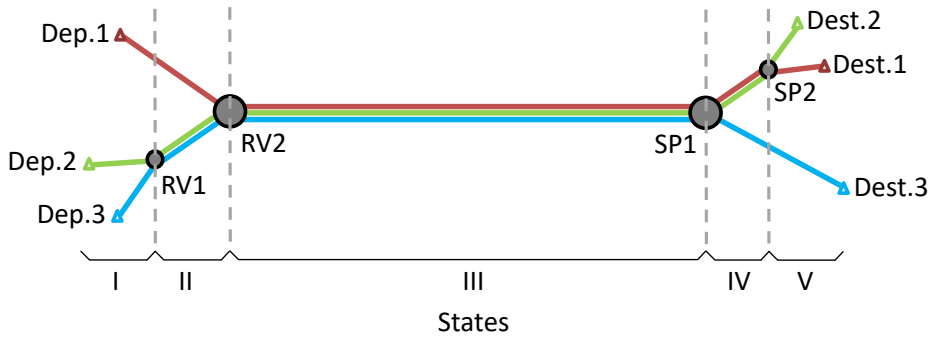

Fig. 7.6: Experiment C: Discrete states representation for three-aircraft formation.

It is easy to see that in the switches among these discrete states, there are two rendezvous points, RV1 and RV2, where RV1 is the first one and RV2 is the second one, and two splitting points, SP1 and SP2 , where SP1 is the first one and SP2 is the second one. In Fig. 7.6, the points RV1, RV2, SP1, and SP2 are represented with grey points. Small triangles have been used to represent the departure and destination of each flight.

Optimal rendezvous and splitting locations and times

Figs. 7.7 and 7.8 represent the three-aircraft routes obtained in cases $C_1, \ldots, C_5$. In these figures, the behavior of the rendezvous and splitting locations, respectively, is detailed. It can be observed that the location of both rendezvous points, RV1 and RV2, and the location of the second splitting point, SP2, do not present significant variations in the different cases. On the contrary, the location of the first splitting point, SP1, notably changes, differing in some cases in more than 1000 km. This variation in the location of SP1, which is the point in which there is a switch between State III and State IV, implies that the three-aircraft formation time and distance largely depend on the fuel savings scheme. Consequently, the formation time and distance in State IV also have a high dependency on it. Results in tables 7.12 and 7.13 confirm this conclusion. It can also be observed in these tables that, in all the considered cases, the formation times and distances corresponding to discrete State II are small compared to other discrete states.

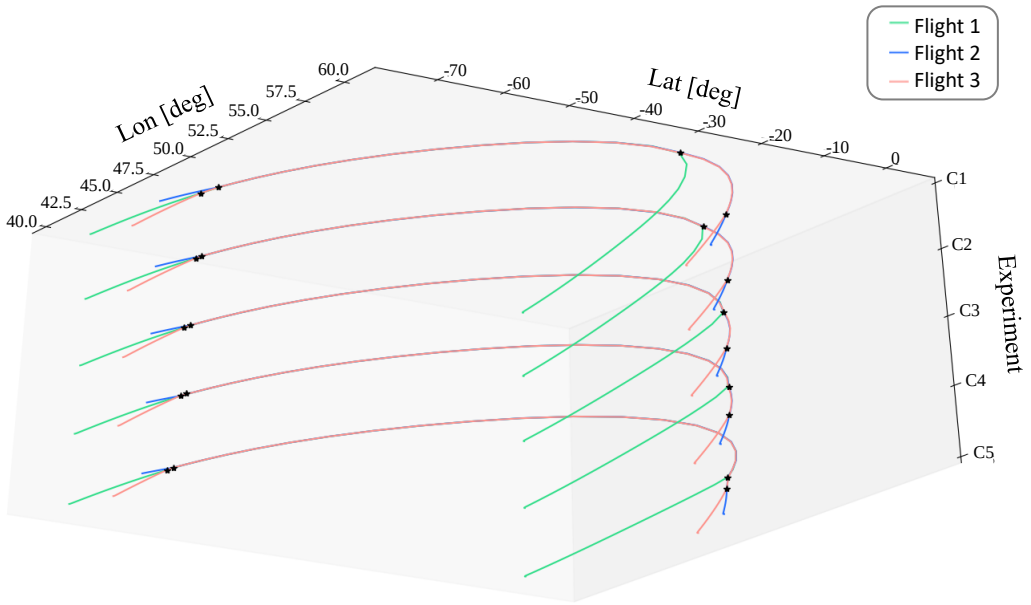

Fig. 7.7: Experiment C: Routes obtained in the different cases considered. Detail of the rendezvous locations.

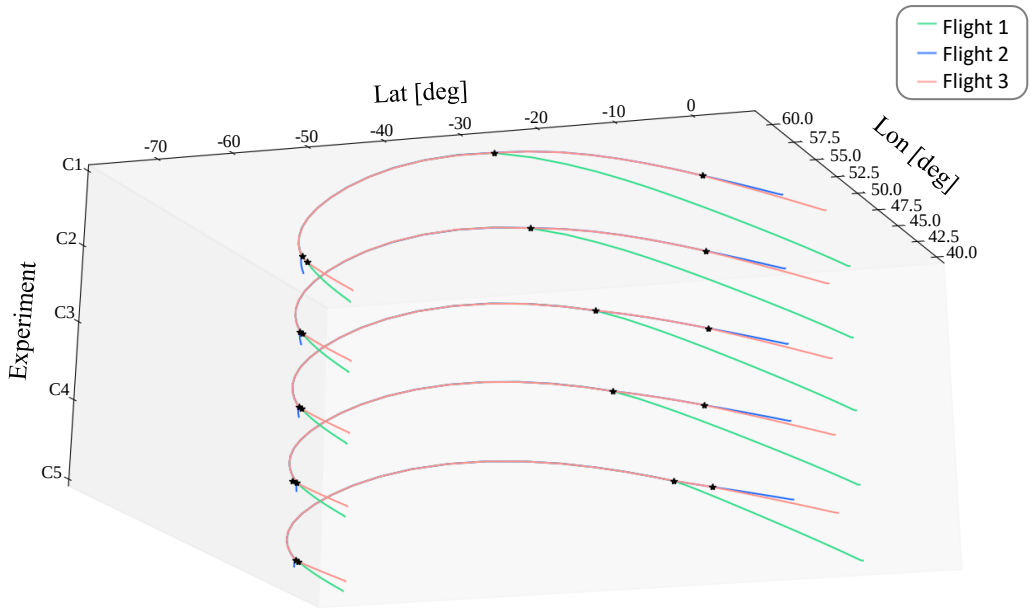

Fig. 7.8: Experiment C: Routes obtained in the different cases considered. Detail of the splitting locations.

	Formation distances $[km]$		
Cases	**State II**	**State III**	**State IV**
C_1	113.53	3008.99	1371.24
C_2	38.19	3323.62	1142.36
C_3	41.01	3743.05	737.69
C_4	44.48	3847.74	595.32
C_5	41.44	4229.41	257.29

Table 7.12: Experiment C: Formation distances for the two- and three-aircraft formation phases.

	Formation times $[h]$		
Cases	**State II**	**State III**	**State IV**
C_1	0.13	3.30	1.72
C_2	0.06	3.69	1.43
C_3	0.05	4.26	0.92
C_4	0.04	4.42	0.84
C_5	0.06	4.92	0.74

Table 7.13: Experiment C: Formation times for the two- and three-aircraft formation phases.

Direct operating costs

The main results related to the objective functional obtained in Experiment C are reported in Table 7.14. In particular, the increase of the flight time of each flight, the reduction or

increase of the fuel burn and the reduction in the DOC with respect to the results obtained assuming each flight is performed as a solo flight, are reported. It can be seen in this table that, for case C_5, the reduction in the DOC is almost 4% comparing to the case in which formation is not allowed.

	Δ Time [%]			**Δ Fuel burn [%]**			
	Flight 1	**Flight 2**	**Flight 3**	**Flight 1**	**Flight 2**	**Flight 3**	**ΔDOC [%]**
C_1	2.28	0.13	0.30	-1.83	-4.17	0.90	-1.14
C_2	2.45	-0.02	0.16	-2.87	-5.81	1.10	-1.80
C_3	2.89	-0.06	0.10	-4.15	-7.39	1.25	-2.51
C_4	2.90	-0.19	0.01	-5.29	-9.14	1.41	-3.25
C_5	3.54	-0.10	0.02	-6.69	-10.64	1.45	-3.97

Table 7.14: Experiment C: Total flight times, fuel burn and DOC reduction compared to solo flights, in the different cases.

Computational time

The average computational time to find the solution has been 15.274 s. For the sake of comparison, the same problem has been solved using a multiphase method [Hartjes et al., 2019]. In this case, 13 different OCP have been solved, since, in this case, there are 13 possible flight phase sequencing options, as shown in [Hartjes et al., 2019]. The average computational time has been 90.948 s. This shows that the method presented in this thesis is able to drastically reduce the computational time to solve formation mission design problems.

7.5 Conclusions

The results of the numerical experiments described in this chapter show that delays and changes in the fuel savings scheme have significant influence on the formation mission. The results show that a reduction of, approximately, 1% and 4% in terms of the DOC can be achieved for two- and three- aircraft formations, respectively, compared to solo flights, in non-optimistic scenarios, as the ones selected in this chapter. The results demonstrate that the proposed method for formation mission design in the absence of uncertainties is fast, accurate and easily scalable. The average computational times to find the solution for two- and three- aircraft mission design problems using a common desktop computer have been around 4 and 15 seconds, respectively, which translates to one half and one sixth of the computational time required by the multiphase method, respectively.

Chapter 8

Stochastic Formation Mission Design Problem

In this chapter, to show the effectiveness of the methodology described in Chapter 6, in solving the formation mission design problem in the presence of uncertainties, the results of two different numerical experiments will be described. All the experiments involve transoceanic eastbound flights operated by Airbus 330-200. In the first experiment, a three-aircraft formation mission design problem is solved, in which uncertainty regarding fuel burn savings is considered. In the second experiment, a two-aircraft formation mission design problem is solved, in which uncertainty regarding departure times of the aircraft is considered. For each experiment, a detailed description of the results is given along with a comparison with the results obtained in the absence of uncertainties and in solo flights. Finally, a sensitivity analysis of the stochastic solutions of the second experiment has been conducted.

8.1 General description of the experiments

The following numerical experiments have been carried out:

- Experiment A: Three-aircraft transoceanic mission design with uncertainty in the fuel burn savings.
- Experiment B: Two-aircraft transoceanic mission design with uncertainty in departure times of the flights.

Both experiments involve transoceanic eastbound flights. Wind data from the ERA-Interim reanalysis database of the ECMWF are used. As mentioned in Chapter 3, in this thesis only the cruise phase has been considered; the rest of the flight phases are neglected. Thus, the initial and final locations of the cruise phase of the flights are assumed to be the latitudes and longitudes of the departure and arrival airports of each flight at cruise altitude. Airbus A330-200 aircraft BADA models are considered for each flight. The initial masses of the aircraft

are assigned, as are the initial and final velocities, which are set at typical cruise values for the selected aircraft models. The initial heading angles are set to the initial heading angles of the orthodromic paths between the initial and final locations of each flight. The time and fuel burn weighting parameters, α_t and α_f, in the objective functional (3.18) are set to 0.3 and 0.7, respectively, based on the CI definition, as explained in Section 3.4.

The numerical experiments have been conducted on a 3.6 GHz Intel Core i9 computer with 32 GB RAM. The computational times reported in the following sections include both the time required to generate the warm-start solution and the time to find the optimal solution of the problem. The warm-start solution is a feasible solution of the problem generated by the NLP solver from an initial guess of the solution. Several initial guesses have been tried to obtain the warm-started solution in order to ensure that the global optimum is reached. Initial guesses for the latitude, the longitude, and the heading angle are generated using the orthodromic paths between the departure and arrival locations of each flight. Typical cruise velocity and fuel consumption of the aircraft model selected are used to generate the initial guesses of the velocity and the mass of each aircraft during the flight, respectively.

8.2 Experiment A: Three-aircraft transoceanic mission design with uncertainty in the fuel burn savings

8.2.1 Description of the experiment

Experiment A involves three transoceanic eastbound flights, Flight 1, Flight 2, and Flight 3, with uncertainty in the fuel burn savings for the trailing aircraft. The three flights considered in this experiment have the following departure and arrival locations:

- Flight 1: New York (`JFK`) - Paris (`CDG`).
- Flight 2: Boston (`BOS`) - Madrid (`MAD`).
- Flight 3: Montreal (`YUL`) - London (`LHR`).

The departure times of Flight 1, Flight 2, and Flight 3 are set to 10:15, 10:30, and 10:50, respectively. The boundary conditions for the state variables of the three aircraft are given in Table 8.1. Flight 1, Flight 2, and Flight 3 are operated by Aircraft 1, Aircraft 2, and Aircraft 3, respectively.

The relative position of each aircraft in the formation is selected in advance. In case of two-aircraft formation flights that include Aircraft 2, Aircraft 2 will be the leader aircraft and Aircraft 1 or Aircraft 3 will be the trailing. In case of two-aircraft formation flights that do not include Aircraft 2, Aircraft 3 will be the leader aircraft and Aircraft 1 will be the trailing. In case of three-aircraft formation flights, Aircraft 2 will be the leader aircraft, Aircraft 3 the intermediate, and Aircraft 1 the trailing.

Symbol	Units	Flight 1	Flight 2	Flight 3
ϕ_I	[deg]	40.64	42.36	45.47
ϕ_F	[deg]	48.85	40.48	51.47
λ_I	[deg]	-73.78	-71.06	-73.74
λ_F	[deg]	2.35	-3.57	-0.12
χ_I	[deg]	+54.26	69.25	+55.53
V_I	[m/s]	240	240	240
V_F	[m/s]	220	220	220
m_I	[kg]	$215\,000$	$210\,000$	$220\,000$

Table 8.1: Experiment A: Boundary conditions of the three flights.

The random variable that represents the fuel burn savings for the trailing aircraft is denoted by θ. This random variable is modeled as a Gaussian random variable with mean 0.1 and standard deviation 0.02, i.e., $\theta \sim \mathcal{N}(0.1, 0.02)$, based on several aerodynamic models and flight tests reported in [Kent and Richards, 2021]. The departure times are fixed.

Solving this problem entails deciding which mode of flight, i.e., formation or solo flight, is optimal, the expected values and standard deviations of the latitude and longitude of the optimal trajectories of each aircraft as functions of time, and the expected values and standard deviation of the timing of the trajectory as functions of the orthodromic distance from the departure locations. They include the expected values and the standard deviations of the arrival times and, in the case of formation flight, the expected values and the standard deviations of the latitude, longitude, and time of the rendezvous and splitting locations.

8.2.2 Results

The sequence of discrete states obtained in the solution is the following:

- State 1: All the aircraft fly solo.
- State 2: Aircraft 1 and Aircraft 2 fly in a two-aircraft formation and Aircraft 3 flies solo.
- State 3: All the aircraft fly in a three-aircraft formation.
- State 4: Aircraft 1 and Aircraft 3 fly in a two-aircraft formation and Aircraft 2 flies solo.
- State 5: All the aircraft fly solo.

Optimal routes

The expected values of the longitude and latitude of the optimal routes obtained in the solution together with the corresponding 95% confidence envelopes are represented on the

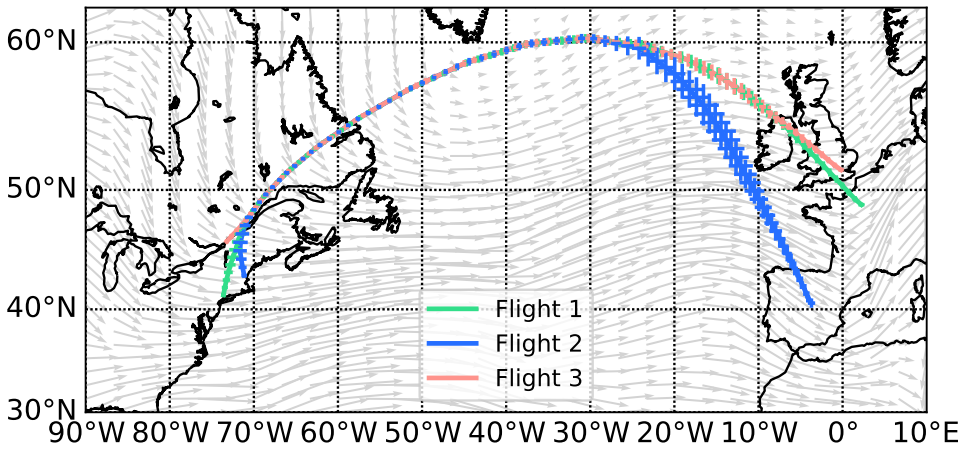

Fig. 8.1: Experiment A: Expected values of the latitude and longitude of the optimal trajectories of each aircraft together with the corresponding 95% confidence envelopes represented on the relevant map together with the wind field.

relevant map together with the wind field in Fig. 8.1 and as functions of time in Fig. 8.2.(a) and Fig. 8.2.(b), respectively.

Optimal state and control variables

The expected values of the rest of the state variables, namely, the mass, the heading angle, and the Mach number, together with the corresponding 95% confidence envelopes are represented as functions of time in Fig. 8.2.(c), Fig. 8.2.(d), and Fig. 8.2.(e), respectively. The expected values of the control variables are represented for the three flights in Fig. 8.3. Green, blue, and red lines correspond to Flight 1, Flight 2, and Flight 3, respectively. For a better understanding of these figures, the portions of the plots of the variables that correspond to formation flight are represented on a gray background. In particular, the portions of the plots that correspond to State 2 and State 4, which includes a two-aircraft formation, are represented on a light gray background, whereas the portion of the plots that correspond to State 3, which includes a three-aircraft formation, is represented on a dark gray background.

It is important to note that all the optimal solutions obtained considering the fuel burn savings that correspond to the nodes of the gPC expansion of the random variable $\theta \sim \mathcal{N}(0.1, 0.02)$ are formation missions with the same structure.

The control variables vary in a quite smooth way.

Optimal rendezvous and splitting times

The expected values of the rendezvous and splitting times are reported in Table 8.2 together with the corresponding 95% confidence interval. State 2, in which Aircraft 1 and

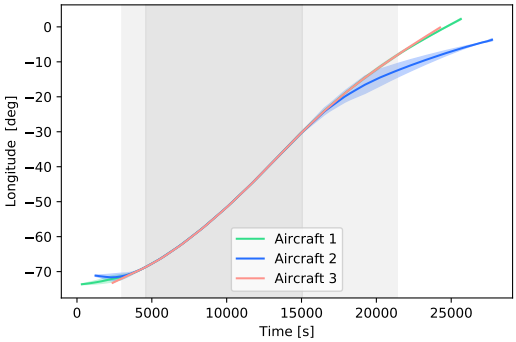

(a) Longitude

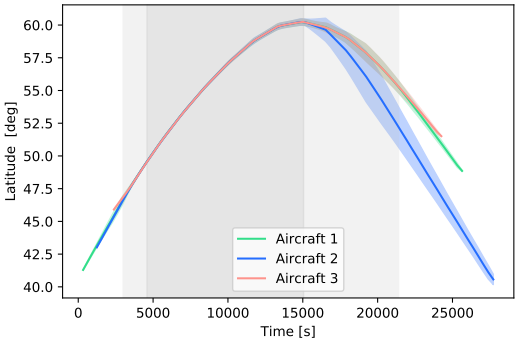

(b) Latitude

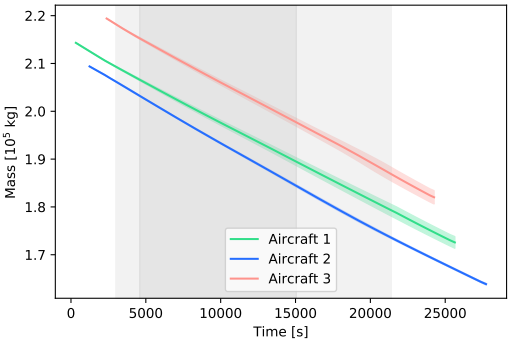

(c) Mass

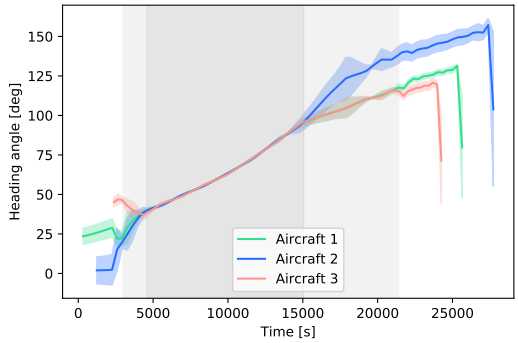

(d) Heading angle

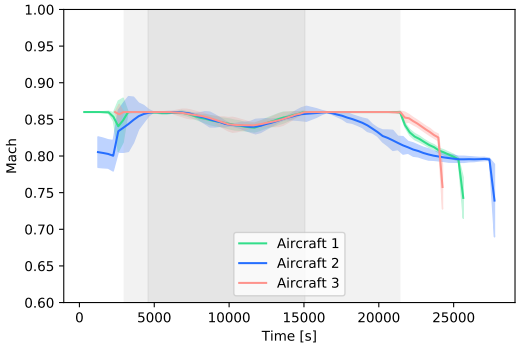

(e) Mach number

Fig. 8.2: Experiment A: Expected values of the state variables of the optimal trajectories of each aircraft together with the corresponding 95% confidence envelopes.

Aircraft 2 fly in formation and Aircraft 3 flies solo, has the shortest duration.

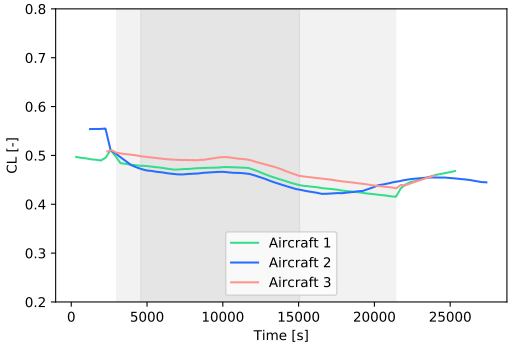

(a) Lift coefficient

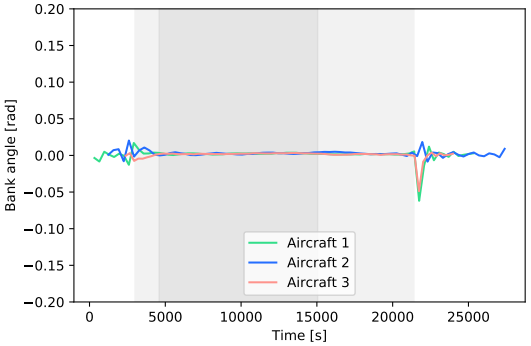

(b) Bank angle

(c) Adimensional thrust

Fig. 8.3: Experiment A: Expected values of the control variables of each aircraft.

Spatial variability

Regarding the spatial variability of the solution, it can be observed in Fig. 8.1, Fig. 8.2.(a), and Fig. 8.2.(b), that both geographical coordinates have a similar behavior. In the first two discrete states, the spatial variability is rather low, and in State 3, it is almost negligible. Then, near the first splitting location, the spatial variability starts increasing for all the flights. Finally, it decreases when the aircraft are approaching the final locations. Hence, the second splitting location has a significant dependency on the random variable θ and, consequently, both the duration and the traveled distance in State 3 have a significant dependency on it. Flight 2 has the greatest spatial variability.

Temporal variability

In addition to the spatial variability, the temporal variability is also quantified in order to have complete information regarding the spatio-temporal variability of the solution. The expected values of the timing of the solution together with the corresponding 95% confidence

envelopes are represented in Fig. 8.4 as functions of the orthodromic distance from the departure location of each flight. It can be observed in this figure that the temporal variability is very low in all the flights. In particular, in Flight 1 and Flight 3, the temporal variability is almost negligible during the whole flight time, whereas, in Flight 2, it starts increasing after the first splitting location. However, despite this increase, it is very low in Flight 2 as well, leading to the conclusion that the temporal variability of all the flights slightly depends on the random variable θ.

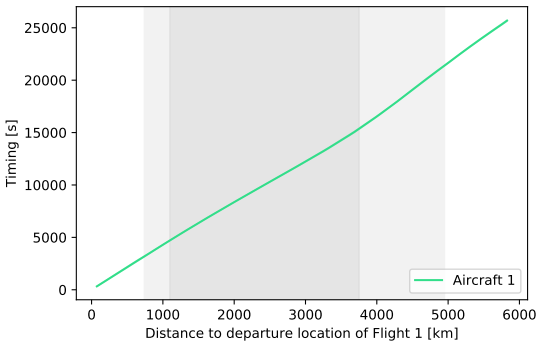

(a) Flight 1

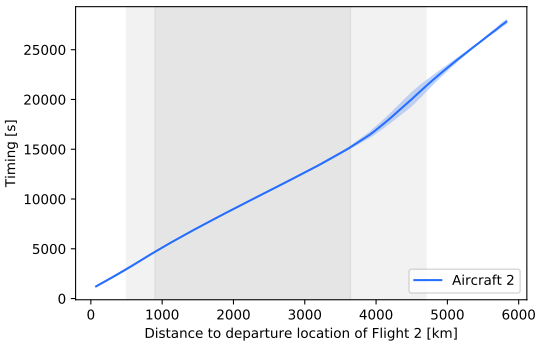

(b) Flight 2

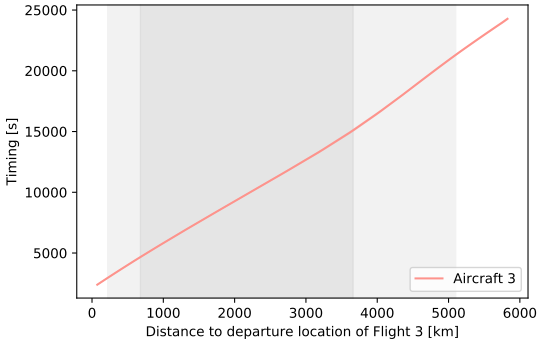

(c) Flight 3

Fig. 8.4: Experiment A: Expected values of the timing of the optimal trajectories of each aircraft together with the corresponding 95% envelopes.

It can be observed in Table 8.2, in which the expected values and the 95% confidence intervals of the rendezvous and splitting times are reported, that the amplitudes of these intervals are lower for the rendezvous times than for the splitting times, but remains fairly small for both of them.

	Expected value	95% confidence interval
First rendezvous time [h]	0.88	[0.87, 0.89]
Second rendezvous time [h]	1.32	[1.32, 1.32]
First splitting time [h]	4.19	[4.17, 4.21]
Second splitting time [h]	5.95	[5.92, 5.98]

Table 8.2: Experiment A: Expected values and 95% confidence intervals of the rendezvous and splitting times.

Direct operating costs

The expected values and the 95% confidence intervals for both the flight time, expressed in hours, and the fuel burn, expressed in tonnes, for each flight are listed in Table 8.3. From the amplitudes of the 95% confidence intervals, it is easy to see that, as already mentioned, the flight time variability is rather low. In contrast, as expected, the uncertainty in the fuel burn savings has a significant impact on the variability of the fuel consumption.

	Flight time [h]		Fuel burn [t]	
	Expected value	95% confidence interval	Expected value	95% confidence interval
Flight 1	7.13	[7.12, 7.15]	42.47	[41.19, 43.74]
Flight 2	7.47	[7.43, 7.52]	46.24	[45.90, 46.58]
Flight 3	6.16	[6.15, 6.18]	38.00	[36.58, 39.42]

Table 8.3: Experiment A: Expected values and 95% confidence intervals of flight times and fuel consumption of each flight.

Comparison with the results obtained in solo flight

To quantify the benefits of formation flight with respect to solo flight, the expected values of the flight time and the fuel consumption, along with the expected value of the corresponding DOC expressed in monetary units, *mu*, are estimated assuming that the three flights are performed as solo flights. The obtained results are reported in Table 8.4. For the sake of comparison, the expected values of the DOC obtained in both formation and solo flights of the three aircraft are reported in Table 8.5. It is remarkable that, in spite of the uncertainties considered in the fuel burn savings for the trailing aircraft, the reduction in the total DOC achieved with formation flight amounts to 2.16%.

	Flight time [h]	Fuel burn [t]	DOC [mu]
Flight 1	7.06	45.73	39635.79
Flight 2	7.32	45.44	39713.60
Flight 3	6.02	39.52	34165.60

Table 8.4: Experiment A: Expected values of flight times, fuel consumption, and DOC in solo flight of the three aircraft.

	Flight 1	Flight 2	Flight 3	Total
DOC solo flight [mu]	39635.79	39713.60	34165.60	113514.99
DOC formation flight [mu]	37429.40	40435.59	33252.80	111117.79
ΔDOC [%]	-5.89	+1.79	-2.75	-2.16

Table 8.5: Experiment A: Expected values of the DOC in solo and formation flights of the three aircraft.

Comparison with the results obtained in deterministic formation mission design

To quantify the effects of the uncertainty in the fuel burn savings for the trailing aircraft on the DOC, the same formation mission is designed in the absence of uncertainty, in which the fuel burn savings for both the trailing and intermediate aircraft are set to 10%. For the sake of comparison, the obtained results in terms of the DOC for the deterministic and stochastic formation missions are summarized in Table 8.6. It can be seen that the increment of the total DOC due to the presence of uncertainties amounts to 1.60%.

	Flight 1	Flight 2	Flight 3	Total
Deterministic DOC [mu]	36178.9	40205.67	32980.96	109365.53
Stochastic DOC [mu] (expected value)	37429.40	40435.59	33252.80	111117.79
ΔDOC [%]	+3.45	+0.57	+0.82	+1.60

Table 8.6: Experiment A: Values of the DOC in deterministic and stochastic formation missions of the three aircraft.

8.3 Experiment B: Two-aircraft transoceanic mission design with uncertainty in the departure times of the flights

8.3.1 Description of the experiment

Experiment B involves two transoceanic eastbound flights, Flight 1 and Flight 2, with uncertainty in the departure times of the flights. The flights considered in this experiment have the same departure and arrival locations and the same boundary values for the state variables as Flight 1 and Flight 2 in Experiment A. They have the following departure and arrival locations:

- Flight 1: New York (`JFK`) - Paris (`CDG`).
- Flight 2: Boston (`BOS`) - Madrid (`MAD`).

The departure times of Flight 1 and Flight 2 are set to 10:15 and 10:30, respectively. The boundary conditions for the state variables of the two aircraft are given in Table 8.1. Flight 1 and Flight 2 are operated by Aircraft 1 and Aircraft 2, respectively.

As in Experiment A, the formation configuration is selected in advance. In case of formation flight, Aircraft 1 will be the trailing aircraft and Aircraft 2 the leader. In this experiment, the fuel burn savings for the trailing aircraft are set to 10%.

The random variables that represent the delays with respect to the scheduled departure times of Flight 1 and Flight 2 from JFK and BOS airports are denoted by θ_1 and θ_2, respectively. These random variables have been modeled using a Gaussian mixture distribution, the parameters of which are estimated from real delay data obtained from the Transtats online database[1] of the U.S. Bureau of Transportation Statistics. This database provides detailed information on the U.S. transportation systems, including data on departure delays by airport and airline. The expectation-maximization algorithm for fitting mixture-of-Gaussian models to data is employed for this purpose [Murphy, 2012]. Departure delay data corresponding to April 2019 are used.

The resulting Gaussian mixture probability density functions that model the random variables θ_1 and θ_2 that represent the departure delays at JFK and BOS airports both have 4 components. The values of the parameters of the Gaussian mixture probability density functions are given in Table 8.7, where $p_{i,j}, i = 1, 2, j = 1, 2, 3, 4$ are the weights of the Gaussian component probability density functions of θ_i, which are probabilities that sum to 1, and $\mu_{i,j}$ and $\sigma_{i,j}$ are their means and standard deviations, respectively. This result is consistent with previous studies on estimation of flight departure delay distributions [Tu et al., 2008]. Fig. 8.5 shows in black the obtained Gaussian mixture distribution of the departure delays of Flight 1 and Flight 2 from JFK and BOS airports, respectively, together with the histogram of the data. A bin width of 2 minutes is used for the histograms. The components of the Gaussian mixture distribution are represented by dotted lines. The mean and the standard deviation of the random variable θ_1 are -1.67 min and 7.69 min, respectively. The mean and the standard deviation of the random variable θ_2 are -0.88 min and 10.37 min, respectively.

	Departure airport	Random variable	$p_{i,1}, p_{i,2}, p_{i,3}, p_{i,4}$	$\mu_{i,1}, \mu_{i,2}, \mu_{i,3}, \mu_{i,4}$	$\sigma_{i,1}, \sigma_{i,2}, \sigma_{i,3}, \sigma_{i,4}$
Flight 1	JFK	θ_1	0.39, 0.17, 0.27, 0.17	-4.94, 11.94, -0.99, -8.91	2.20, 7.17, 2.93, 2.89
Flight 2	BOS	θ_2	0.24, 0.56, 0.06, 0.14	-1.76, -6.61, 28.67, 10.92	3.39, 3.70, 5.68, 5.78

Table 8.7: Experiment B: Estimated parameters of the Gaussian mixture probability density functions that model the departure delays of the flights.

As in Experiment A, solving this problem entails deciding which mode of flight is optimal, the expected values and standard deviations of the latitude and longitude of the optimal trajectories of each aircraft as functions of time, and the expected values and standard deviation of the timing of the trajectory as functions of the distance.

8.3.2 Results

The sequence of discrete states obtained in the solution is the following:

- State 1: Both aircraft fly solo.

[1] https://www.transtats.bts.gov/

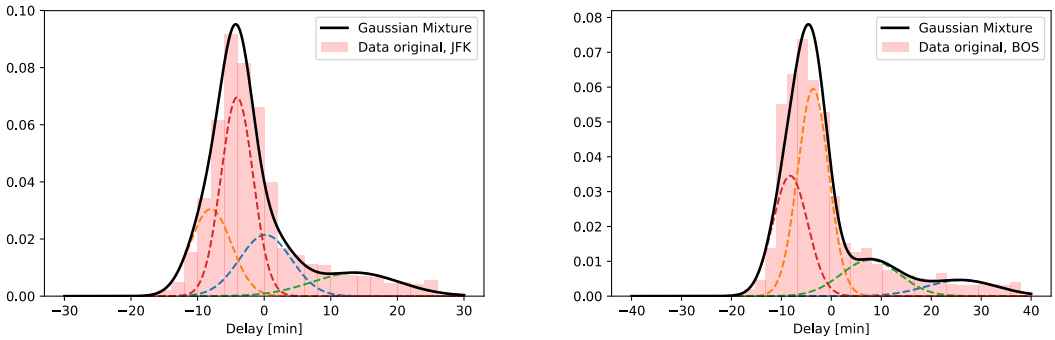

(a) θ_2, departure delay of Flight 1, JFK airport

(b) θ_2, departure delay of Flight 2, BOS airport

Fig. 8.5: Experiment B: Estimated probability density functions of the random variables θ_1 and θ_2 that represent the departure delays of each flight.

- State 2: The aircraft fly in formation.
- State 3: Both aircraft fly solo.

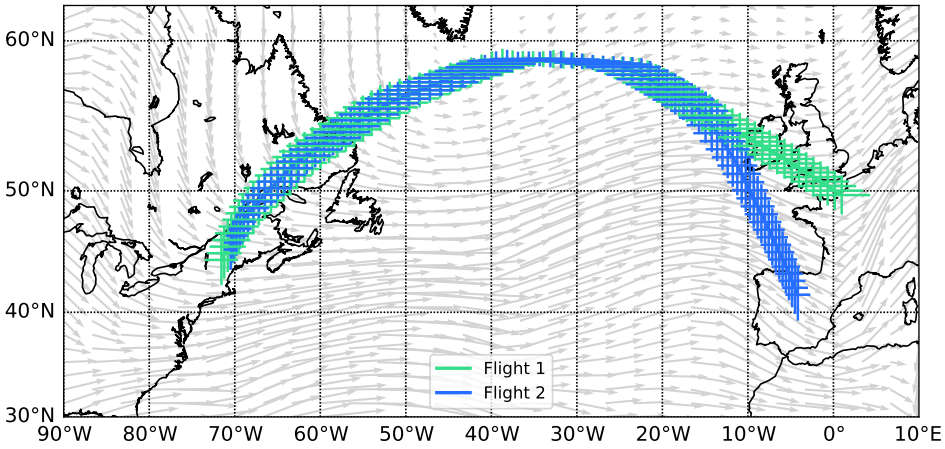

Fig. 8.6: Experiment B: Expected values of the longitude and latitude of the optimal trajectories of each aircraft together with the corresponding 95% confidence envelopes represented on the relevant map together with the wind field.

Optimal routes

The expected values of the longitude and latitude of the optimal routes obtained in the solution together with the corresponding 95% confidence envelopes are represented on the relevant map together with the wind field in Fig. 8.6 and as functions of time in Fig. 8.7.(a).

Optimal state and control variables

The expected values of the rest of the state variables, namely, the mass, the heading angle, and the Mach number, together with the corresponding 95% confidence envelopes are represented as functions of time in Fig. 8.7.(c), Fig. 8.7.(d), and Fig. 8.7.(e), respectively. The expected values of the control variables are represented for the two flights in Fig. 8.8. Green and blue lines correspond to Flight 1 and Flight 2, respectively. As in Experiment A, the portions of the plots of the variables that correspond to State 2, in which the aircraft fly in formation, are represented on a gray background.

It is important to note that all the optimal solutions obtained considering the fuel burn savings that correspond to the nodes of the gPC expansion of the two random variables are formation missions with the same structure.

The control variables vary in a quite smooth way. Comparing the expected values of the state variables and the corresponding 95% confidence envelopes represented as functions of time in Fig. 8.7 with the corresponding ones of Experiment A given in Fig. 8.2, the high variability in every state variable of each flight is striking. In particular, the Mach number variability in the early part of the flight is especially worthy of note. This is due to the fact that anticipations and delays in the departure times of the flights are compensated by increments and reductions of their velocities.

Optimal rendezvous and splitting times

The expected values of the rendezvous and splitting times are reported in Table 8.8 together with the corresponding 95% confidence intervals. State 2, in which the aircraft fly in formation, has the longest duration.

Spatial variability

Regarding the spatial variability of the solution, it can be observed in Fig. 8.6, Fig. 8.7.(a), and Fig. 8.7.(b) that the longitude variability is greater in State 2, in which the aircraft fly in formation. In contrast, the latitude variability has a minimum in State 2, which is located around the maximum value of this geographical coordinate. Aircraft 2, the leading aircraft, has the greatest spatial variability.

Temporal variability

As in Experiment A, in addition to the spatial variability, the temporal variability is also quantified in order to have complete information regarding the spatio-temporal variability of the solution. The expected values of the timing of the solution together with the corresponding 95% confidence envelopes are represented in Fig. 8.9, as functions of the orthodromic distance from the departure locations of each flight. It can be observed in this figure that the temporal

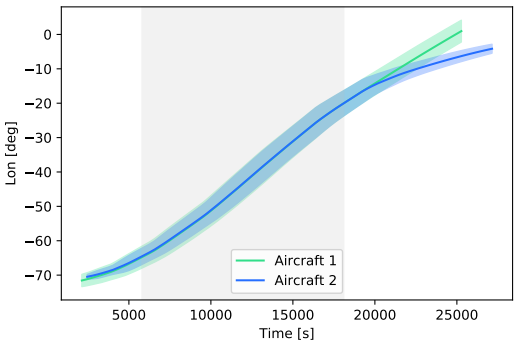

(a) Longitude

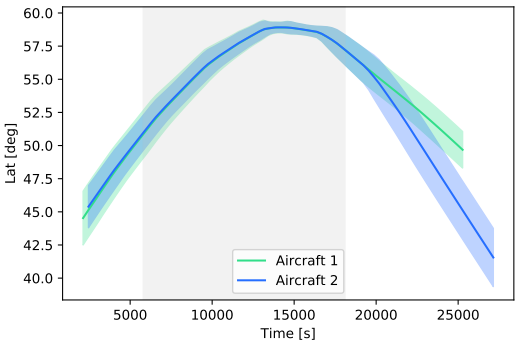

(b) Latitude

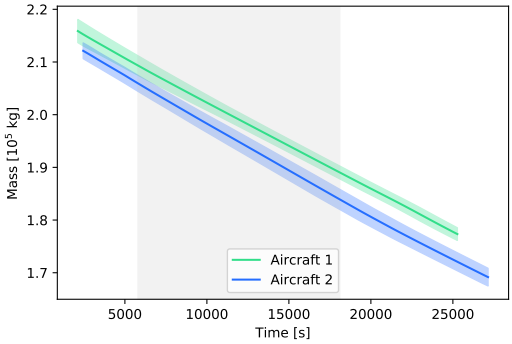

(c) Mass

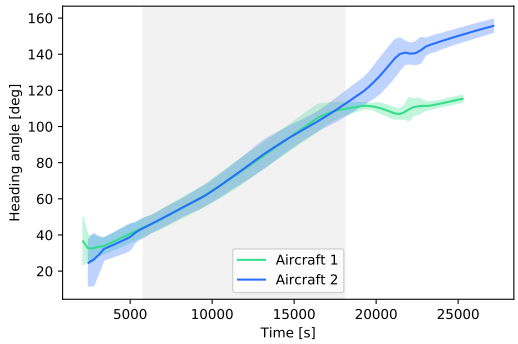

(d) Heading angle

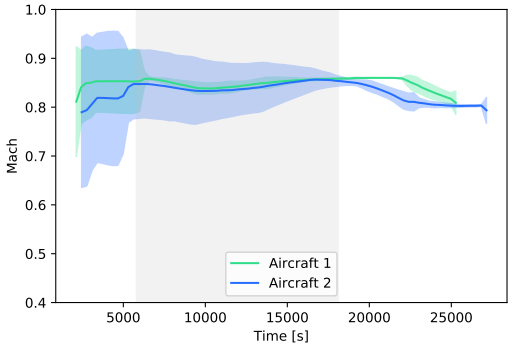

(e) Mach number

Fig. 8.7: Experiment B: Expected values of the state variables of the optimal trajectories of each aircraft together with the corresponding 95% confidence envelopes.

variability has a similar behavior for both flights, remaining nearly constant throughout the flight. As in the case of spatial variability, the temporal variability of the flights in Experiment B is considerably greater than the temporal variability of the flights in Experiment A. As expected, uncertainty in the departure times of the flights has a significant impact on the

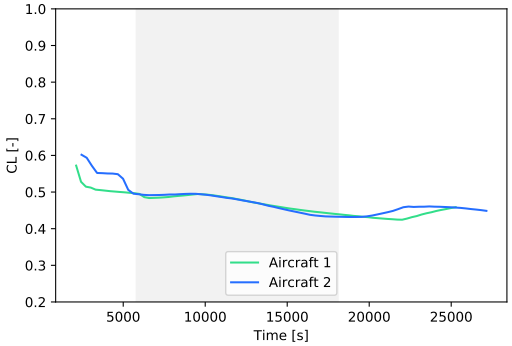

(a) Lift coefficient

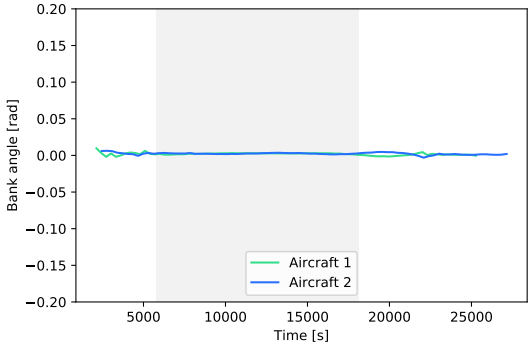

(b) Bank angle

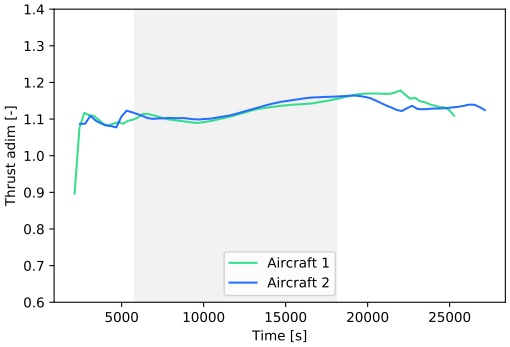

(c) Adimensional thrust

Fig. 8.8: Experiment B: Expected values of the control variables of each aircraft.

temporal variability of the trajectories, more than the uncertainty in the fuel burn savings for the trailing aircraft.

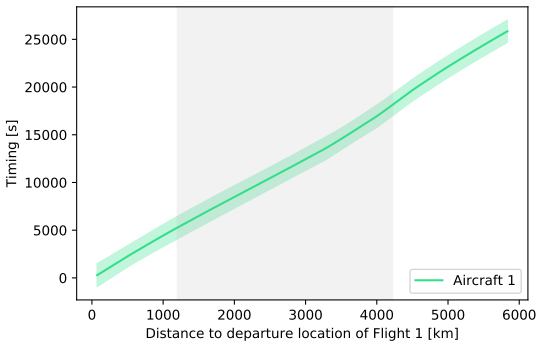

(a) Flight 1

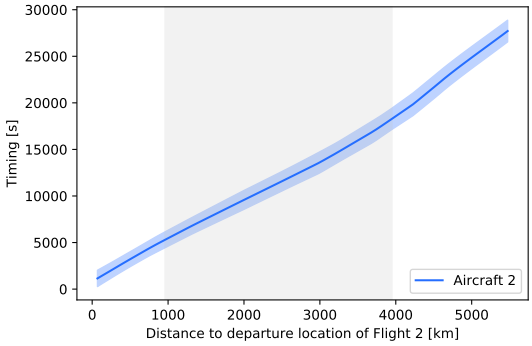

(b) Flight 2

Fig. 8.9: Experiment B: Expected values of the timing of the optimal trajectories of each aircraft together with the corresponding 95% envelopes.

It can be observed in Table 8.8, in which the expected values and the 95% confidence intervals of the rendezvous and splitting times are reported, that the amplitudes of these intervals are similar for the rendezvous and splitting times, being, in both cases, considerably greater than the amplitudes of the 95% confidence intervals of the rendezvous and splitting times obtained in Experiment A.

	Expected value	**95% confidence interval**
Rendezvous time [h]	1.61	[1.29, 1.94]
Splitting time [h]	5.03	[4.71, 5.34]

Table 8.8: Experiment B: Expected values and 95% confidence intervals of the rendezvous and splitting times.

Direct operating costs

The expected values and the 95% confidence intervals for both the flight time, expressed in hours, and the fuel burn, expressed in tonnes, for each flight are listed in Table 8.9. From the amplitudes of the 95% confidence intervals, it is easy to see that, as already mentioned, the flight time variability is rather high. Additionally, the uncertainty in the departure times also has a significant impact on the variability of the fuel consumption.

	Flight time [h]		**Fuel burn [t]**	
	Expected value	**95% confidence interval**	**Expected value**	**95% confidence interval**
Flight 1	7.18	[6.86, 7.50]	43.58	[42.52, 44.63]
Flight 2	7.70	[7.37, 8.02]	46.69	[46.27, 47.11]

Table 8.9: Experiment B: Expected values and 95% confidence intervals of flight times and fuel consumption of each flight.

Comparison with the results obtained in solo flight

To quantify the benefits of formation flight with respect to solo flight, the expected values of the flight time and the fuel consumption along with the expected value of the corresponding DOC expressed in monetary units, *mu*, for the two solo flights, given in the first two rows of Table 8.4, are compared to the expected values of the DOC obtained in formation flight. The obtained results are reported in Table 8.10. It can be observed that, in the presence of uncertainties regarding the departure times of the flights, the probability density funcion of which is estimated from real departure delay data, small benefits are expected in terms of the reduction of the total DOC, which amount to only 0.11%. However, in real-life scenarios, some mitigation measures could be implemented to reduce the negative impact of flight delays on the benefits of formation flight such as adjusting the flight plan of the formation mission before departure when one of the flights of a formation is delayed.

	Flight 1	Flight 2	Total
DOC solo flight [mu]	39635.79	39713.60	79349.39
DOC formation flight [mu]	38260.39	40999.01	79259.39
ΔDOC [%]	-3.59	+3.14%	-0.11

Table 8.10: Experiment B: Expected values of the DOC in solo and formation flights of the two aircraft.

Comparison with the results obtained in deterministic formation missions

To quantify the effects of the uncertainty in the departure delays on the DOC, the same formation mission is designed in the absence of uncertainty, in which no delays are considered. For the sake of comparison, the obtained results in terms of the DOC for the deterministic and stochastic formation missions are summarized in Table 8.11. It can be seen that the increment of the total DOC due to the presence of uncertainties amounts to 3.76%.

	Flight 1	Flight 2	Total
Deterministic DOC [mu]	36178.90	40205.67	76384.57
Stochastic DOC [mu] (expected value)	38260.39	40999.01	79259.39
ΔDOC [%]	+5.75	+1.97	+3.76

Table 8.11: Experiment B: Values of the DOC in deterministic and stochastic formation missions of the two aircraft.

Based on the results of the two experiments, it is possible to conclude that uncertainties have a significant impact on the formation flight benefits in terms of the reduction of the DOC. In particular, the uncertainties regarding the departure times have a far greater impact on the DOC than the uncertainties regarding the fuel burn savings. These results demonstrate that formation flight is economically beneficial in the presence of uncertainties regarding the fuel savings for the trailing aircraft and in the departure times of the aircraft.

In the next section, a sensitivity analysis of the solution of this experiment to the random variables that represent the departure times of the flights is carried out. The purpose of this analysis is to quantify how much uncertainty in each component of the solution is due to the different sources of uncertainty considered in the experiment.

8.3.3 Sensitivity analysis

In this section, following Section 6.3, a variance-based sensitivity analysis of the results obtained in Experiment B is conducted through the computation of the Sobol' indices. The aim of this variance-based sensitivity analysis is to quantify what proportion of the variance of the latitude and the longitude of flight k of the solution of the formation mission design problem, $\lambda_k(t,\theta)$ and $\phi_k(t,\theta)$, respectively, is due to the variance of each departure delays of Flight 1 and Flight 2, θ_1 and θ_2, respectively.

The analysis of the sensitivity of the components of the solution obtained in Experiment

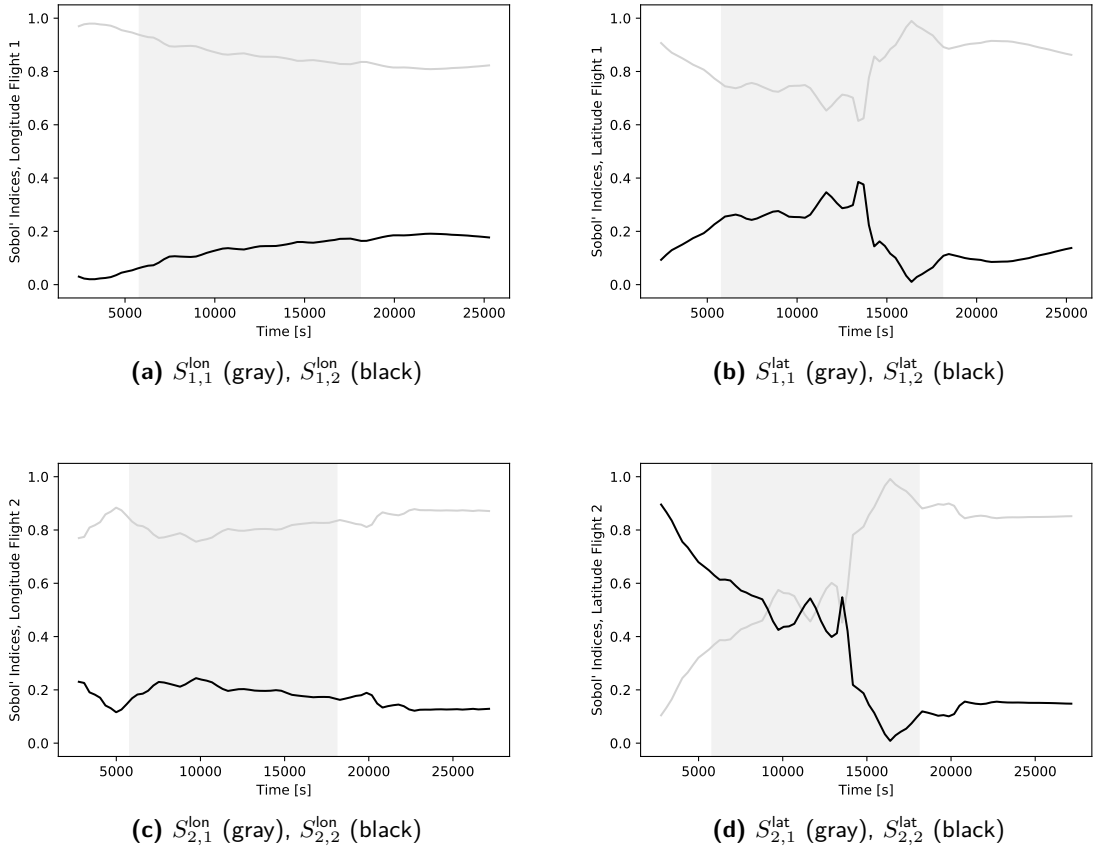

(a) $S^{\text{lon}}_{1,1}$ (gray), $S^{\text{lon}}_{1,2}$ (black)

(b) $S^{\text{lat}}_{1,1}$ (gray), $S^{\text{lat}}_{1,2}$ (black)

(c) $S^{\text{lon}}_{2,1}$ (gray), $S^{\text{lon}}_{2,2}$ (black)

(d) $S^{\text{lat}}_{2,1}$ (gray), $S^{\text{lat}}_{2,2}$ (black)

Fig. 8.10: Experiment B: Sobol' indices of the geographical coordinates of the optimal trajectories of each flight. Gray and black lines correspond to the random variables θ_1 and θ_2, respectively.

B to the two random variables θ_1 and θ_2 that represent the departure delays of Flight 1 and Flight 2, respectively, is carried out employing this approach. The Sobol' indices of the latitude and longitude of Flight $k, k = 1, 2$ with respect to the random variable $\theta_j, j = 1, 2$ are denoted by $S^{\text{lat}}_{k,j}$ and $S^{\text{lon}}_{k,j}$, respectively. They represent the proportions of the variance of the geographical coordinates of the optimal route of Flight k that is due to the variance of the departure time of Flight j. The Sobol' indices of the longitude and latitude of the optimal routes obtained in the solution of Experiment B are represented as functions of time in Fig. 8.10, in which Sobol' indices associated with θ_1 and θ_2 are plotted in gray and black, respectively.

It can be seen in Fig. 8.10.(a) and Fig. 8.10.(b) that during the whole flight, most of the variance of both geographical coordinates of the optimal route of Flight 1 is due to the variance of the random variable θ_1. In particular, the percentage of the variance of the longitude of Flight 1 due to the variance of θ_1 is around 90%, while the percentage of the variance of the latitude of Flight 1 due to the variance of the same random variable is between

60% and 90% during the whole flight time.

It can be seen in Fig. 8.10.(c) and Fig. 8.10.(d) that during the whole flight, most of the variance of the longitude of the optimal route of Flight 2 is due to the variance of the random variable θ_1. In contrast, the relative influence of the variance of the random variables θ_1 and θ_2 on the variance of the latitude of the optimal route of Flight 2 changes along the flight. In particular, in the first part of Flight 2, up to 8000 seconds, approximately, the variance of the random variable θ_2 has the most influence on the variance of the latitude of Flight 2. After that, there is an intermediate part of Flight 2, between 8000 and 14000 seconds, approximately, in which the variances of θ_1 and θ_2 have a similar influence on the variance of the latitude of Flight 2. Finally, in the last part of Flight 2, the influence of the variance of θ_1 on the variance of the latitude of Flight 2 becomes predominant, reaching a percentage of 90%.

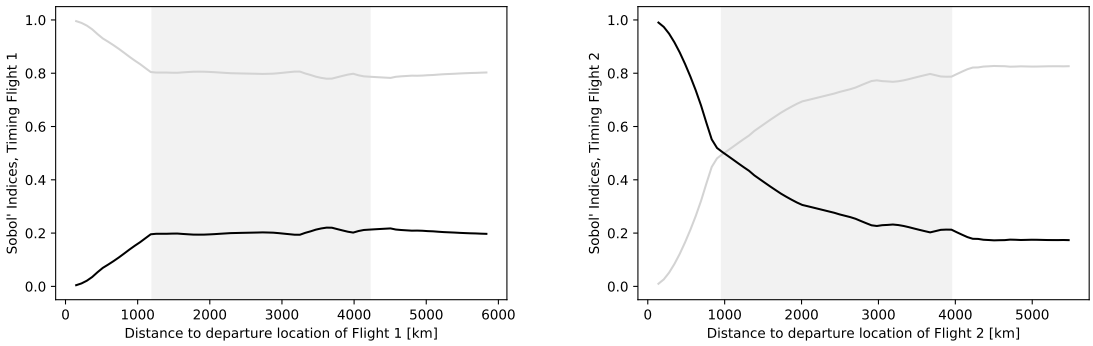

(a) $S^{\text{timing}}_{1,1}$ (gray), $S^{\text{timing}}_{1,2}$ (black), Flight 1

(b) $S^{\text{timing}}_{2,1}$ (gray), $S^{\text{timing}}_{2,2}$ (black), Flight 2

Fig. 8.11: Experiment B: Sobol' indices of the timing of the optimal trajectories of each flight. Gray and black lines correspond to the random variables θ_1 and θ_2, respectively.

The Sobol' indices of the timing of Flight $k, k = 1, 2$ with respect to the random variable $\theta_j, j = 1, 2$ are denoted by $S^{\text{timing}}_{k,j}(d_k)$, where d_k is the orthodromic distance of flight k from the departure location. They numerically quantify the proportion of the variance of the timing of the optimal route of flight k that is due to the variance of θ_j. The Sobol' indices of the timing of the optimal routes obtained in the solution of Experiment B are represented as functions of the orthodromic distance in Fig. 8.11, in which Sobol' indices associated with θ_1 and θ_2 are plotted in gray and black, respectively. It can be seen in this figure that, during the whole flight, most of the variance of the timing of the optimal route of Flight 1 is due to the variance of the random variable θ_1, with a percentage of about 80%. On the contrary, the relative influence of the variance of the random variables θ_1 and θ_2 on the variance of the timing of the optimal route of Flight 2 changes along the flight. In particular, in the first part of Flight 2, up to the distance of 1000 km, approximately, the variance of θ_2 has the most influence on the variance of the timing of the optimal route of Flight 2. After that, the

influence of the variance of θ_1 on the variance of the timing of the optimal route of Flight 2 becomes predominant, reaching a percentage of 80%.

8.4 Conclusions

The results of the numerical experiments described in this chapter show that uncertainties have a significant impact on the potential benefits of a formation mission. In particular, the uncertainties regarding the departure times have a greater impact on the direct operating costs than the uncertainties regarding the fuel burn savings. The results reveal that the increment of the direct operating costs due to the presence of uncertainties amounts to 1.60% and 3.76% in Experiment A and Experiment B, respectively. However, even in the presence of uncertainties, reductions of the direct operating costs are expected with formation flight compared to solo flight in both experiments. The results also give interesting additional information, revealing, for instance, that one random variable may have predominant influence on the variability of a component of the solution. They also indicate that the relative influence of the random variables on the variability of a component of the solution may change during the flight. The results of the numerical experiments described in this chapter show that the proposed methodology is an effective tool for solving the formation mission design problem for commercial aircraft in the presence of uncertainties.

Chapter 9

Conclusions and Future Research

In this thesis, the formation mission design problem in the presence of uncertainties has been solved using stochastic optimal control techniques, with the aim of demonstrating the economical feasibility of formation flight in commercial aviation.

First, the formation mission design problem for commercial aircraft has been studied in the absence of uncertainties. A novel framework to solve the problem has been presented, in which the formation mission is modeled as a switched dynamical system, aircraft are assumed to have two flight modes, namely solo and formation flight, and the discrete state of the switched dynamical system is the result of their combination. The discrete dynamics of the system has been modeled using logical constraints in disjunctive form. Thus, the formation mission design problem has been formulated as an optimal control problem for a switched dynamical system with logical constraints in disjunctive form. The optimal control approach allows accurate flight dynamics models and meteorological forecast to be taken into account, improving trajectory predictability and the estimation of both flight time and fuel consumption of the aircraft involved in the formation mission design problem.

The switched optimal control problem has been solved using the embedding approach. The embedding approach is a unifying technique able to efficiently tackle both the switching dynamics and the logical constrains of the switched optimal control problem, transforming it into a smooth optimal control problem, which has been solved using classical numerical optimal control techniques. Specifically, direct numerical optimal control techniques based on pseudospectral knotting methods have been used. The main advantages of this approach are that the multiphase formulation is avoided, as well as the use of binary variables, decreasing the computational time and effort in finding the solution. This approach is substantially different from previous approaches, which are based on exhaustively analyzing every possible formation mission individually and then comparing the results. Additionally, this approach is easily scalable to design formation mission problems with an arbitrary number of aircraft.

Several numerical experiments have been conducted with two and three transoceanic flights. Additionally, an analysis of the solutions has also been carried out in order to study how the delays in the departure time and changes in the fuel saving scheme influence the formation mission. The results indicate that delays and changes in the fuel savings scheme have significant influence on the formation mission. This suggests that a deeper understanding of the effects of uncertainties in these and other parameters on the formation mission is needed.

Therefore, the formation mission design problem for commercial aircraft in the presence of uncertainties has been addressed. Uncertainties are represented by random variables characterized by probability density functions. The formation mission design problem in the presence of uncertainties has been formulated as an stochastic switched optimal control problem and solved using the generalized polynomial chaos expansion, by means of which the original stochastic switched optimal control problem is transformed into an equivalent deterministic switched optimal control problem in a higher dimensional state space. The generalized polynomial chaos expansion allows, not only a statistical analysis, but also a sensitivity analysis of the stochastic solutions to be conducted at a low computational cost to estimate the relative contribution of each random variable to the variability of the components of the solution.

Several numerical experiments have been conducted with two and three transoceanic flights. The results of the numerical experiments indicate that uncertainties have a significant impact on the potential benefits of a formation mission. The results of the sensitivity analysis reveal that one random variable may have predominant influence on the variability of a component of the solution. They also indicate that the relative influence of the random variables on the variability of a component of the solution may change during the flight.

The results of the numerical experiments demonstrate that formation flight is economically beneficial in the presence of realistic levels of uncertainty in the fuel savings for the trailing aircraft and in the departure times of the aircraft. The results of the numerical experiments also show that the proposed frameworks for formation mission design in the presence of uncertainty is fast and accurate. These features, makes the proposed approach suitable to be incorporated in a ground-based system which could be used by flight dispatchers as a support system to design formation missions for airlines or airline alliances. The computational time of the proposed algorithm makes it suitable for the strategic and tactical planning phases of the flight, as well as for the operational phase, that is, during the flight.

9.1 Open problems and future research

Due to the complexity of the formation flight planning problem, after studying the formation mission design problem, there are several open problems, which will subject of future research. They will be described in this section.

As said in Chapter 2, the formation flight planning problem can be split into two

subproblems, namely the partner allocation problem and the formation mission design problem. The former, which consists in establishing how to group a set of longhaul flights into smaller subsets that contain potential partners of beneficial formation missions in terms of the overall DOC, has not been studied in this thesis. Thus, due to its close relation with the formation mission design problem, the partner allocation problem will be one of the first to be studied. Preliminary research indicates that this problem could be solved by first calculating the optimal solo flight trajectories using the numerical optimal control methods described in Chapter 5 and, then, applying a suitable spatiotemporal geo-referenced data clustering algorithm [Ansari et al., 2020] such as those introduced in [Vieira et al., 2009] and [Jeung et al., 2010], to solve the problem of finding objects that move together in a spatiotemporal geo-referenced dataset, which are referred to as flocks or convoys. In [Aung and Tan, 2010] an extended version of this problem is studied, in which the members of the convoy can change over time.

As explained in Chapter 3, a fuel consumption reduction model has been employed for the trailing aircraft, instead of an induced drag reduction model. Therefore, to improve the estimations of the benefits achieved by formation flight and, consequently, the DOC of the formation mission, the latter model should be adopted.

In all the experiments described in this thesis, only one type of formation has been considered and the leader of the formation has been set in advance. Therefore, to improve the methodology proposed in this thesis, after a thorough study of the aerodynamics of formation flight, some other functionalities should be included, such as the possibility of choosing the optimal type of formation for a given formation mission and the optimal positions of the leader and the trailing aircraft in the formation.

In this thesis, accurate dynamic models of the aircraft have been considered to solve the formation mission design problem. However, some simplifying assumptions, which have been outlined in Chapter 3, have been introduced, such as the reduced two degree of freedom point variable-mass dynamic aircraft model. Therefore, to improve the accuracy of the solutions and the predictability of the resulting aircraft trajectories, a non-reduced three degree of freedom point variable-mass dynamic aircraft model should be employed.

Although the wind field has been included in the dynamic models of the aircraft in all the numerical experiments, it has been considered as a deterministic vector field, which is not a realistic assumption. Therefore, to improve the accuracy of the solutions and the predictability of the resulting aircraft trajectories, uncertainties regarding the wind forecast should be considered. Being a random function of space and time, the wind field should be modeled as a stochastic process. Although the generalized polynomial chaos expansion can be employed to represent stochastic processes, specific techniques are needed for their representation, such as the Karhunen–Loève expansion.

In Experiment B described in Chapter 8, two sources of uncertainties have been considered, namely the departure time of the flights, which have been quantified using the generalized polynomial chaos expansion. However, they have been assumed to be independent random

variables. In the presence of dependent random variables, the Vine Copula technique [Torre et al., 2019] must be used before applying the generalized polynomial chaos expansion. In both cases, increasing the number of sources of uncertainties considered in the problem, increases the dimensionality of the problem and, consequently, sparse grid numerical methods should be used such as the Smolyak sparse quadrature [Xiu, 2010].

Finally, most realistic instances of the formation mission design problem could be solved including probabilistic constraints, also known as chance constraints [Kim and Braatz, 2012] in the formulation of the problem. Chance constraints can be included in the formulation of the problem using the generalized polynomial chaos expansion.

Bibliography

[Abeyratne, 2020] Abeyratne, R. (2020). The outcome of the 40th ICAO assembly: A new look at ICAO? *Air and Space Law*, 45(1).

[Abrantes et al., 2021] Abrantes, I., Ferreira, A. F., Silva, A., and Costa, M. (2021). Sustainable aviation fuels and imminent technologies-CO_2 emissions evolution towards 2050. *Journal of Cleaner Production*, 313:127937.

[Airbus, a] Airbus. `https://www.airbus.com/en/newsroom/press-releases/2021-11-airbus-and-its-partners-demonstrate-how-sharing-the-skies-can-save`. Accessed: 2021-11-18.

[Airbus, b] Airbus. `https://www.airbus.com/en/innovation/disruptive-concepts/biomimicry/fellofly`. Accessed: 2022-01-10.

[Alwan and Liu, 2018] Alwan, M. S. and Liu, X. (2018). *Theory of Hybrid Systems: Deterministic and Stochastic*. Springer.

[Ansari et al., 2020] Ansari, M. Y., Ahmad, A., Khan, S. S., Bhushan, G., et al. (2020). Spatiotemporal clustering: A review. *Artificial Intelligence Review*, 53(4):2381–2423.

[Assembly 40th, 2019] Assembly 40th, I. `https://www.icao.int/Meetings/a40/Documents/WP/wp_317_en.pdf`. Accessed: 2021-11-21.

[Aung and Tan, 2010] Aung, H. H. and Tan, K.-L. (2010). Discovery of evolving convoys. In Gertz, M. and Ludäscher, B., editors, *International Conference on Scientific and Statistical Database Management*, pages 196–213. Springer.

[Bengea et al., 2011] Bengea, S., Uthaichana, K., Zěfran, M., and DeCarlo, R. A. (2011). Optimal control of switching systems via embedding into continuous optimal control problem. In Levine, W. S., editor, *The Control Handbook: Advanced Methods*, chapter 31, pages 31–1 – 31–23. CRC Press.

[Bengea and DeCarlo, 2005] Bengea, S. C. and DeCarlo, R. A. (2005). Optimal control of switching systems. *Automatica*, 41:11–27.

[Betts, 2010] Betts, J. T. (2010). *Practical Methods for Optimal Control and Estimation using Nonlinear Programming*. SIAM.

[Bieniawski et al., 2014] Bieniawski, S. R., Clark, R. W., Rosenzweig, S. E., and Blake, W. E. (2014). Summary of flight testing and results for the formation flight for aerodynamic benefit program. In *Proceedings of the 52nd Aerospace Sciences Meeting*, National Harbor, MD, USA.

[Blake and Flanzer, 2016] Blake, W. B. and Flanzer, T. C. (2016). Optimal routing for drag-reducing formation flight: A restricted case. *Journal of Guidance, Control, and Dynamics*, 39(1):173–176.

[Blatman and Sudret, 2010] Blatman, G. and Sudret, B. (2010). An adaptive algorithm to build up sparse polynomial chaos expansions for stochastic finite element analysis. *Probabilistic Engineering Mechanics*, 25(2):183–197.

[Bower et al., 2009] Bower, G. C., Flanzer, T. C., and Kroo, I. M. (2009). Formation geometries and route optimization for commercial formation flight. In *Proceedings of the 27th AIAA Applied Aerodynamics Conference*, San Antonio, TX, USA.

[Buhmann, 2003] Buhmann, M. D. (2003). *Radial Basis Functions: Theory and Implementations*. Cambridge University Press.

[Camilleri, 2018] Camilleri, M. A. (2018). Aircraft operating costs and profitability. In *Travel Marketing, Tourism Economics and the Airline Product*, chapter 12, pages 191–204. Springer.

[Caprace et al., 2019] Caprace, D.-G., Winckelmans, G., Chatelain, P., and Eldredge, J. D. (2019). Wake vortex detection and tracking for aircraft formation flight. In *Proceedings of the AIAA Aviation 2019 Forum*, Dallas, TX, USA.

[Cavalier et al., 1990] Cavalier, T. M., Pardalos, P. M., and Soyster, A. L. (1990). Modeling and integer programming techniques applied to propositional calculus. *Computers and Operations Research*, 17(6):561–570.

[Cook et al., 2015] Cook, A., Blom, H. A., Lillo, F., Mantegna, R. N., Micciche, S., Rivas, D., Vázquez, R., and Zanin, M. (2015). Applying complexity science to air traffic management. *Journal of Air Transport Management*, 42:149–158.

[Dee et al., 2011] Dee, D. P., Uppala, S. M., et al. (2011). The ERA–Interim reanalysis: Configuration and performance of the data assimilation system. *Quarterly Journal of the Royal Meteorological Society*, 137(656):553–597.

[Durango et al., 2016] Durango, G. J., Lawson, C., and Shahneh, A. Z. (2016). Formation flight investigation for highly efficient future civil transport aircraft. *The Aeronautical Journal*, 120(1229):1081–1100.

[Eurocontrol, 2013] Eurocontrol (2013). User manual for the Base of Aircraft Data (BADA). Technical Report 130416, Eurocontrol.

[Fahroo and Ross, 2000] Fahroo, F. and Ross, I. M. (2000). A spectral patching method for direct trajectory optimization. *Journal of the Astronautical Sciences*, 48(2):269–286.

[Fahroo and Ross, 2008] Fahroo, F. and Ross, I. M. (2008). Advances in pseudospectral methods for optimal control. In *Proceedings of the AIAA Guidance, Navigation and Control Conference and Exhibit*, Honolulu, HI, USA.

[Falck et al., 2021] Falck, R., Gray, J. S., Ponnapalli, K., and Wright, T. (2021). Dymos: A Python package for optimal control of multidisciplinary systems. *Journal of Open Source Software*, 6(59):2809.

[Flanzer et al., 2014] Flanzer, T. C., Bieniawski, S. R., and Blake, W. B. (2014). Operational analysis for the formation flight for aerodynamic benefit program. In *Proceedings of the 52nd Aerospace Sciences Meeting*, National Harbor, MD, USA.

[Flanzer et al., 2020] Flanzer, T. C., Bieniawski, S. R., and Brown, J. A. (2020). Advances in cooperative trajectories for commercial applications. In *Proceedings of the AIAA SciTech 2020 Forum*, Orlando, FL, USA.

[Garg, 2011] Garg, D. (2011). *Advances in Global Pseudospectral Methods for Optimal Control*. PhD thesis, University of Florida, Gainesville, FL, USA.

[Garg et al., 2011] Garg, D., Patterson, M. A., Francolin, C., Darby, C. L., Huntington, G. T., Hager, W. W., and Rao, A. V. (2011). Direct trajectory optimization and costate estimation of finite-horizon and infinite-horizon optimal control problems using a Radau pseudospectral method. *Computational Optimization and Applications*, 49(2):335–358.

[Garg et al., 2009] Garg, D., Patterson, M. A., Hager, W., Rao, A. V., Benson, D. A., and Huntington, G. T. (2009). An overview of three pseudospectral methods for the numerical solution of optimal control problems. *Advances in the Astronautical Sciences*, 135:1–17.

[Haalas et al., 2014] Haalas, D. J., Bieniawski, S. R., Whitehead, B., Flanzer, T., and Blake, W. B. (2014). Formation flight for aerodynamic benefit simulation development and validation. In *Proceedings of the 52nd Aerospace Sciences Meeting*, National Harbor, MD, USA.

[Hallock and Holzäpfel, 2018] Hallock, J. N. and Holzäpfel, F. (2018). A review of recent wake vortex research for increasing airport capacity. *Progress in Aerospace Sciences*, 98:27–36.

[Hart et al., 2012] Hart, W. E., Laird, C. D., Watson, J.-P., Woodruff, D. L., Hackebeil, G. A., Nicholson, B. L., and Siirola, J. D. (2012). *Pyomo-Optimization Modeling in Python*. Springer.

[Hartjes et al., 2018] Hartjes, S., van Hellenberg Hubar, M. E., and Visser, H. G. (2018). Multiple-phase trajectory optimization for formation flight in civil aviation. In Dolega, B., Glebocki, R., Kordos, D., and Zugaj, M., editors, *Advances in Aerospace Guidance, Navigation and Control*, pages 389–405. Springer.

[Hartjes et al., 2019] Hartjes, S., Visser, H. G., and van Hellenberg Hubar, M. E. (2019). Trajectory optimization of extended formation flights for commercial aviation. *Aerospace*, 6(9):100.

[Héder, 2017] Héder, M. (2017). From NASA to EU: the evolution of the TRL scale in Public Sector Innovation. *The Innovation Journal*, 22(2):1–23.

[Hu et al., 2005] Hu, J., Prandini, M., and Sastry, S. (2005). Aircraft conflict prediction in the presence of a spatially correlated wind field. *IEEE Transactions on Intelligent Transportation Systems*, 6(3):326 – 340.

[Hull, 2007] Hull, D. G. (2007). *Fundamentals of Airplane Flight Mechanics*. Springer.

[Huntington, 2007] Huntington, G. T. (2007). *Advancement and analysis of a Gauss pseudospectral transcription for optimal control problems*. PhD thesis, Massachusetts Institute of Technology, Cambridge, MA, USA.

[Huntington and Rao, 2008] Huntington, G. T. and Rao, A. V. (2008). Comparison of global and local collocation methods for optimal control. *Journal of Guidance, Control, and Dynamics*, 31(2):432–436.

[IATA, 2013] IATA (2013). Technology roadmap, 4th Edition. Technical report, International Air Transport Association.

[IATA, 2016] IATA (2016). Press Release No. 59. IATA forecasts passenger demand to double over 20 years. `https://www.iata.org/en/pressroom/pr/2016-10-18-02/`. Accessed: 2021-12-19.

[ICAO, 1944] ICAO (1944). Convention on international civil aviation. Annex 2. Technical report, International Civil Aviation Organization.

[ICAO, 2016] ICAO (2016). Environmental report 2016. Aviation and climate change. Technical report, International Civil Aviation Organization.

[ICAO, 2017] ICAO (2017). Airline operating costs and productivity. Technical report, International Civil Aviation Organization.

[IPCC, 2018] IPCC (2018). Global warming of 1.5C. Technical report, The Intergovernmental Panel on Climate Change.

[Jeung et al., 2010] Jeung, H., Yiu, M. L., Zhou, X., Jensen, C. S., and Shen, H. T. (2010). Discovery of convoys in trajectory databases. *Proceedings of the VLDB Endowment*, 1(1):1068–1080.

[Kent and Richards, 2014] Kent, T. and Richards, A. (2014). Accounting for the effect of ground delay on commercial formation flight. In *Proceedings of the 2014 UKACC International Conference on Control*, Loughborough, United Kingdom.

[Kent and Richards, 2015] Kent, T. E. and Richards, A. G. (2015). Analytic approach to optimal routing for commercial formation flight. *Journal of Guidance, Control, and Dynamics*, 38(10):1872–1884.

[Kent and Richards, 2021] Kent, T. E. and Richards, A. G. (2021). Potential of formation flight for commercial aviation: Three case studies. *Journal of Aircraft*, 58(2):1–14.

[Kim and Braatz, 2012] Kim, K. K. K. and Braatz, R. D. (2012). Probabilistic analysis and control of uncertain dynamic systems: Generalized polynomial chaos expansion approaches. In *Proceedings of the 2012 American Control Conference*, Montreal, QC, Canada.

[Klavins, 2004] Klavins, E. (2004). Communication complexity of multi-robot systems. In Boissonnat, J., Burdick, J., Goldberg, K., and Hutchinson, S., editors, *Algorithmic Foundations of Robotics V*, pages 275–291. Springer.

[Kless et al., 2013] Kless, J. E., Aftosmis, M. J., Ning, S. A., and Nemec, M. (2013). Inviscid analysis of extended-formation flight. *AIAA Journal*, 51(7):1703–1715.

[Klöwer et al., 2021] Klöwer, M., Allen, M., Lee, D., Proud, S., Gallagher, L., and Skowron, A. (2021). Quantifying aviation's contribution to global warming. *Environmental Research Letters*, 16(10):104027.

[Lai et al., 2022] Lai, Y. Y., Christley, E., Kulanovic, A., Teng, C.-C., Björklund, A., Nordensvärd, J., Karakaya, E., and Urban, F. (2022). Analysing the opportunities and challenges for mitigating the climate impact of aviation: A narrative review. *Renewable and Sustainable Energy Reviews*, 156:111972.

[Lee et al., 2009] Lee, D. S., Fahey, D. W., Forster, P. M., Newton, P. J., Wit, R. C., Lim, L. L., Owen, B., and Sausen, R. (2009). Aviation and global climate change in the 21st century. *Atmospheric Environment*, 43(22-23):3520–3537.

[Li et al., 2014] Li, X., Nair, P. B., Zhang, Z., Gao, L., and Gao, C. (2014). Aircraft robust trajectory optimization using nonintrusive polynomial chaos. *Journal of Aircraft*, 51(5):1592–1603.

[Lissaman and Shollenberger, 1970] Lissaman, P. B. S. and Shollenberger, C. A. (1970). Formation flight of birds. *Science*, 168(3934):1003–1005.

[Liu et al., 2019] Liu, C., Jiang, B., Patton, R. J., and Zhang, K. (2019). Integrated fault-tolerant control for close formation flight. *IEEE Transactions on Aerospace and Electronic Systems*, 56(2):839–852.

[Marks and Gollnick, 2016] Marks, T. and Gollnick, V. (2016). Influence of aircraft type and order on fuel savings gained by two aircraft formations. In *Proceedings of the 30th Congress of the International Council of the Aeronautical Science*, Deajeon, South Korea.

[Matsuno et al., 2015] Matsuno, Y., Tsuchiya, T., Wei, J., Hwang, I., and Matayoshi, N. (2015). Stochastic optimal control for aircraft conflict resolution under wind uncertainty. *Aerospace Science and Technology*, 43:77–88.

[Michel et al., 2020] Michel, D.-T., Dolfi-Bouteyre, A., Goular, D., Augère, B., Planchat, C., Fleury, D., Lombard, L., Valla, M., and Besson, C. (2020). Onboard wake vortex localization with a coherent 1.5 μm Doppler LiDAR for aircraft in formation flight configuration. *Optics Express*, 28(10):14374–14385.

[Murphy, 2012] Murphy, K. P. (2012). *Machine learning: A probabilistic perspective*. The MIT Press.

[Ning et al., 2011] Ning, A., Flanzer, T. C., and Kroo, I. M. (2011). Aerodynamic performance of extended formation flight. *Journal of Aircraft*, 48(3):855–865.

[Ning, 2011] Ning, S. A. (2011). *Aircraft Drag Reduction Through Extended Formation Flight*. PhD thesis, Stanford University, Standord, CA, USA.

[Patterson and Rao, 2014] Patterson, M. A. and Rao, A. V. (2014). GPOPS-II: A MATLAB software for solving multiple-phase optimal control problems using hp-adaptive Gaussian quadrature collocation methods and sparse nonlinear programming. *ACM Transactions on Mathematical Software*, 41(1):1–37.

[Prandini and Hu, 2009] Prandini, M. and Hu, J. (2009). Application of reachability analysis for stochastic hybrid systems to aircraft conflict prediction. *IEEE Transactions on Automatic Control*, 54(4):913 – 917.

[Rao et al., 2009] Rao, A. V., Benson, D., Huntington, G. T., Francolin, C., Darby, C. L., and Patterson, M. (2009). *User's Manual for GPOPS Version 2.1: A MATLAB Package for Dynamic Optimization Using the Gauss Pseudospectral Method*.

[Rivas and Vazquez, 2016] Rivas, D. and Vazquez, R. (2016). Uncertainty. In Cook, A. and Rivas, D., editors, *Complexity Science in Air Traffic Management*. Routledge.

[Ross, 2020] Ross, I. (2020). Enhancements to the DIDO optimal control toolbox. *arXiv preprint arXiv:2004.13112*.

[Ross and Fahroo, 2004] Ross, I. M. and Fahroo, F. (2004). Pseudospectral knotting methods for solving optimal control problems. *Journal of Guidance, Control, and Dynamics*, 27(3):397–405.

[Saltelli et al., 2008] Saltelli, A., Ratto, M., Andres, T., Campolongo, F., Cariboni, J., Gatelli, D., Saisana, M., and Tarantola, S. (2008). *Global Sensitivity Analysis. The Primer*. John Wiley & Sons.

[Seo et al., 2017] Seo, J., Kim, Y., Kim, S., and Tsourdos, A. (2017). Collision avoidance strategies for unmanned aerial vehicles in formation flight. *IEEE Transactions on Aerospace and Electronic Systems*, 53(6):2718–2734.

[Shapiro, 2003] Shapiro, A. (2003). Monte Carlo Sampling Methods. In Ruszczynski, A. and Shapiro, A., editors, *Stochastic Programming*, volume 10 of *Handbooks in Operations Research and Management Science*, pages 353–425. Elsevier.

[Shone et al., 2021] Shone, R., Glazebrook, K., and Zografos, K. G. (2021). Applications of stochastic modeling in air traffic management: Methods, challenges and opportunities for solving air traffic problems under uncertainty. *European Journal of Operational Research*, 292:1–26.

[Slotnick, 2014] Slotnick, J. P. (2014). Computational aerodynamic analysis for the formation flight for aerodynamic benefit program. In *Proceedings of the 52nd Aerospace Sciences Meeting*, National Harbor, MD, USA.

[Sudret, 2008] Sudret, B. (2008). Global sensitivity analysis using polynomial chaos expansions. *Reliability Engineering and System Safety*, 93:964–979.

[Tierno et al., 2012] Tierno, M. Á. G., Cortés, M. P., and Márquez, C. P. (2012). *Mecánica del vuelo*. Ibergaceta.

[Torre et al., 2019] Torre, E., Marelli, S., Embrechts, P., and Sudret, B. (2019). A general framework for data-driven uncertainty quantification under complex input dependencies using vine copulas. *Probabilistic Engineering Mechanics*, 55:1–16.

[Trucchia et al., 2019] Trucchia, A., Egorova, V., Pagnini, G., and Rochoux, M. (2019). On the merits of sparse surrogates for global sensitivity analysis of multi-scale nonlinear problems: Application to turbulence and fire-spotting model in wildland fire simulators. *Communications in Nonlinear Science and Numerical Simulation*, 73:120–145.

[Tu et al., 2008] Tu, Y., Ball, M. O., and Jank, W. S. (2008). Estimating flight departure delay distributions—a statistical approach with long-term trend and short-term pattern. *Journal of the American Statistical Association*, 103(481):112–125.

[Vachon et al., 2002] Vachon, M. J., Ray, R., Walsh, K., and Ennix, K. (2002). F/A-18 aircraft performance benefits measured during the autonomous formation flight project. In *Proceedings of the AIAA Atmospheric Flight Mechanics Conference and Exhibit*, Monterey, CA, USA.

[Vechtel et al., 2018] Vechtel, D., Fischenberg, D., and Schwithal, J. (2018). Flight dynamics simulation of formation flight for energy saving using LES-generated wake flow fields. *CEAS Aeronautical Journal*, 9(4):735–746.

[Vieira et al., 2009] Vieira, M. R., Bakalov, P., and Tsotras, V. J. (2009). On-line discovery of flock patterns in spatio-temporal data. In *Proceedings of the 17th ACM SIGSPATIAL International Conference on Advances in Geographic Information Systems*, Seattle, WA, USA.

[Voskuijl, 2017] Voskuijl, M. (2017). Cruise range in formation flight. *Journal of Aircraft*, 54(6):2184–2191.

[Wächter and Biegler, 2006] Wächter, A. and Biegler, L. T. (2006). On the implementation of an interior-point filter line-search algorithm for large-scale nonlinear programming. *Mathematical programming*, 106(1):25–57.

[Wei et al., 2008] Wei, S., Zěfran, M., and DeCarlo, R. A. (2008). Optimal control of robotic systems with logical constraints: Application to UAV path planning. In *Proceedings of the 2008 IEEE International Conference on Robotics and Automation*, Pasadena, CA, USA.

[Wieselsberger, 1914] Wieselsberger, C. (1914). Beitrag zur Erklärung des Winkelfluges einiger Zugvögel. *Zeitschrift für Flugtechnik und Motorluftschiffahrt.*, 5:225–229.

[Xiu, 2010] Xiu, D. (2010). *Numerical Methods for Stochastic Computations. A Spectral Method Approach*. Princeton University Press.

[Xu et al., 2014] Xu, J., Ning, S. A., Bower, G., and Kroo, I. (2014). Aircraft route optimization for formation flight. *Journal of Aircraft*, 51(2):490–501.

[Zhu, 2019] Zhu, Y. (2019). *Uncertain Optimal Control*. Springer.